New nitric oxide-releasing indomethacin derivatives with 1,3-thiazolidine-4-one scaffold: Design, synthesis, in silico and in vitro studies

Alexandru Sava, Frederic Buron, Sylvain Routier, Alina Panainte, Nela Bibire, Lenuţa Profire

New nitric oxide-releasing indomethacin derivatives with 1,3-thiazolidine-4-one scaffold: design, synthesis, *in silico* and *in vitro* studies

Alexandru Sava[a,b], Frederic Buron[b], Sylvain Routier[b,1,*], Alina Panainte[a], Nela Bibire[a], Lenuţa Profire[c,1,*]

[a]*Department of Analytical Chemistry, Faculty of Pharmacy, "Grigore T. Popa" University of Medicine and Pharmacy of Iaşi, 16 University Street, Iasi, Romania*

[b]*Institut de Chimie Organique et Analytique ICOA, CNRS UMR 7311, Université d'Orléans, Orléans, France*

[c]*Department of Pharmaceutical Chemistry, Faculty of Pharmacy, "Grigore T. Popa" University of Medicine and Pharmacy of Iaşi, 16 University Street, Iasi, Romania*

*Corresponding author at: Department of Pharmaceutical Chemistry, Faculty of Pharmacy, "Grigore T. Popa" University of Medicine and Pharmacy of Iași, 16 University Street, Iasi, Romania, E-mail address: lenuta.profire@umfiasi.ro (L.P.); Institut de Chimie Organique et Analytique ICOA, CNRS UMR 7311, Université d'Orléans, France, sylvain.routier@univ-orleans.fr (S.R.)

[1]Both authors contributed equally as senior authors.

ABSTRACT

In this study we present design and synthesis of nineteen new nitric oxide-releasing indomethacin derivatives with 1,3-thiazolidine-4-one scaffold (NO-IND-TZDs) (**6a-s**), as a new safer and efficient multi-targets strategy for inflammatory diseases. The chemical structure of all synthesized derivatives (intermediaries and finals) was proved by NMR and mass spectroscopic analysis. In order to study the selectivity of NO-IND-TZDs for COX isoenzymes (COX-1 and COX-2) a molecular docking study was performed using AutoDock 4.2.6 software. Based on docking results, COX-2 inhibitors were designed and **6o** appears as the most selective derivative which showed an improved selective index compared with indomethacin (IND) and diclofenac (DCF), used as reference drugs. The biological evaluation of **6a-s**, using *in vitro* assays has included the anti-inflammatory and antioxidant effects as well as the nitric oxide (NO) release. Referring to the anti-inflammatory effects, the most active compound was **6i**, which was more

active than IND and aspirin (ASP) in term of denaturation effect, on bovine serum albumin (BSA), as indirect assay to predict the anti-inflammatory effect. An appreciable anti-inflammatory effect, in reference with IND and ASP, was also showed by **6k**, **6c**, **6q**, **6o**, **6j, 6d**. The antioxidant assay revealed the compound **6n** as the most active, being 100 times more active than IND. The compound **6n** showed also the most increase capacity to release NO, which means is safer in terms of gastro-intestinal side effects. The ADME-Tox study revealed also that the NO-IND-TZDs are generally proper for oral administration, having optimal physico-chemical and ADME properties. We can conclude that the compounds **6i** and **6n** are promising agents and could be included in further investigations to study in more detail their pharmaco-toxicological profile.

Key words: indomethacin, 1,3-thiazolidine-4-one, nitric oxide, docking study, cyclooxygenase, inflammation.

1. Introduction

The inflammation is a crucial physiological response of the human body to any kind of aggression in order for restoring the body homeostasis [1–3]. Moreover, uncontrolled and persistent inflammation may develop itself into a chronic malady [4,5], which becomes the fundamental basis for the pathogenesis of many chronic diseases such as rheumatoid arthritis [6], inflammatory bowel disease [7], metabolic disorders (diabetes mellitus and obesity) [8–10], cardiovascular disorders (ischemic heart disease, atherosclerosis) [11,12], neurodegenerative diseases (Parkinson's and Alzheimer's disease) [13–15] and cancer [16], many of which are life-threatening [17,18].

Non-steroidal anti-inflammatory drugs (NSAIDs) are principal drugs which are used to treat different conditions where inflammation is involved [19]. They inhibit cyclooxygenase (COX) enzyme in a wide variety of systems, ranging from microsomal enzyme synthesis to different cells and tissues [20]. Therefore, COX inhibition has become definitively the main mechanism that is responsible for both therapeutic and side effects of these drugs [21,22]. Briefly, despite the clinical benefits of NSAIDs through nonselective COX inhibition or to the relative COX-1 and COX-2 inhibition, long term use of them increase the incidence of side effects (gastrointestinal, renal, allergic skin reactions, increased risk of acute coronary syndromes, bleeding) [21,23–25].

Indomethacin (IND) is one of the most relevant NSAID used worldwide for the treatment of acute and chronic rheumatoid arthritis and other inflammatory rheumatic diseases, episodes of acute gout and acute musculoskeletal pain [26,27]. However, it was documented that long-term clinical usage of IND is responsible for a wide range of side effects including gastrointestinal (GI) irritation, bleeding and ulceration, digestive disorders (nausea, vomiting, abdominal pain, diarrhea or constipation), increased anxiety, headache, dizziness, peripheral edema, arterial hypertension, tachycardia, kidney and liver dysfunction, allergic and anaphylactic reactions [26,28].

To improve clinical effectiveness of NSAIDs, two platform strategies are currently emerging [29,30]. The first one is drugs combination, in order to reduce the side effects of NSAIDs, and the second one is referring to a single compound can hit multiple targets (single drug-multiple targets).

Nitric oxide releasing non-steroidal anti-inflammatory drugs (NO-NSAIDs) are a new class of anti-inflammatory drugs consisting of a traditional NSAID to which a NO releasing moiety has been covalently attached by a spacer [31,32]. NO is an endogenous short-lived free radical, produced in mammalians cells through nitric oxide synthase mediated conversion of L-arginine to L-citruline [33–36]. It is known that NO has a key role in a wide variety of physiological and pathophysiological processes, such as inflammation, vasodilatation, platelet adhesion, thrombosis neurotransmission, neuronal communication and wound healing [37–39]. Referring to NO-NSAIDs is recognized that NO is a critical mediator of GI mucosal defense and suppresses the NSAIDs side effects mediated by COX-1 inhibition such as suppression of reduction in mucosal blood flow, synthesis of mucosal cytoprotective prostaglandins (especially PGE_2) and over-expression of inflammatory mediators (plasma tumor necrosis factor alpha (TNF-α) and the leukocyte–endothelial cell adherence) [37,40,41]. Moreover, based the beneficial cardiovascular effect of NO, were developed nitric-oxide selective COX-2 inhibitors (NO-COXIBs) which proved to be safer than classical COX-2 inhibitors [21,42].

On other hand, the 1,3-thiazolidine-4-one scaffold serve as a core for many synthetic compounds of great interest in medicinal chemistry [43]. This scaffold is a structural component of various natural products, like thiamine (vitamin B_1), acidomycin (isolated from *Strepomyces* strains) [44,45] and many metabolic products (cytotoxic cyclopeptides) of fungi and primitive marine animals [46]. Several thiazolidine-4-one based drugs such as ralitoline (anticonvulsant),

etozoline (loop diuretic) and pioglitazone (oral anti-diabetic drug) have already been approved for therapeutic use (Fig. 1). The literature reports for thiazolidine-4-one scaffold other important biological effects such as anti-inflammatory, antioxidant, platelet-activating factor (PAF) antagonist, cyclooxygenase (COX) inhibition, tumor necrosis factor antagonist as well as anticancer, anticonvulsant, antimicrobial, antiviral and anti HIV effects [47–52].

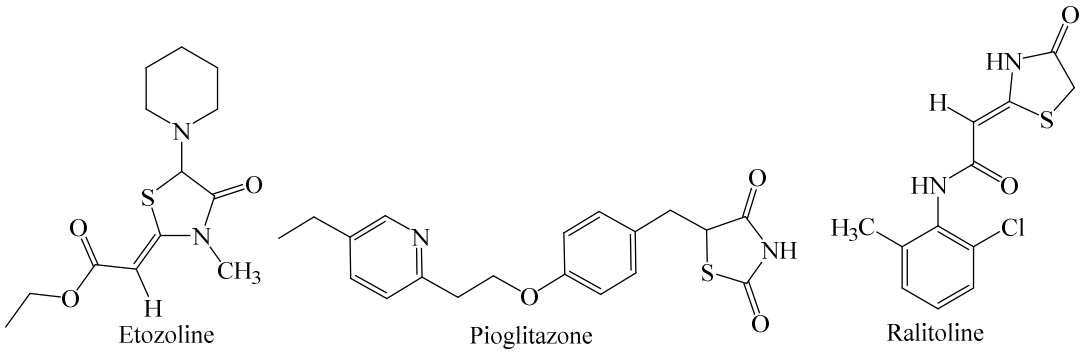

Fig. 1. Representative drugs containing the thiazolidinone core.

To attach a thiazolidine-4-one scaffold to indomethacin structure a carbohydrazide linker was used. This group is often used in medicinal chemistry due to its: (i) synthetic feasibility and functionalization by reacting with a variety of chemical substances, (ii) plasma stability and (iii) stereo chemical nature which allows the conjugated hydrophobic subunit to link at binding pocket in a favorable and stable configuration [53–55]. Carbohydrazide group is an important pharmacophore, presents in several drugs, such as rimonabant (the first selective cannabinoid receptor blocker, with anorectic anti-obesity effect) [56–58], nitrofurantoin (antibacterial drug used to treat bladder infections), carbazochrome (haemostatic agent), nifuroxazide (a nitrofuran antibiotic) [59,60] and dantrolene (a postsynaptic muscle relaxant) (Fig. 2) [53,54,61].

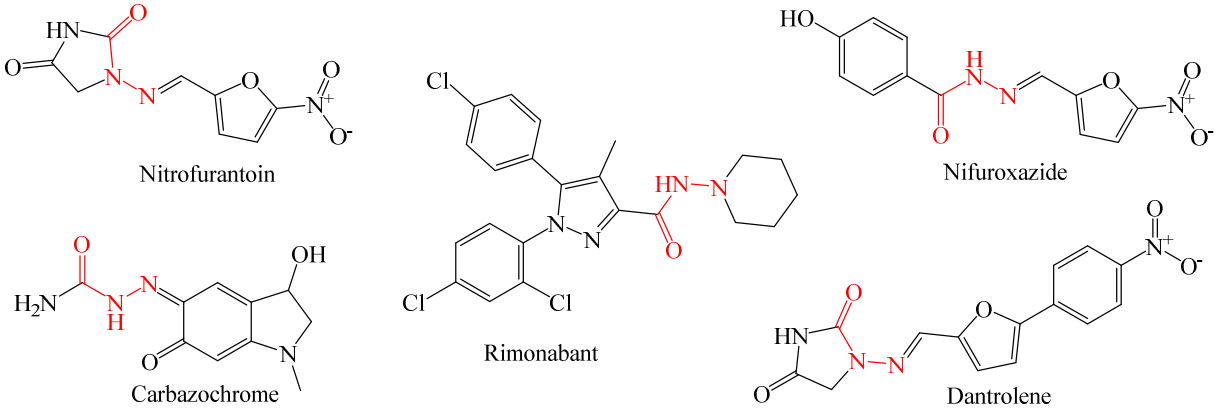

Fig. 2. Representative drugs containing the carbohydrazide group.

Based on arguments presented above we have developed new nitric oxide-releasing indomethacin derivatives with 1,3-thiazolidine-4-one scaffold (NO-IND-TZDs), as safer and efficient multi-targets therapeutic strategy. In this study we present the design and synthesis of NO-IND-TZDs as well as biological evaluation in terms of COX isoenzyme inhibition selectivity, based on molecular docking study, anti-inflammatory and antioxidant effects and also their capacity to release NO.

2. Material and methods

2.1. Chemistry

General information. All solvents used for chemical synthesis were of analytical grade or HPLC *p.a*. quality unless otherwise stated. The anhydrous solvents needed for certain reactions have been distilled or dried according to standard procedures prior to use: dichloromethane has been distilled under P_2O_5 and acetonitrile has been dried on cartridge by a GT S100 station. The progress of the reaction and purity of synthesized compounds were monitored by thin layer chromatography (TLC), using 2×5 cm pre-coated silicagel 60 F254 aluminium plate (Merck) and UV lamp exposure at 254 nm. Column chromatography purifications are performed on Merck 40-70 mM silicagel (230-240 mesh) or on C18 AIT 40-60 m silicagel. The ^{1}H NMR (250 MHz or 400 MHz), ^{13}C NMR (63 MHz or 101 MHz) and ^{19}F NMR (376 MHz) spectra were recorded on Bruker Avance DPX250 (250, 131 MHz) or Bruker Avance II (400 MHz) spectrometer. Chemical shifts (δ H, δ C) and coupling constant values (*J*) are given in *ppm* and *Hz*, respectively. An internal standard of tetramethylsilane (TMS, δ H = 0, δ C = 0) in $CDCl_3$ and DMSO-d_6 was used. High resolution mass spectrometry (HRMS) has been made on a Bruker maXis mass spectrometer within the "Research Federation" platform between ICOA and CBM (FR2708).

*2.1.1. General procedure for the synthesis of the halide-ethoxy-benzaldehyde derivatives (**2a-s**)*

To a solution of hydroxybenzaldehydes (**1a-s)** (1.0 Eq.) in acetonitrile (150 mL), 1,2-dibromoethane or bis(2-chloroethyl)ether (10.0 Eq.) and potassium carbonate (2.0 Eq.) were added, according to the method reported in the literature [62–64], which was adapted to our synthesis in terms of the ratio of reagents, solvent, time of reaction, purification method. The mixture was stirred overnight under reflux and progress of reaction was monitored by TLC.

After cooling to room temperature, distilled water (4 x 50 mL) was added and the mixture was extracted with diethyl ether (50 mL). The combined organic layers were washed with brine (50 mL), dried over anhydrous magnesium sulfate and concentrated under reduced pressure. The crude products were purified by flash chromatography (silicagel, petroleum ether/ethyl acetate) to give the pure products (**2a-s**).

*2.1.1.1. 4-(2-Bromoethoxy)benzaldehyde **(2a)** was obtained from 4-hydroxybenzaldehyde (**1a**)* as a yellow oil in 96% yield. ^{1}H NMR (400 MHz, DMSO-d_6) δ = 3.77 – 3.90 (m, 2H), 4.39 – 4.49 (m, 2H), 7.16 (d, *J* = 8.7 Hz, 2H), 7.88 (d, *J* = 8.7 Hz, 2H), 9.88 (s, 1H). ^{13}C NMR (101 MHz, DMSO-d_6) δ = 31.5 (CH_2), 68.5 (CH_2), 115.5 ($2CH_{Ar}$), 130.4 (C_q), 132.2 ($2CH_{Ar}$), 163.2 (C_q), 191.7 (C = O). HRMS (EI-MS) *m/z* calcd for $C_9H_9BrO_2$: 227.9786 $[M-H]^+$, found: 227.9855. Rf (petroleum ether/ethyl acetate = 6/4) 0.68.

*2.1.1.2. 4-(2-Bromoethoxy)-3-fluorobenzaldehyde **(2b)*** was obtained from 3-fluoro-4-hydroxybenzaldehyde (**1b**) as a white solid in 91% yield, m.p. 61-63°C. ^{1}H NMR (400 MHz, DMSO-d_6) δ = 3.87 (dd, *J* = 6.0 HZ, 4.7 Hz, 2H), 4.53 (dd, *J* = 6.1 Hz, 4.7 Hz, 2H), 7.41 (t, *J* = 8.3 Hz, 1H), 7.71 (dd, *J* = 11.3 Hz, 2.0 Hz, 1H), 7.77 (ddd, *J* = 8.3 Hz, 2.0 Hz, 1.0 Hz, 1H), 9.87 (d, *J*= 2.0 Hz, 1H). ^{13}C NMR (101 MHz, DMSO-d_6) δ = 30.7 (CH_2), 69.0 (CH_2), 114.9 (d, *J* = 1.7 Hz, CH_{Ar}), 115.4 (d, *J* = 18.4 Hz, CH_{Ar}), 128.2 (d, *J* = 3.1 Hz, CH_{Ar}), 130.1 (d, *J* = 5.0 Hz, C_q), 151.0 (d, *J* = 10.7 Hz, C_q), 151.5 (d, *J* = 247.3 Hz, C_qF), 190.8 (d, *J* = 2.2 Hz, C = O).
^{19}F NMR (376 MHz, DMSO-d_6) δ = -133.32 (ddd, *J* = 10.9 Hz, 8.3 Hz, 2.1 Hz). HRMS (EI-MS) *m/z* calcd for $C_9H_8FBrO_2$: 245.9692 $[M-H]^+$, found: 245.9762. Rf (petroleum ether/ethyl acetate = 7/3) 0.65.

*2.1.1.3. 4-(2-Bromoethoxy)-3-chlorobenzaldehyde **(2c)*** was obtained from 3-chloro-4-hydroxybenzaldehyde (**1c**) as a white solid in 95% yield, m.p. 62-64 °C.^{1}H NMR (400 MHz, DMSO-d_6) δ = 3.82 - 3.92 (m, 2H), 4.50 - 4.59 (m, 2H), 7.38 (d, *J* = 8.5 Hz, 1H), 7.89 (dd, *J* = 8.5 Hz, 2.0 Hz, 1H), 7.97 (d, *J* = 2.0 Hz, 1H), 9.88 (s, 1H). ^{13}C NMR (101 MHz, DMSO-d_6) δ = 30.6 (CH_2), 69.1 (CH_2), 114.0 (CH_{Ar}), 122.3 (C_q), 130.4 (C_q), 130.6 (CH_{Ar}), 130.8 (CH_{Ar}), 157.9 (C_q), 190.7 (C = O). HRMS (EI-MS) *m/z* calcd for $C_9H_8BrClO_2$: 261.9396 $[M-H]^+$, found: 261.9468. Rf (petroleum ether/ethyl acetate = 5/5) 0.74.

*2.1.1.4. 3-Bromo-4-(2-bromoethoxy)benzaldehyde **(2d)*** was obtained from 3-bromo-4-hydroxybenzaldehyde (**1d**) as a white solid in 86% yield, m.p. 64-66 °C. ^{1}H NMR (400 MHz,

DMSO-d_6) δ = 3.82 - 3.90 (m, 2H), 4.50 - 4.58 (m, 2H), 7.33 (d, *J* = 8.5 Hz, 1H), 7.91 (dd, *J* = 8.5 Hz, 2.0 Hz, 1H), 8.11 (d, *J* = 2.0 Hz, 1H), 9.86 (s, 1H). ^{13}C NMR (101 MHz, DMSO-d_6) δ = 30.6 (CH_2), 69.2 (CH_2), 111.7 (C_q), 113.8 (CH_{Ar}), 130.9 (C_q), 131.1 (CH_{Ar}), 134.1 (CH_{Ar}), 158.8 (C_q), 190.5 (C = O). HRMS (EI-MS) *m/z* calcd for $C_9H_8Br_2O_2$: 305.8891 $[M-H]^+$, found: 305.8962. Rf (petroleum ether/ethyl acetate = 6/4) 0.57.

2.1.1.5. 4-(2-Bromoethoxy)-3-methoxybenzaldehyde ***(2e)*** was obtained from 4-hydroxy-3-methoxybenzaldehyde (**1e**) as white needle-shaped crystals in 86% yield, m.p. 66-68 °C. ^{1}H NMR (400 MHz, DMSO-d_6) δ =3.84 (dd, *J* = 6.0 Hz, 4.9 Hz, 2H), 3.85 (s, 3H), 4.43 (dd, *J* = 6.1 Hz, 4.8 Hz, 2H), 7.20 (d, *J* = 8.2 Hz, 1H), 7.42 (d, *J* = 2.0 Hz, 1H), 7.54 (dd, *J* = 8.2 Hz, 2.0 Hz, 1H), 9.85 (s, 1H). ^{13}C NMR (101 MHz, DMSO-d_6) δ =30.9 (CH_2), 55.6 (CH_3), 68.6 (CH_2), 110.0 (CH_{Ar}), 112.6 (CH_{Ar}), 125.9 (CH_{Ar}), 130.1 (C_q), 149.2 (C_q), 152.7 ($3C_q$), 191.5 (C = O). HRMS (EI-MS) *m/z* calcd for $C_{10}H_{11}BrO_3$: 257.9892 $[M-H]^+$, found: 257.9962. Rf (petroleum ether/ethyl acetate = 6/4) 0.55.

2.1.1.6. 4-(2-Bromoethoxy)-3-ethoxybenzaldehyde ***(2f)*** was obtained from 3-ethoxy-4-hydroxybenzaldehyde (**1e**) as yellowish white needle-shaped crystals in 65% yield, m.p. 65-67 °C. ^{1}H NMR (400 MHz, DMSO-d_6) δ = 1.35 (t, *J* = 6.9 Hz, 3H), 3.83 (dd, *J* = 6.1 Hz, 5.0 Hz, 2H), 4.12 (q, *J* = 6.9 Hz, 2H), 4.43 (dd, *J* = 6.1 Hz, 5.0 Hz, 2H), 7.20 (d, *J* = 8.3 Hz, 1H), 7.41 (d, *J* = 1.9 Hz, 1H), 7.53 (dd, *J* = 8.2 Hz, 1.9 Hz, 1H), 9.84 (s, 1H). ^{13}C NMR (101 MHz, DMSO-d_6) δ = 14.6 (CH_3), 30.9 (CH_2), 64.1 (CH_2), 68.6 (CH_2), 111.7 (CH_{Ar}), 113.2 (CH_{Ar}), 125.6 (CH_{Ar}), 130.2 (C_q), 148.5 (C_q), 153.0 (C_q), 191.4 (C = O). HRMS (EI-MS) *m/z* calcd for $C_{11}H_{13}BrO_3$: 272.0048 $[M-H]^+$, found: 272.0119. Rf (petroleum ether/ethyl acetate = 6/4) 0.55.

2.1.1.7. 4-(2-Bromoethoxy)-3-nitrobenzaldehyde ***(2g)*** was obtained from 4-hydroxy-3-nitrobenzaldehyde (**1g**) as greenish yellow solid in 85% yield, m.p. 68-70 °C. ^{1}H NMR (400 MHz, DMSO-d_6) δ = 3.80 - 3.88 (m, 2H), 4.60 - 4.68 (m, 2H), 7.59 (d, *J* = 8.7 Hz, 1H), 8.18 (dd, *J* = 8.7 Hz, 2.0 Hz, 1H), 8.43 (d, *J* = 2.0 Hz, 1H), 9.96 (s, 1H). ^{13}C NMR (101 MHz, DMSO-d_6) δ = 30.3 (CH_2), 69.8 (CH_2), 115.8 (CH_{Ar}), 126.3 (CH_{Ar}), 129.1 (C_q), 134.8 (CH_{Ar}), 139.6 (C_q), 154.6 (C_q), 190.4 (C = O). HRMS (EI-MS) *m/z* calcd for $C_9H_8BrNO_4$: 272.9637 $[M-H]^+$, found: 272.9708. Rf (petroleum ether/ethyl acetate = 7/3) 0.70.

2.1.1.8. 4-(2-Bromoethoxy)-3,5-dimethoxybenzaldehyde ***(2h)*** was obtained from 4-hydroxy-3,5-dimethoxybenzaldehyde (**1h**) as white solid in 95% yield, m.p. 64-66 °C. ^{1}H NMR (400 MHz,

DMSO-d_6) δ = 3.69 (t, *J* = 5.9 Hz, 2H), 3.87 (s, 6H), 4.27 (t, *J* = 5.9 Hz, 2H), 7.27 (s, 2H), 9.89 (s, 1H). ^{13}C NMR (101 MHz, DMSO-d_6) δ = 31.6 (CH_2), 56.2 ($2CH_3$), 72.4 (CH_2), 106.7 ($2CH_{Ar}$), 131.9 (C_q), 141.2 (C_q), 153.2 ($2C_q$), 191.9 (C = O). HRMS (EI-MS) *m/z* calcd for $C_{11}H_{13}BrO_4$: 287.9997 $[M-H]^+$, found: 288.0068. Rf (petroleum ether/ ethyl acetate =7/3) 0.50.

2.1.1.9. 4-(2-Bromoethoxy)-3,5-dichlorobenzaldehyde ***(2i)*** was obtained from 3,5-dichloro-4-hydroxybenzaldehyde (**1h**) as white solid in 95% yield, m.p. 67-69 °C. ^{1}H NMR (400 MHz, DMSO-d_6) δ = 3.76 -3.92 (m, 2H), 4.35 - 4.49 (m, 2H), 8.0 (s, 2H), 9.91 (s, 1H).^{13}C NMR (101 MHz, DMSO-d_6) δ = 31.2 (CH_2), 73.4 (CH_2), 129.4 ($2C_q$), 130.0 ($2CH_{Ar}$), 133.6 (C_q), 154.7 (C_q), 190.2 (C = O). HRMS (EI-MS) *m/z* calcd for $C_9H_7BrCl_2O_2$: 295.9006 $[M-H]^+$, found: 295.9072. Rf (petroleum ether/ethyl acetate = 8/2) 0.66.

2.1.1.10. 4-(2-Bromoethoxy)-3-chloro-5-methoxybenzaldehyde ***(2j)*** was obtained from 3-chloro-4-hydroxy-5-methoxybenzaldehyde (**1j**) as white needle-shaped crystals in 86% yield, m.p. 65-67 °C. ^{1}H NMR (400 MHz, DMSO-d_6) δ =3.67 – 3.83 (m, 2H), 3.92 (s, 3H), 4.30 – 4.49 (m, 2H), 7.52 (d, *J* = 1.8 Hz, 1H), 7.65 (d, *J* = 1.8 Hz, 1H), 9.89 (s, 1H). ^{13}C NMR (101 MHz, DMSO-d_6) δ =31.6 (CH_2), 56.4 (CH_3), 72.9 (CH_2), 111.1 (CH_{Ar}), 124.1 (CH_{Ar}), 127.6 (C_q), 132.6 (C_q), 148.2 (C_q), 153.6 (C_q), 191.1 (C = O). HRMS (EI-MS) *m/z* calcd for $C_{10}H_{10}BrClO_3$: 291.9502 $[M-H]^+$, found: 291.9573. Rf (petroleum ether/ethyl acetate = 6/4) 0.64.

2.1.1.11. 3-(2-Bromoethoxy)benzaldehyde ***(2k)*** was obtained from 3-hydroxybenzaldehyde (**1k**) as a colorless oil in 91% yield. ^{1}H NMR (400 MHz, DMSO-d_6) δ = 3.76 – 3.90 (m, 2H), 4.32 – 4.47 (m, 2H), 7.26 - 7.33 (m, 1H), 7.44 (d, *J* = 2.7 Hz, 1H), 7.49 - 7.56 (m, 2H), 9.97 (s, 1H). ^{13}C NMR (101 MHz, DMSO-d_6) δ = 31.1 (CH_2), 68.0 (CH_2), 114.0 (CH_{Ar}), 121.4 (CH_{Ar}), 122.7 (CH_{Ar}), 130.4 (CH_{Ar}), 137.6 (C_q), 158.4 (C_q), 192.7 (C = O). HRMS (EI-MS) *m/z* calcd for $C_9H_9BrO_2$: 227.9786 $[M-H]^+$, found: 227.9856. Rf (petroleum ether/ethyl acetate = 7/3) 0.57.

2.1.1.12. 3-(2-Bromoethoxy)-4-methoxybenzaldehyde ***(2l)*** was obtained from 3-hydroxy-4-methoxybenzaldehyde (**1l**) as white solid in 88% yield, m.p. 64-66 °C. ^{1}H NMR (400 MHz, DMSO-d_6) δ = 3.74 - 3.85 (m, 2H), 3.89 (s, 3H), 4.31 - 4.44 (m, 2H), 7.19 (d, *J* = 8.3 Hz, 1H), 7.41 (d, *J* = 1.9 Hz, 1H), 7.58 (dd, *J* = 8.3 Hz, 1.9 Hz, 1H), 9.83 (s, 1H). ^{13}C NMR (101 MHz, DMSO-d_6) δ = 31.1 (CH_2), 56.0 (CH_3), 68.6 (CH_2), 111.6 (CH_{Ar}), 111.8 (CH_{Ar}), 126.4 (CH_{Ar}), 129.6 (C_q), 147.7 (C_q), 154.4 (C_q), 191.3 (C = O). HRMS (EI-MS) *m/z* calcd for $C_{10}H_{11}BrO_3$: 257.9892 $[M-H]^+$, found: 257.9965. Rf (petroleum ether/ethyl acetate = 5/5) 0.64.

2.1.1.13. 3-(2-Bromoethoxy)-4-nitrobenzaldehyde ***(2m)*** was obtained from 3-hydroxy-4-nitrobenzaldehyde (**1m**) as brown solid in 80% yield, m.p. 69-71 °C. ^{1}H NMR (400 MHz, DMSO-d_6) δ = 3.76 -3.88 (m, 2H), 4.54 - 4.70 (m, 2H), 7.68 (dd, *J* = 8.2 Hz, 1.5 Hz, 1H), 7.86 (d, *J* = 1.5 Hz, 1H), 8.07 (d, *J* = 8.2 Hz, 1H), 10.06 (s, 1H). ^{13}C NMR (101 MHz, DMSO-d_6) δ =30.5 (CH_2), 69.5 (CH_2), 115.6 (CH_{Ar}), 122.2 (CH_{Ar}), 125.4 (CH_{Ar}), 139.5 (C_q), 143.1 (C_q), 150.4 (C_q), 191.9 (C = O). HRMS (EI-MS) *m/z* calcd for $C_9H_8BrNO_4$: 272.9637 $[M-H]^+$, found: 272.9714. Rf (petroleum ether/ethyl acetate = 4/4) 0.65.

2.1.1.14. 5-(2-Bromoethoxy)-2-nitrobenzaldehyde ***(2n)*** was obtained from 5-hydroxy-2-nitrobenzaldehyde (**1n**) as green solid in 86% yield, m.p. 67-69 °C. ^{1}H NMR (400 MHz, DMSO-d_6) δ = 3.81 - 3.89 (m, 2H), 4.51 - 4.62 (m, 2H), 7.29 (d, *J* = 2.8 Hz, 1H), 7.40 (dd, *J* = 9.0 Hz, 2.9 Hz, 1H), 8.19 (d, *J* = 9.0 Hz, 1H), 10.29 (s, 1H). ^{13}C NMR (101 MHz, DMSO-d_6) δ = 30.8 (CH_2), 68.9 (CH_2), 114.3 (CH_{Ar}), 118.7 (CH_{Ar}), 127.3 (CH_{Ar}), 134.2 (C_q), 142.1 (C_q), 162.1 (C_q), 189.8 (C = O). HRMS (EI-MS) *m/z* calcd for $C_9H_8BrNO_4$: 272.9637 $[M-H]^+$, found: 272.9709. Rf (petroleum ether/ethyl acetate = 6/4) 0.65.

2.1.1.15. 2-Bromo-3-(2-bromoethoxy)-4-methoxybenzaldehyde ***(2o)*** was obtained from 2-bromo-3-hydroxy-4-methoxybenzaldehyde (**1o**) as a white solid in 90% yield, m.p. 70-72 °C. ^{1}H NMR (400 MHz, DMSO-d_6) δ = 3.79 (t, *J* = 5.8Hz, 2H), 3.94 (s, 3H), 4.29 (t, *J* = 5.8 Hz, 2H), 7.27 (dd, *J* = 8.7 Hz, 0.8 Hz, 1H), 7.68 (d, *J* = 8.7 Hz, 1H), 10.10 (d, *J* = 0.8 Hz, 1H). ^{13}C NMR (101 MHz, DMSO-d_6) δ = 31.4 (CH_2), 56.6 (CH_3), 72.5 (CH_2), 112.2 (CH_{Ar}), 121.4 (C_q), 126.7 (C_q), 126.9 (CH_{Ar}), 144.3 (C_q), 158.1 (C_q), 190.4 (C = O). HRMS (EI-MS) *m/z* calcd for $C_{10}H_{10}Br_2O_3$: 335.8997 $[M-H]^+$, found: 335.9070. Rf (petroleum ether/ethyl acetate = 6/4) 0.66.

2.1.1.16. 2-(2-Bromoethoxy)benzaldehyde ***(2p)*** was obtained from 2-hydroxybenzaldehyde (**1p**) as a greenish yellow oil in 92% yield. ^{1}H NMR (400 MHz, DMSO-d_6) δ = 3.82 - 3.93 (m, 2H), 4.42 - 4.54 (m, 2H), 7.11 (ddt, *J* = 7.3 Hz, 0.9 Hz, 1H), 7.26 (ddd, *J* = 8.4 Hz, 0.9 Hz, 0.5 Hz, 1H), 7.61 - 7.75 (m, 2H), 10.45 (s, 1H). ^{13}C NMR (101 MHz, DMSO-d_6) δ = 31.3 (CH_2), 68.5 (CH_2), 114.1 (CH_{Ar}), 121.3 (CH_{Ar}), 124.5 (C_q), 127.4 (CH_{Ar}), 136.4 (CH_{Ar}), 160.4 (C_q), 189.1 (C = O). HRMS (EI-MS) *m/z* calcd for $C_9H_9BrO_2$: 227.9786 $[M-H]^+$, found: 227.9856. Rf (petroleum ether/ethyl acetate = 7.5/2.5) 0.56.

2.1.1.17. 4-(2-(2-Chloroethoxy)ethoxy)benzaldehyde ***(2q)*** was obtained from 4-hydroxy-benzaldehyde (**1a**) and bis(2-chloroethyl)ether as a fine white needle crystals in 79% yield, m.p.

65-67 °C. ^{1}H NMR (400 MHz, DMSO-d_6) δ = 3.74 (s, 4H), 3.77 - 3.88 (m, 2H), 4.16 - 4.29 (m, 2H), 7.08 - 7.17 (m, 2H), 7.79 - 7.91 (m, 2H), 9.87 (s, 1H). ^{13}C NMR (101 MHz, DMSO-d_6) δ = 43.5 (CH_2), 67.6 (CH_2), 68.6 (CH_2), 70.6 (CH_2), 114.9 ($2CH_{Ar}$), 129.7 (C_q), 131.8 ($2CH_{Ar}$), 163.4 (C_q), 191.3 (C = O). HRMS (EI-MS) *m/z* calcd for $C_{11}H_{13}ClO_3$: 228.0553 $[M-H]^+$, found: 228.0626. Rf (petroleum ether/ethyl acetate = 6/4) 0.50.

2.1.1.18.*4-(2-(2-Chloroethoxy)ethoxy)-3-methoxybenzaldehyde* **(2r)** was obtained from 4-hydroxy-3-methoxybenzaldehyde (**1e**) and bis(2-chloroethyl)ether as a fine white needle crystals in 88% yield, m.p. 64-66 °C. ^{1}H NMR (250 MHz, DMSO-d_6) δ = 3.64 - 3.80 (m, 4H), 3.78 - 3.89 (m, 5H), 4.15 - 4.28 (m, 2H), 7.18 (d, *J* = 8.7 Hz, 1H), 7.40 (d, *J* = 1.9 Hz, 1H), 7.53 (dd, *J* = 8.3 Hz, 1.9 Hz, 1H), 9.84 (s, 1H).^{13}C NMR (101 MHz, DMSO-d_6) δ = 43.5 (CH_2), 55.6 (CH_3), 68.1 (CH_2), 68.6 (CH_2), 70.7 (CH_2), 109.8 (CH_{Ar}), 112.3 (CH_{Ar}), 125.9 (CH_{Ar}), 129.8 (C_q), 149.2 (C_q), 153.4 (C_q), 191.3 (C = O). HRMS (EI-MS) *m/z* calcd for $C_{12}H_{15}ClO_4$: 258.0659 $[M-H]^+$, found: 258.0731. Rf (petroleum ether/ethyl acetate = 5/5) 0.46.

2.1.1.19. 4-(2-(2-Chloroethoxy)ethoxy)-3-ethoxybenzaldehyde ***(2s)*** was obtained from 3-ethoxy 4-hydroxybenzaldehyde (**1f**) and bis(2-chloroethyl)ether as a fine white needle crystals in 83% yield, m.p. 64-66 °C.^{1}H NMR (250 MHz, DMSO-d_6) δ = 1.35 (t, *J* = 6.9 Hz, 3H), 3.68 -3.81 (m, 4H), 3.81 - 3.88 (m, 2H), 4.10 (q, *J* = 6.9 Hz, 2H), 4.17 -4.27 (m, 2H), 7.19 (d, *J* = 8.3 Hz, 1H), 7.39 (d, *J* = 1.9 Hz, 1H), 7.52 (dd, *J* = 8.3 Hz, 1.9 Hz, 1H), 9.83 (s, 1H). ^{13}C NMR (101 MHz, DMSO-d_6) δ = 14.6 (CH_3), 43.5 (CH_2), 63.9 (CH_2), 68.3 (CH_2), 68.6 (CH_2), 70.8 (CH_2), 111.2 (CH_{Ar}), 112.6 (CH_{Ar}), 125.7 (CH_{Ar}), 129.8 (C_q), 148.5 (C_q), 153.6 (C_q), 191.4 (C = O). HRMS (EI-MS) *m/z* calcd for $C_{13}H_{17}ClO_4$: 272.0815 $[M-H]^+$, found: 272.0889. Rf (petroleum ether/ethyl acetate = 4/6) 0.66.

2.1.2. General procedure for the synthesis of the nitrate ester benzaldehyde derivatives ***(3a-s)***

To a solution of the appropriate halide derivative, **2a-s** (1.0 Eq.), in acetonitrile (50 mL), silver nitrate (1.5 Eq.) was added and the mixture was stirred under reflux and darkness for approximately 12 h, according to the method reported in the literature [65–67], which was adapted to our synthesis in terms of the ratio of reagents, solvent, time of reaction, purification method. Then brine was added to precipitate the excess of silver nitrate. After filtration, the mixture was extracted twice with diethyl ether (50 mL). The combined organic layers were washed with water (50 mL) and brine (50 mL), dried over anhydrous magnesium sulfate, filtered

and concentrated under reduced pressure. The crude products were purified by flash chromatography (silicagel, petroleum ether/ethyl acetate) to give the pure products (**3a-s**).

2.1.2.1. 2-(4-Formylphenoxy)ethyl nitrate ***(3a)*** was obtained from 4-(2-bromoethoxy) benzaldehyde (**2a)** as yellow oil in 95% yield. ^{1}H NMR (400 MHz, DMSO-d_6) δ = 4.39 - 4.50 (m, 2H), 4.88 - 4.95 (m, 2H), 7.11 - 7.20 (m, 2H), 7.84 - 7.93 (m, 2H), 9.88 (s, 1H). ^{13}C NMR (101 MHz, DMSO-d_6) δ = 64.5 (CH_2), 71.7 (CH_2), 115.0 ($2CH_{Ar}$), 130.1 (C_q), 131.8 ($2CH_{Ar}$), 162.7 (C_q), 191.3(C = O). HRMS (EI-MS) *m/z* calcd for $C_9H_9NO_5$: 211.0481 $[M-H]^+$, found: 211.0554. Rf (petroleum ether/ethyl acetate = 6/4) 0.42.

2.1.2.2. 2-(2-Fluoro-4-formylphenoxy)ethyl nitrate ***(3b)*** was obtained from 4-(2-bromoethoxy)-3-fluorobenzaldehyde (**2b)** as borrow oil in 99% yield. ^{1}H NMR (400 MHz, DMSO-d_6) δ = 4.46 - 4.61 (m, 2H), 4.86 - 5.03 (m, 2H), 7.43 (t, *J* = 8.3 Hz, 1H), 7.71 (dd, *J* = 11.3 Hz, 1.9 Hz, 1H), 7.78 (ddd, *J* = 8.3 Hz, 1.9 Hz, 1.0 Hz, 1H), 9.87 (d, *J* = 2.1 Hz, 1H). ^{13}C NMR (101 MHz, DMSO-d_6) δ = 65.6 (CH_2), 71.5 (CH_2), 114.8 (d, *J* = 1.6 Hz, CH_{Ar}), 115.4 (d, *J* = 18.2 Hz, CH_{Ar}), 128.2 (d, *J* = 3.2 Hz, CH_{Ar}), 130.2 (d, *J* = 5.0 Hz, C_q), 151.0 (d, *J* = 10.7 Hz, C_q), 151.6 (d, *J* = 247.4 Hz, C_qF), 190.8 (d, *J* = 2.1 Hz, C =O). ^{19}F NMR (376 MHz, DMSO-d_6) δ = -133.32 (ddd, *J* = 10.9 Hz, 8.3 Hz, 2.1 Hz). HRMS (EI-MS) *m/z* calcd for $C_9H_8FNO_5$: 229.0387 $[M-H]^+$, found: 229.0459. Rf (petroleum ether/ethyl acetate = 5/5) 0.45.

2.1.2.3. *2-(2-Chloro-4-formylphenoxy)ethyl nitrate* **(3c)** was obtained from 4-(2-bromoethoxy)-3-chlorobenzaldehyde (**2c)** as pale yellow solid in 85% yield, m.p. 58-60 °C. ^{1}H NMR (400 MHz, DMSO-d_6) δ = 4.51 - 4.58 (m, 2H), 4.91 - 5.00 (m, 2H), 7.40 (d, *J* = 8.5 Hz, 1H), 7.89 (dd, *J* = 8.5Hz, 2.0 Hz, 1H), 7.96 (d, *J* = 2.0 Hz, 1H), 9.87 (s, 1H). ^{13}C NMR (101 MHz, DMSO-d_6) δ = 65.8 (CH_2), 71.3 (CH_2), 113.9 (CH_{Ar}), 122.3 (C_q), 130.5 (C_q), 130.6 (CH_{Ar}), 130.7 (CH_{Ar}), 157.8 (C_q), 190.7 (C = O). HRMS (EI-MS) *m/z* calcd for $C_9H_8ClNO_5$: 245.0091 $[M-H]^+$, found: 245.0162. Rf (petroleum ether/ethyl acetate = 4/6) 0.68.

2.1.2.4. 2-(2-Bromo-4-formylphenoxy)ethyl nitrate ***(3d)*** was obtained from 3-bromo-4-(2-bromo-ethoxy)benzaldehyde (**2d**) as yellow oil in 85% yield ^{1}H NMR (400 MHz, DMSO-d_6) δ = 4.50 - 4.57 (m, 2H), 4.90 - 5.00 (m, 2H), 7.35 (d, *J* = 8.6 Hz, 1H), 7.92 (dd, *J* = 8.5 Hz, 2.0 Hz, 1H), 8.10 (d, *J* = 2.0 Hz, 1H), 9.86 (s, 1H). ^{13}C NMR (101 MHz, DMSO-d_6) δ = 65.9 (CH_2), 71.3 (CH_2), 111.6 (C_q), 113.8 (CH_{Ar}), 130.9 (C_q), 131.0 (CH_{Ar}), 134.0 (CH_{Ar}), 158.7 (C_q), 190.5 (C =

O). HRMS (EI-MS) *m/z* calcd for $C_9H_8BrNO_5$: 288.9586 $[M-H]^+$, found: 288.9657. Rf (petroleum ether/ethyl acetate = 7/3) 0.23.

2.1.2.5. 2-(4-Formyl-2-methoxyphenoxy)ethyl nitrate ***(3e)*** was obtained from 4-(2-bromoethoxy)-3-methoxybenzaldehyde (**2e**) as yellow oil in 99% yield. ^{1}H NMR (400 MHz, DMSO-d_6) δ = 3.84 (s, 3H), 4.39 - 4.46 (m, 2H), 4.88 - 4.95 (m, 2H), 7.22 (d, *J* = 8.3 Hz, 1H), 7.42 (d, *J* = 1.9 Hz, 1H), 7.55 (dd, *J* = 8.3 Hz, 1.9 Hz, 1H), 9.85 (s, 1H). ^{13}C NMR (101 MHz, DMSO-d_6) δ = 55.6 (CH_3), 65.0 (CH_2), 71.7 (CH_2), 109.9 (CH_{Ar}), 112.5 (CH_{Ar}), 125.8 (CH_{Ar}), 130.2 (C_q), 149.2 (C_q), 152.6 (C_q), 191.5 (C = O). HRMS (EI-MS) *m/z* calcd for $C_{10}H_{11}NO_6$: 241.0586 $[M-H]^+$, found: 241.0659. Rf (petroleum ether/ethyl acetate = 6/4) 0.43.

2.1.2.6. 2-(2-Ethoxy-4-formylphenoxy)ethyl nitrate ***(3f)*** was obtained from 4-(2-bromoethoxy)-3-ethoxybenzaldehyde (**2f**) as yellow oil in 92% yield ^{1}H NMR (400 MHz, DMSO-d_6) δ =1.34 (t, *J* = 6.9 Hz, 3H), 4.09 (q, *J* = 6.9 Hz, 2H), 4.39 - 4.46 (m, 2H), 4.89 - 4.96 (m, 2H), 7.21 (d, *J* = 8.3 Hz, 1H), 7.40 (d, *J* = 1.9 Hz, 1H), 7.53 (dd, *J* = 8.2 Hz, 1.9 Hz, 1H), 9.84 (s, 1H). ^{13}C NMR (101 MHz, DMSO-d_6) δ = 14.5 (CH_3), 64.0 (CH_2), 65.2 (CH_2), 71.6 (CH_2), 111.4 (CH_{Ar}), 113.1 (CH_{Ar}), 125.5 (CH_{Ar}), 130.3 (C_q), 148.5 (C_q), 152.8 (C_q), 191.4 (C = O). HRMS (EI-MS) *m/z* calcd for $C_{11}H_{13}NO_6$: 255.0743 $[M-H]^+$, found: 255.0816. Rf (petroleum ether/ethyl acetate = 6/4) 0.52.

2.1.2.7. *2-(4-Formyl-2-nitrophenoxy)ethyl nitrate* **(3g)** was obtained from 4-(2-bromoethoxy)-3-nitrobenzaldehyde (**2g**) as pale yellow solid in 60% yield, m.p. 55-57 °C. ^{1}H NMR (400 MHz, DMSO-d_6) δ = 4.59 - 4.70 (m, 2H), 4.89 - 5.00 (m, 2H), 7.61 (d, *J* = 8.7 Hz, 1H), 8.19 (dd, *J* = 8.7 Hz, 2.0 Hz, 1H), 8.43 (d, *J* = 2.0 Hz, 1H), 9.96 (s, 1H). ^{13}C NMR (101 MHz, DMSO-d_6) δ = 66.6 (CH_2), 71.1 (CH_2), 115.8 (CH_{Ar}), 126.4 (CH_{Ar}), 129.2 (C_q), 134.9 (CH_{Ar}), 139.6 (C_q), 154.7 (C_q), 190.4 (C = O). HRMS (EI-MS) *m/z* calcd for $C_9H_8N_2O_7$: 256.0332 $[M-H]^+$, found: 256.0404. Rf (petroleum ether/ethyl acetate = 3/7) 0.57.

2.1.2.8. 2-(4-Formyl-2,6-dimethoxyphenoxy)ethyl nitrate ***(3h)*** was obtained from 4-(2-bromo-ethoxy)-3,5-dimethoxybenzaldehyde (**2h**) as pale yellow solid in 92% yield, m.p. 52-54 °C. ^{1}H NMR (400 MHz, DMSO-d_6) δ = 3.85 (s, 6H), 4.18 - 4.35 (m, 2H), 4.70 - 4.87 (m, 2H), 7.26 (s, 2H), 9.89 (s, 1H). ^{13}C NMR (101 MHz, DMSO-d_6) δ = 56.1 ($2CH_3$), 68.7 (CH_2), 72.8 (CH_2), 106.6 ($2CH_{Ar}$), 132.1(C_q), 141.0 (C_q), 153.3 ($2C_q$), 191.9 (C = O). HRMS (EI-MS) *m/z* calcd for $C_{11}H_{13}NO_7$: 271.0692 $[M-H]^+$, found: 271.0765. Rf (petroleum ether/ethyl acetate = 2/8) 0.20.

2.1.2.9. 2-(2,6-Dichloro-4-formylphenoxy)ethyl nitrate ***(3i)*** was obtained from 4-(2-bromoethoxy)-3,5-dichlorobenzaldehyde (**2i**) as white solid in 54% yield, m.p. 49-51 °C. ^{1}H NMR (250 MHz, DMSO-d_6) δ = 4.33 - 4.55 (m, 2H), 4.79 - 5.04 (m, 2H), 8.02 (s, 2H), 9.91 (s, 1H). ^{13}C NMR (101 MHz, DMSO-d_6) δ = 68.5 (CH_2), 72.4 (CH_2), 129.4 ($2C_q$), 130.0 ($2CH_{Ar}$), 133.6 (C_q), 154.7 (C_q), 190.2 (C = O). HRMS (EI-MS) *m/z* calcd for $C_9H_7Cl_2NO_5$: 278.9701 $[M-H]^+$, found: 278.9775. Rf (petroleum ether/ethyl acetate = 8/2) 0.52.

2.1.2.10. 2-(2-Chloro-4-formyl-6-methoxyphenoxy)ethyl nitrate ***(3j)*** was obtained from 4-(2-bromoethoxy)-3-chloro-5-methoxybenzaldehyde (**2j**) as borrow oil in 98% yield. ^{1}H NMR (400 MHz, DMSO-d_6) δ = 3.91 (s, 3H), 4.33 - 4.45 (m, 2H), 4.79 - 4.90 (m, 2H), 7.52 (d, *J* = 1.8 Hz, 1H), 7.64 (d, *J* = 1.8 Hz, 1H), 9.89 (s, 1H). ^{13}C NMR (101 MHz, DMSO-d_6) δ = 56.4 (CH_3), 69.2 (CH_2), 72.7 (CH_2), 111.1 (CH_{Ar}), 124.0 (CH_{Ar}), 127.6 (C_q), 132.8 (C_q), 148.0 (C_q), 153.6 (C_q), 191.0 (C = O). HRMS (EI-MS) *m/z* calcd for $C_{10}H_{10}ClNO_6$: 275.0197 $[M-H]^+$, found: 275.0270. Rf (petroleum ether/ethyl acetate = 6/4) 0.55.

2.1.2.11. 2-(3-Formylphenoxy)ethyl nitrate ***(3k)*** was obtained from 3-(2-bromoethoxy) benzaldehyde (**2k**) as yellow oil in 86% yield. ^{1}H NMR (400 MHz, DMSO-d_6) δ = 4.33 - 4.44 (m, 2H), 4.86 - 4.95 (m, 2H), 7.25 - 7.35 (m, 1H), 7.39 - 7.49 (m, 1H), 7.48 - 7.61 (m, 2H), 9.97 (s, 1H). ^{13}C NMR (101 MHz, DMSO-d_6) δ = 64.3 (CH_2), 71.8 (CH_2), 113.8 (CH_{Ar}), 121.4 (CH_{Ar}), 122.9 (CH_{Ar}), 130.4 (CH_{Ar}), 137.7 (C_q), 158.4 (C_q), 192.8 (C = O). HRMS (EI-MS) *m/z* calcd for $C_9H_9NO_5$: 211.0481 $[M-H]^+$, found: 211.0554. Rf (petroleum ether/ethyl acetate = 8/2) 0.38.

2.1.2.12. 2-(5-Formyl-2-methoxyphenoxy)ethyl nitrate ***(3l)*** was obtained from 3-(2-bromoethoxy)-4-methoxybenzaldehyde (**2l**) as pale yellow solid in 87% yield, m.p. 50-52 °C. ^{1}H NMR (400 MHz, DMSO-d_6) δ = 3.88 (s, 3H), 4.34 - 4.41 (m, 2H), 4.87 - 4.94 (m, 2H), 7.20 (d, *J* = 8.3 Hz, 1H), 7.44 (d, *J* = 1.9 Hz, 1H), 7.60 (dd, *J* = 8.3 Hz, 1.9 Hz, 1H), 9.84 (s, 1H). ^{13}C NMR (101 MHz, DMSO-d_6) δ = 56.0 (CH_3), 65.0 (CH_2), 71.8 (CH_2), 111.5 (CH_{Ar}), 111.7 (CH_{Ar}), 126.6 (CH_{Ar}), 129.6 (C_q), 147.6 (C_q), 154.4 (C_q), 191.3 (C = O). HRMS (EI-MS) *m/z* calcd for $C_{10}H_{11}NO_6$: 241.0586 $[M-H]^+$, found: 241.0660. Rf (petroleum ether/ethyl acetate = 7/3) 0.35.

2.1.2.13. 2-(5-Formyl-2-nitrophenoxy)ethyl nitrate ***(3m)*** was obtained from 3-(2-bromoethoxy)-4-nitrobenzaldehyde (**2m**) as orange solid in 99% yield, m.p. 56-58 °C. ^{1}H NMR (400 MHz, DMSO-d_6) δ = 4.58 - 4.65 (m, 2H), 4.89 - 4.96 (m, 2H), 7.70 (dd, *J* = 8.2 Hz, 1.2 Hz, 1H), 7.87

(d, *J* = 1.3 Hz, 1H), 8.08 (d, *J* = 8.2 Hz, 1H), 10.07 (s, 1H). ^{13}C NMR (101 MHz, DMSO-d_6) δ = 66.3 (CH_2), 71.2 (CH_2), 115.3 (CH_{Ar}), 122.4 (CH_{Ar}), 125.5 (CH_{Ar}), 139.5 (C_q), 143.0 (C_q), 150.5 (C_q), 192.0 (C = O). HRMS (EI-MS) *m/z* calcd for $C_9H_8N_2O_7$: 256.0332 $[M-H]^+$, found: 256.0406. Rf (petroleum ether/ethyl acetate = 5/5) 0.58.

2.1.2.14. 2-(3-formyl-4-nitrophenoxy)ethyl nitrate ***(3n)*** was obtained from 5-(2-bromoethoxy)-2-nitrobenzaldehyde (**2n**) as brown solid in 99% yield, m.p. 52-54 °C. ^{1}H NMR (400 MHz, DMSO-d_6) δ = 4.46 - 4.62 (m, 2H), 4.85 - 5.01 (m, 2H), 7.30 (d, *J* = 2.9 Hz, 1H), 7.40 (dd, *J* = 9.0 Hz, 2.9 Hz, 1H), 8.19 (d, *J* = 9.0 Hz, 1H), 10.29 (s, 1H). ^{13}C NMR (101 MHz, DMSO-d_6) δ = 65.4 (CH_2), 71.5 (CH_2), 114.2 (CH_{Ar}), 118.8 (CH_{Ar}), 127.2 (CH_{Ar}), 134.2 (C_q), 142.2 (C_q), 162.0 (C_q), 189.8 (C = O). HRMS (EI-MS) *m/z* calcd for $C_9H_8N_2O_7$: 256.0332 $[M-H]^+$, found: 256.0404. Rf (petroleum ether/ethyl acetate = 7/3) 0.40.

2.1.2.15. 2-(2-Bromo-3-formyl-6-methoxyphenoxy)ethyl nitrate ***(3o)*** was obtained from 2-bromo-3-(2-bromoethoxy)-4-methoxybenzaldehyde (**2o**) as brown solid in 99% yield, m.p. 66-68 °C. ^{1}H NMR (400 MHz, DMSO-d_6) δ = 3.93 (s, 3H), 4.25 - 4.34 (m, 2H), 4.80 - 4.92 (m, 2H), 7.29 (dd, *J* = 8.7 Hz, 0.7 Hz, 1H), 7.69 (d, *J* = 8.7 Hz, 1H), 10.10 (d, *J* = 0.7 Hz, 1H). ^{13}C NMR (101 MHz, DMSO-d_6) δ = 56.7 (CH_3), 68.8 (CH_2), 72.7 (CH_2), 112.2 (CH_{Ar}), 121.3 (C_q), 126.7 (C_q), 127.1 (CH_{Ar}), 144.3 (C_q), 158.1 (C_q), 190.3 (C = O). HRMS (EI-MS) *m/z* calcd for $C_{10}H_{10}BrNO_6$: 318.9691 $[M-H]^+$, found: 318.9765. Rf (petroleum ether/ethyl acetate = 7/3) 0.38.

2.1.2.16. 2-(2-Formylphenoxy)ethyl nitrate ***(3p)*** was obtained from 2-(2-bromoethoxy) benzaldehyde (**2p**) as yellow oil in 83% yield. ^{1}H NMR (250 MHz, DMSO-d_6) δ = 4.40 - 4.54 (m, 2H), 4.92 - 5.05 (m, 2H), 7.09 (tt, *J* = 7.5 Hz, 0.9 Hz, 1H), 7.18 - 7.30 (m, 1H), 7.58 - 7.66 (m, 1H), 7.66 - 7.76 (m, 1H), 10.36 (d, *J* = 0.8 Hz, 1H). ^{13}C NMR (101 MHz, DMSO-d_6) δ = 66.5 (CH_2), 71.3 (CH_2), 114.1 (CH_{Ar}), 121.3 (CH_{Ar}), 124.5 (C_q), 127.4 (CH_{Ar}), 136.4 (CH_{AR}), 160.4 (C_q), 189.1 (C = O).HRMS (EI-MS) *m/z* calcd for $C_9H_9NO_5$: 211.0481 $[M-H]^+$, found: 211.0551. Rf (petroleum ether/ethyl acetate = 8/2) 0.21.

2.1.2.17. 2-(2-(4-Formylphenoxy)ethoxy)ethyl nitrate ***(3q)*** was obtained from 4-(2-(2-chloro-ethoxy)ethoxy)benzaldehyde (**2q**) as yellow needle-shaped crystals in 86% yield, m.p. 51-53 °C. ^{1}H NMR (400 MHz, DMSO-d_6) δ = 3.69 - 3.89 (m, 4H), 4.13 - 4.28 (m, 2H), 4.60 - 4.76 (m, 2H), 7.08 - 7.18 (m, 2H), 7.79 - 7.93 (m, 2H), 9.87 (s, 1H). ^{13}C NMR (101 MHz, DMSO-d_6) δ = 66.6 (CH_2), 67.6 (CH_2), 68.7 (CH_2), 72.9 (CH_2), 115.0 ($2CH_{Ar}$), 129.7 (C_q), 131.8 ($2CH_{Ar}$),

163.4(C_q), 191.3 (C = O). HRMS (EI-MS) *m/z* calcd for $C_{11}H_{13}NO_6$: 255.0743 $[M-H]^+$, found: 255.0817. Rf (petroleum ether/ethyl acetate = 4/6) 0.58.

2.1.2.18. 2-(2-(4-Formyl-2-methoxyphenoxy)ethoxy)ethyl nitrate ***(3r)*** was obtained from 4-(2-(2-chloroethoxy)ethoxy)-3-methoxybenzaldehyde (**2r**) as brown oil in 86% yield. ^{1}H NMR (400 MHz, DMSO-d_6) δ = 3.71 - 3.87 (m, 7H), 4.15 - 4.27 (m, 2H), 4.63 - 4.74 (m, 2H), 7.18 (d, *J* = 8.3 Hz, 1H), 7.40 (d, *J* = 1.9 Hz, 1H), 7.53 (dd, *J* = 8.3 Hz, 1.9 Hz, 1H), 9.84 (s, 1H). ^{13}C NMR (101 MHz, DMSO-d_6) δ = 55.5 (CH_3), 66.6 (CH_2), 68.0 (CH_2), 68.7 (CH_2), 72.9 (CH_2), 109.7 (CH_{Ar}), 112.2 (CH_{Ar}), 125.9 (CH_{Ar}), 129.8 (C_q), 149.2 (C_q), 153.3 (C_q), 191.3 (C = O). HRMS (EI-MS) *m/z* calcd for $C_{12}H_{15}NO_7$: 285.0849 $[M-H]^+$, found: 285.0918. Rf (petroleum ether/ethyl acetate = 4/6) 0.59.

2.1.2.19. 2-(2-(2-Ethoxy-4-formylphenoxy)ethoxy)ethyl nitrate ***(3s)*** was obtained from 4-(2-(2-chloroethoxy)ethoxy)-3-ethoxybenzaldehyde (**2s**) as brown solid in 60% yield, m.p. 55-57 °C. ^{1}H NMR (400 MHz, DMSO-d_6) δ = 1.35 (t, *J* = 6.9 Hz, 3H), 3.77 - 3.88 (m, 4H), 4.10 (q, *J* = 6.9 Hz, 2H), 4.16 -4.28 (m, 2H), 4.63 - 4.74 (m, 2H), 7.18 (d, *J* = 8.2 Hz, 1H), 7.39 (d, *J* = 1.9 Hz, 1H), 7.52 (dd, *J* = 8.2 Hz, 1.9 Hz, 1H), 9.83 (s, 1H). ^{13}C NMR (101 MHz, DMSO-d_6) δ = 14.5 (CH_3), 63.9 (CH_2), 66.7 (CH_2), 68.2 (CH_2), 68.7 (CH_2), 72.9 (CH_2), 111.2 (CH_{Ar}), 112.6 (CH_{Ar}), 125.7 (CH_{Ar}), 129.8 (C_q), 148.4 (C_q), 153.5 (C_q), 191.4 (C = O). HRMS (EI-MS) *m/z* calcd for $C_{13}H_{17}NO_7$: 299.1005 $[M-H]^+$, found: 299.1083. Rf (petroleum ether/ethyl acetate = 4/6) 0.62.

*2.1.3. Synthesis of 2-(1-(4-chlorobenzoyl)-5-methoxy-2-methyl-1H-indol-3-yl)acetohydrazide (****4****)*

To a suspension of indomethacin (1.0 Eq., 45.5 mmol) in acetonitrile (300 mL), hydroxybenzotriazole (HOBt, 1.1 Eq., 54.6 mmol) and 1-ethyl-3-(3-dimethylaminopropyl) carbodiimide (EDC, 1.0 Eq., 54.6 mmol) were added and the mixture was stirred at room temperature for 3h, according to the method reported in the literature [68,69], which was adapted to our synthesis in terms of the ratio of reagents, solvent, time of reaction, purification method. The resulting mixture was then slowly added drop wise, at 0-5°C, to a solution of hydrazine (2.0 Eq., 91mmol) and cyclohexene (1 mL) in acetonitrile (200 mL). The mixture was kept at this temperature for 1 h and then was diluted with distilled water (500 mL), when a precipitated is formed, which was collected by filtration. The indomethacin hydrazide was obtained in 95% yield, m.p. 202-204 °C. ^{1}H NMR (400 MHz, DMSO-d_6) δ = 2.26 (s, 3H), 3.46 (s, 2H), 3.78 (s,

3H), 4.25 (s, 2H), 6.71 (dd, *J* = 9.0Hz, 2.5 Hz, 1H), 6.92 (d, *J* = 9.0 Hz, 1H), 7.16 (d, *J* = 2.5 Hz, 1H), 7.61 - 7.75 (m, 4H), 9.22 (s, 1H). ^{13}C NMR (101 MHz, DMSO-d_6) δ = 13.3 (CH_3), 29.3(CH_2), 55.4(CH_3), 102.1 (CH_{Ar}), 111.1 (CH_{Ar}), 114.0 (C_q), 114.5 (CH_{Ar}), 129.0 ($2CH_{Ar}$), 130.2 (C_q), 130.8 (C_q), 131.1 ($2CH_{Ar}$), 134.2 (C_q), 135.2 (C_q), 137.5(C_q), 155.5 (C_q), 167.8 (C_q), 168.8 (C_q). HRMS (EI-MS) *m/z* calcd for $C_{19}H_{18}ClN_3O_3$: 371.1037 $[M-H]^+$, found: 371.1106.Rf (dichloromethane/methanol = 9.6/0.4) 0.57.

*2.1.4. General procedure for the synthesis of the indomethacin hydrazone derivatives (**5a–s**)*

To a suspension of indomethacin hydrazide (**4**, 1.0 Eq.) in absolute ethanol, the corresponding nitrate ester benzaldehyde (**3a-s**) (1.1 Eq.) was added in presence of catalytic amount of hydrochloric acid. The mixture was stirred for 12 h under reflux when an extensive precipitated was formed. After cooling at room temperature, the precipitate was collected by filtration, washed with cold water (80 mL), ethyl ether (30 mL), dried over anhydrous magnesium sulfate, filtered and concentrated under reduced pressure. The corresponding indomethacin hydrazone derivatives (**5a**-**e**) were obtained in near quantitative yields (90–98%) and were used without isolation for the final step of synthesis.

*2.1.5. General procedure for the synthesis of the nitric oxide-releasing indomethacin derivatives with 1,3-thiazolidine-4-one scaffold (**6a-s**)*

To a suspension of indomethacin hydrazone derivatives (**5a-s**) (1.0 Eq.) in dry toluene (80 mL), mercaptoacetic acid (1.5 Eq.) was added in presence of few amount of anhydrous magnesium sulfate (2-3 g), using a Dean Stark equipment and applying a modified method [49,70,71]. The mixture was stirred for 14 h at 110°C, after that was cooled at room temperature and the solvent was removed under reduced pressure. The residue was taken up with ethyl acetate (30 mL), filtered and the filtrate was successively washed with a diluted aqueous solution of sodium bicarbonate (20 mL), water and finally with brine. The combined organic layers were dried over anhydrous magnesium sulfate and solvent was removed under reduced pressure to get a crude product that was purified by column chromatography (silicagel, petroleum ether/ethyl acetate or acetonitrile/toluene) to give the pure products (**6a-s**).

*2.1.5.1. 2-(4-(3-(2-(1-(4-Chlorobenzoyl)-5-methoxy-2-methyl-1H-indol-3-yl)acetamido)-4-oxo-thiazolidin-2-yl)phenoxy)ethyl nitrate (**6a**)* was obtained from *2*-(4-((2-(2-(1-(4-chlorobenzoyl)-5-methoxy-2-methyl-1*H*-indol-3-yl)acetyl)hydrazineylidene)methyl)phenoxy)ethyl nitrate **(5a)**

as pale yellow solid in 56% yield, m.p. 169-171 °C. ^{1}H NMR (250 MHz, DMSO-d_6) δ = 2.10 (s, 3H), 3.49 (s, 2H), 3.70 (s, 3H), 3.70 (d, *J* = 15.9 Hz, 1H), 3.86 (dd, *J* = 15.9 Hz, 1.7, 1H), 4.22 - 4.34 (m, 2H), 4.83 - 4.94 (m, 2H), 5.71 (s, 1H), 6.68 (dd, *J* = 9.0 Hz, 2.5 Hz, 1H), 6.88 (d, *J* = 8.7 Hz, 2H), 6.94 (d, *J* = 9.0 Hz, 1H), 7.00 (d, *J* = 2.5 Hz, 1H), 7.28 (d, *J* = 8.7 Hz, 2H), 7.65 (s, 4H), 10.35 (s, 1H). ^{13}C NMR (101 MHz, DMSO-d_6) δ = 13.2 (CH_3), 28.7 (CH_2), 29.2 (CH_2), 55.3 (CH_3), 61.1 (CH), 64.1 (CH_2), 71.9 (CH_2), 101.6 (CH_{AR}), 111.6 (CH_{Ar}), 113.2 (C_q), 114.4 ($3CH_{Ar}$), 129.0 ($2CH_{Ar}$), 129.2 ($2CH_{Ar}$), 130.1 (C_q), 130.4 (C_q), 130.5 (C_q), 131.1 ($2CH_{Ar}$), 134.2 (C_q), 135.2 (C_q), 137.6 (C_q), 155.5 (C_q), 158.3 (C_q), 167.8 (C_q), 168.4 (C_q), 168.7 (C_q). HRMS (EI-MS) *m/z* calcd for $C_{30}H_{27}ClN_4O_8S$: 638.1238, $[M-H]^+$ found: 638.1299. Rf (petroleum ether/ethyl acetate = 2/8) 0.46.

2.1.5.2. *2-(4-(3-(2-(1-(4-Chlorobenzoyl)-5-methoxy-2-methyl-1H-indol-3-yl)acetamido)-4-oxo-thiazolidin-2-yl)-2-fluorophenoxy)ethyl nitrate* **(6b)** was obtained from 2-(4-((2-(2-(1-(4-chlorobenzoyl)-5-methoxy-2-methyl-1*H*-indol-3-yl)acetyl)hydrazineylidene)methyl)-2-fluoro-phenoxy)ethyl nitrate **(5b)** as pale yellow solid in 45% yield, m.p. 154-156 °C. ^{1}H NMR (400 MHz, DMSO-d_6) δ = 2.12 (s, 3H), 3.50 (s, 2H), 3.70 (s, 3H), 3.70 (d, *J* = 15.8 Hz, 1H), 3.90 (dd, *J* = 15.8 Hz, 1.8 Hz, 1H), 4.28 - 4.43 (m, 2H), 4.80 - 5.00 (m, 2H), 5.72 (s, 1H), 6.67 (dd, *J* = 9.0 Hz, 2.5 Hz, 1H), 6.92 (d, *J* = 9.0 Hz, 1H), 6.98 (d, *J* = 2.5 Hz, 1H), 7.00 - 7.10 (m, 2H), 7.29 (dd, *J* = 12.2 Hz, 1.8 Hz, 1H), 7.65 (s, 4H), 10.38 (s, 1H). ^{19}F NMR (376 MHz, DMSO-d_6) δ = 133.67 (dd, *J* = 12.1 Hz, 7.4 Hz). ^{13}C NMR (101 MHz, DMSO-d_6) δ = 13.2 (CH_3), 28.7 (CH_2), 29.1 (CH_2), 55.3 (CH_3), 60.6 (CH), 65.3 (CH_2), 71.7 (CH_2), 101.5 (CH_{Ar}), 111.5 (CH_{Ar}), 113.1 (C_q), 114.4 (C_q), 114.5 (CH_{Ar}), 115.2 (d, *J* =19.1 Hz, CH_{Ar}), 124.3 (d, *J* =3.3 Hz, CH_{Ar}), 129.0 ($2CH_{Ar}$) , 130.1 (C_q), 130.5 (C_q), 131.1 ($2CH_{Ar}$), 131.9 (d, *J* =5.9 Hz, C_q), 134.1 (C_q), 135.3 (C_q), 137.6 (C_q), 146.1 (d, *J* =10.7 Hz, C_q), 151.4 (d, *J* =244.9 Hz, C_qF), 155.5 (C_q), 167.8 (C_q), 168.4 (C_q), 168.7 (C_q). ^{19}F NMR (376 MHz, DMSO-d_6) δ = -133.67 (dd, *J* =12.1 Hz, 7.4 Hz). HRMS (EI-MS) *m/z* calcd for $C_{30}H_{26}ClFN_4O_8S$: 656.1144, $[M-H]^+$ found: 656.1206. Rf (petroleum ether/ethyl acetate = 2/8) 0.54.

2.1.5.3. *2-(2-Chloro-4-(3-(2-(1-(4-chlorobenzoyl)-5-methoxy-2-methyl-1H-indol-3-yl)acetamido) -4-oxothiazolidin-2-yl)phenoxy)ethyl nitrate* **(6c)** was obtained from 2-(2-chloro-4-((2-(2-(1-(4-chlorobenzoyl)-5-methoxy-2-methyl-1*H*-indol-3-yl)acetyl)hydrazineylidene)methyl)phenoxy) ethyl nitrate **(5c)** as pale yellow solid in 40% yield, m.p. 137-139 °C. ^{1}H NMR (250 MHz, DMSO-d_6) δ = 2.12 (s, 3H), 3.51 (s, 2H), 3.69 (s, 3H), 3.70 (dd, *J* = 15.9 Hz, 0.8 Hz, 1H), 3.91

(dd, *J* = 15.9 Hz, 1.8 Hz, 1H), 4.28 - 4.45 (m, 2H), 4.79 - 5.02 (m, 2H), 5.72 (s, 1H), 6.67 (dd, *J* = 9.0 Hz, 2.5 Hz, 1H), 6.94 (d, *J* = 9.0 Hz, 0.4 Hz, 1H), 6.99 (d, *J* = 2.5 Hz, 1H), 7.03 (d, *J* = 8.6 Hz, 1H), 7.23 (dd, *J* = 8.6 Hz, 2.2 Hz, 1H), 7.49 (d, *J* = 2.2 Hz, 1H), 7.65 (s, 4H), 10.40 (s, 1H). ^{13}C NMR (101 MHz, DMSO-d_6) δ =13.7 (CH_3) , 29.2 (CH_2), 29.6 (CH_2), 55.8 (CH_3), 61.0 (CH), 65.9 (CH_2), 72.0 (CH_2), 102.0 (CH_{Ar}), 112.0 (CH_{Ar}), 113.6 (C_q), 114.0 (CH_{Ar}), 114.9 (CH_{Ar}), 122.0 (C_q), 128.4 (CH_{Ar}), 129.5 ($2CH_{Ar}$), 129.6 (CH_{Ar}), 130.6 (C_q), 130.9 (C_q), 131.6 ($2CH_{Ar}$), 132.6 (C_q), 134.6 (C_q), 135.7 (C_q), 138.1 (C_q), 154.0 (C_q), 156.0 (C_q), 168.3 (C_q), 169.0 (C_q), 169.1 (C_q). HRMS (EI-MS) *m/z* calcd for $C_{30}H_{26}Cl_2N_4O_8S$: 672.0848, $[M-H]^+$ found: 672.0914. Rf (toluene/acetonitrile = 6/4) 0.60.

2.1.5.4. *2-(2-Bromo-4-(3-(2-(1-(4-chlorobenzoyl)-5-methoxy-2-methyl-1H-indol-3-yl)acetamido) -4-oxothiazolidin-2-yl)phenoxy)ethyl nitrate* **(6d)** was obtained from 2-(2-bromo-4-((2-(2-(1-(4-chlorobenzoyl)-5-methoxy-2-methyl-1*H*-indol-3-yl)acetyl)hydrazineylidene)methyl)phenoxy) ethyl nitrate **(5d)** as pale yellow solid in 38% yield, m.p. 167-169 °C. ^{1}H NMR (400 MHz, DMSO-d_6) δ = 2.11 (s, 3H), 3.50 (s, 2H), 3.69 (s, 3H), 3.70 (d, *J* = 15.9 Hz, 1H), 3.91 (dd, *J* = 15.9 Hz, 1.8 Hz, 1H), 4.27 - 4.42 (m, 2H), 4.81 - 5.00 (m, 2H), 5.72 (s, 1H), 6.67 (dd, *J* = 9.0 Hz, 2.6 Hz, 1H), 6.94 (d, *J* = 9.0 Hz, 1H), 6.98 (s, 1H), 7.00 (d, *J* = 6.2 Hz, 1H), 7.27 (dd, *J* = 8.6 Hz, 2.2 Hz, 1H), 7.63 (d, *J* = 2.2 Hz, 1H), 7.59 - 7.71 (m, 4H), 10.40 (s, 1H). ^{13}C NMR (101 MHz, DMSO-d_6) δ = 13.2 (CH_3), 28.7 (CH_2), 29.2 (CH_2), 55.3 (CH_3), 60.4 (CH), 65.5 (CH_2), 71.5 (CH_2), 101.5 (CH_{Ar}), 111.1 (CH_{Ar}), 111.61 (CH_{Ar}), 113.12 (C_q), 113.3 (CH_{Ar}), 114.4 (C_q), 128.6 (CH_{Ar}), 129.0 ($2CH_{Ar}$), 130.08 (CH_{Ar}), 130.5 (C_q), 131.1 ($2CH_{Ar}$), 132.1 (C_q), 132.5 (C_q), 134.2 (C_q), 135.2 (C_q), 137.6 (C_q), 154.4 (C_q), 155.5 (C_q), 167.8 (C_q), 168.44 (C_q), 168.7 (C_q). HRMS (EI-MS) *m/z* calcd for $C_{30}H_{26}BrClN_4O_8S$: 716.0343, $[M-H]^+$ found: 716.0404. Rf (petroleum ether/ethyl acetate = 2/8) 0.50.

2.1.5.5. *2-(4-(3-(2-(1-(4-Chlorobenzoyl)-5-methoxy-2-methyl-1H-indol-3-yl)acetamido)-4-oxo-thiazolidin-2-yl)-2-methoxyphenoxy)ethyl nitrate* **(6e)** was obtained from 2-(4-((2-(2-(1-(4-chlorobenzoyl)-5-methoxy-2-methyl-1*H*-indol-3-yl)acetyl)hydrazineylidene)methyl)-2-methoxy-phenoxy)ethyl nitrate **(5e)** as pale yellow solid in 35% yield, m.p. 174-176 °C. ^{1}H NMR (400 MHz, DMSO-d_6) δ = 2.09 (s, 3H), 3.51 (s, 2H), 3.69 (s, 3H), 3.70 (s, 3H), 3.71 (d, *J* = 15.3 Hz, 1H), 3.85 (dd, *J* = 15.9 Hz, 1.7 Hz, 1H), 4.19 - 4.29 (m, 2H), 4.83 - 4.90 (m, 2H), 5.73 (s, 1H), 6.67 (dd, *J* = 9.0 Hz, 2.6 Hz, 1H), 6.80 - 6.89 (m, 2H), 6.92 (d, *J* = 9.0 Hz, 1H), 6.99 (s, 2H), 7.65 (d, *J* = 1.4 Hz, 4H), 10.34 (s, 1H). ^{13}C NMR (101 MHz, DMSO-d_6) δ = 13.2 (CH_3), 28.7

(CH_2), 29.3 (CH_2), 39.99 (CH_2) , 55.3 (CH_3), 55.5 (CH_3), 61.5 (CH), 64.9 (CH_2), 72.0 (CH_2), 101.6 (CH_{Ar}), 111.0 (CH_{Ar}), 111.5 (CH_{Ar}), 113.1 (CH_{Ar}), 113.2 (C_q), 114.4 (CH_{Ar}), 120.1 (CH_{Ar}), 129.0 ($2CH_{Ar}$), 130.1 (C_q), 130.5 (C_q), 131.1 ($2CH_{Ar}$), 134.2 (C_q), 135.2 (C_q), 137.6 (C_q), 147.8 (C_q), 149.1 (C_q), 155.5 (C_q), 167.8 (C_q), 168.4 (C_q), 168.9 (C_q). HRMS (EI-MS) *m/z* calcd for $C_{31}H_{29}ClN_4O_9S$: 668.1344, $[M-H]^+$ found: 668.1407. Rf (petroleum ether/ethyl acetate = 2/8) 0.43.

2.1.5.6. *2-(4-(3-(2-(1-(4-Chlorobenzoyl)-5-methoxy-2-methyl-1H-indol-3-yl)acetamido)-4-oxo-thiazolidin-2-yl)-2-ethoxyphenoxy)ethyl nitrate* **(6f)** was obtained from 2-(4-((2-(2-(1-(4-chlorobenzoyl)-5-methoxy-2-methyl-1*H*-indol-3-yl)acetyl)hydrazineylidene)methyl)-2-ethoxy-phenoxy)ethyl nitrate **(5f)** as pale yellow solid in 32% yield, m.p. 170-172 °C. ^{1}H NMR (400 MHz, DMSO-d_6) δ = 1.27 (t, *J* = 6.9 Hz, 3H), 2.09 (s, 3H), 3.50 (s, 2H), 3.69 (s, 3H), 3.70 (d, *J* = 15.9 Hz, 1H), 3.80 - 4.02 (m, 3H), 4.22 - 4.29 (m, 2H), 4.83 - 4.90 (m, 2H), 5.71 (s, 1H), 6.67 (dd, *J* = 9.0 Hz, 2.5 Hz, 1H), 6.81 - 6.90 (m, 2H), 6.91 (d, *J* = 9.0 Hz, 1H), 6.97 (d, *J* = 2.0 Hz, 1H), 7.00 (d, *J* = 2.5 Hz, 1H), 7.65 (s, 4H), 10.33 (s, 1H). ^{13}C NMR (101 MHz, DMSO-d_6) δ = 13.1 (CH_3), 14.6 (CH_3), 28.7 (CH_2), 29.3 (CH_2), 55.3 (CH_3), 61.4 (CH), 63.9 (CH_2), 65.3 (CH_2), 721.0 (CH_2), 101.6 (CH_{Ar}), 111.5 (CH_{Ar}), 112.5 (CH_{Ar}), 113.2 (C_q), 113.9 (CH_{Ar}), 114.4 (CH_{Ar}), 120.2 (CH_{Ar}), 129.0 ($2CH_{Ar}$), 130.1 (C_q), 130.5 (C_q), 131.1 ($2CH_{Ar}$), 131.3 (C_q), 134.1 (C_q), 135.2 (C_q), 137.6 (C_q), 148.0(C_q), 148.5 (C_q), 155.5 (C_q), 167.8 (C_q), 168.4 (C_q), 168.8 (C_q). HRMS (EI-MS) *m/z* calcd for $C_{32}H_{31}ClN_4O_9S$: 682.1500, $[M-H]^+$ found: 682.1561. Rf (toluene/acetonitrile = 6/4) 0.58.

2.1.5.7. *2-(4-(3-(2-(1-(4-Chlorobenzoyl)-5-methoxy-2-methyl-1H-indol-3-yl)acetamido)-4-oxo-thiazolidin-2-yl)-2-nitrophenoxy)ethyl nitrate* (**6g)** was obtained from 2-(4-((2-(2-(1-(4-chlorobenzoyl)-5-methoxy-2-methyl-1*H*-indol-3-yl)acetyl)hydrazineylidene)methyl)-2-nitro-phenoxy)ethyl nitrate **(5g)** as pale yellow solid in 25% yield, m.p. 165-167 °C. ^{1}H NMR (250 MHz, DMSO-d_6) δ = 2.13 (s, 3H), 3.50 (s, 2H), 3.68 (s, 3H), 3.73 (d, *J* = 16.0 Hz, 1H), 3.94 (dd, *J* = 16.0 Hz, 1.8 Hz, 1H), 4.37 - 4.54 (m, 2H), 4.80 - 4.99 (m, 2H), 5.82 (s, 1H), 6.66 (dd, *J* = 9.0 Hz, 2.5 Hz, 1H), 6.90 (d, *J* = 9.0 Hz, 1H), 6.95 (d, *J* = 2.5 Hz, 1H), 7.26 (d, *J* = 8.8 Hz, 1H), 7.60 (dd, *J* = 8.8 Hz, 2.3 Hz, 1H), 7.65 (s, 4H), 7.93 (d, 2.3 Hz, 1H), 10.41 (s, 1H). ^{13}C NMR (101 MHz, DMSO-d_6) δ = 13.2 (CH_3), 28.8 (CH_2), 29.1 (CH_2), 55.3 (CH_3), 60.1 (CH_2), 66.1 (CH_2), 71.2 (CH_2), 101.4 (CH_{Ar}), 111.(CH_{Ar}), 113.0 (C_q), 114.4 (CH_{Ar}), 115.2 (CH_{Ar}), 124.3 (CH_{Ar}), 129.0 ($2CH_{Ar}$), 130.0 (C_q), 130.4 (C_q), 131.1 ($2CH_{Ar}$), 131.5 (C_q), 133.7 (C_q), 134.1 (C_q),

135.3 (C_q), 137.6 (C_q), 139.1 (C_q), 150.9 (C_q), 155.5 (C_q), 167.8 (C_q), 168.5 (C_q), 168.6 (C_q). HRMS (EI-MS) *m/z* calcd for $C_{30}H_{26}ClN_5O_{10}S$: 683.1089, $[M-H]^+$ found: 683.1154. Rf (toluene/acetonitrile = 6/4) 0.53.

2.1.5.8. *2-(4-(3-(2-(1-(4-Chlorobenzoyl)-5-methoxy-2-methyl-1H-indol-3-yl)acetamido)-4-oxothiazolidin-2-yl)-2,6-dimethoxyphenoxy)ethyl nitrate* **(6h)** was obtained from 2-(4-((2-(2-(1-(4-chlorobenzoyl)-5-methoxy-2-methyl-1*H*-indol-3-yl)acetyl)hydrazineylidene)methyl)-2,6-dimethoxyphenoxy)ethyl nitrate **(5h)** as pale yellow solid in 42% yield, m.p. 174-176 °C. ^{1}H NMR (400 MHz, DMSO-d_6) δ = 2.08 (s, 3H), 3.55 (s, 2H), 3.70 (s, 10H), 3.88 (dd, *J* = 15.9 Hz, 1.7 Hz, 1H), 4.01 - 4.17 (m, 2H), 4.62 - 4.84 (m, 2H), 5.75 (s, 1H), 6.67 (dd, *J* = 8.9 Hz, 2.5 Hz, 1H), 6.69 (s, 2H), 6.91 (d, *J* = 8.9 Hz, 1H), 7.02 (d, *J* = 2.5Hz, 1H), 7.65 (s, 4H), 10.39 (s, 1H). ^{13}C NMR (101 MHz, DMSO-d_6) δ = 13.1 (CH_3), 28.8 (CH_2), 29.2 (CH_2), 55.3 (CH_3), 55.9 ($2CH_3$), 61.7 (CH), 68.5 (CH_2), 72.8 (CH_2), 101.6 (CH_{Ar}), 104.3 ($2CH_{Ar}$), 111.5 (CH_{Ar}), 113.1 (C_q), 114.5 (CH_{Ar}), 129.0 ($2CH_{Ar}$), 130.1 (C_q), 130.6 (C_q), 131.1 ($2CH_{Ar}$), 134.1 (C_q), 134.4 (C_q), 135.3 (C_q), 135.9 (C_q), 137.6 (C_q), 152.8 ($2C_q$), 155.5 (C_q), 167.8 (C_q), 168.5 (C_q), 169.1 (C_q). HRMS (EI-MS) *m/z* calcd for $C_{32}H_{31}ClN_4O_{10}S$: 698.1449, $[M-H]^+$ found: 698.1512. Rf (petroleum ether/ethyl acetate = 2/8) 0.57.

2.1.5.9. *2-(2,6-Dichloro-4-(3-(2-(1-(4-chlorobenzoyl)-5-methoxy-2-methyl-1H-indol-3-yl)acetamido)-4-oxothiazolidin-2-yl)phenoxy)ethyl nitrate* **(6i)** was obtained from 2-(2,6-dichloro-4-((2-(2-(1-(4-chlorobenzoyl)-5-methoxy-2-methyl-1*H*-indol-3-yl)acetyl)hydrazineylidene)methyl) phenoxy)ethyl nitrate **(5i)** as pale yellow solid in 53% yield, m.p. 138-140 °C. ^{1}H NMR (250 MHz, DMSO-d_6) δ = 2.12 (s, 3H), 3.54 (s, 2H), 3.70 (d, *J* = 15.8 Hz , 1H), 3.72 (s, 3H), 3.98 (dd, *J* = 15.8 Hz, 1.8 Hz, 1H), 4.20 - 4.38 (m, 2H), 4.79 - 4.98 (m, 2H), 5.77 (d, *J* = 1.6 Hz, 1H), 6.67 (dd, *J* = 9.0 Hz, 2.5 Hz, 1H), 6.92 (d, *J* = 9.0 Hz, 0.4 Hz, 1H), 7.02 (d, *J* = 2.5 Hz, 1H), 7.55 (s, 2H), 7.59 - 7.70 (m, 4H), 10.45 (s, 1H). ^{13}C NMR (101 MHz, DMSO-d_6) δ = 13.1 (CH_3), 28.8 (CH_2), 29.0 (CH_2), 55.3 (CH_3), 59.8 (CH), 69.4 (CH_2), 72.4 (CH_2), 101.5 (CH_{Ar}), 111.5 (CH_{Ar}), 113.0 (C_q), 114.5 (CH_{Ar}), 128.2 ($2C_q$), 128.3 ($2CH_{Ar}$), 129.0 ($2CH_{Ar}$), 130.1 (C_q), 130.5 (C_q), 131.1 ($2CH_{Ar}$), 134.1 (C_q), 135.2 (C_q), 137.5 (C_q), 137.6 (C_q), 150.1 (C_q), 155.5 (C_q), 167.8 (C_q), 168.5 (C_q), 168.7 (C_q). HRMS (EI-MS) *m/z* calcd for $C_{30}H_{25}Cl_3N_4O_8S$: 706.0459, $[M-H]^+$ found: 707.0519. Rf (toluene/acetonitrile = 6/4) 0.64.

2.1.5.10. *2-(2-Chloro-4-(3-(2-(1-(4-chlorobenzoyl)-5-methoxy-2-methyl-1H-indol-3-yl)acetamido)-4-oxothiazolidin-2-yl)-6-methoxyphenoxy)ethyl nitrate* **(6j)** was obtained from 2-(2-chloro-4-((2-(2-(1-(4-chlorobenzoyl)-5-methoxy-2-methyl-1*H*-indol-3-yl)acetyl)hydrazineylidene)methyl)-6-methoxyphenoxy)ethyl nitrate **(5j)** as pale yellow solid in 35% yield, m.p. 144-146 °C. ^{1}H NMR (400 MHz, DMSO-d_6) δ = 2.10 (s, 3H), 3.54 (d, *J* = 2.3 Hz, 2H), 3.70 (s, 3H), 3.71 (d, *J* = 15.9 Hz, 1H), 3.73 (s, 3H), 3.92 (dd, *J* = 15.9 Hz, 1.8 Hz, 1H), 4.18 - 4.25 (m, 2H), 4.78 - 4.85 (m, 2H), 5.75 (s, 1H), 6.67 (dd, *J* = 9.0 Hz, 2.5 Hz, 1H), 6.91 (d, *J* = 9.0 Hz, 1H), 7.01 (d, *J* = 2.5 Hz, 1H), 7.04 (d, *J* = 2.0 Hz, 1H), 7.10 (d, *J* = 2.0 Hz, 1H), 7.60 - 7.70 (m, 4H), 10.43 (s, 1H). ^{13}C NMR (101 MHz, DMSO-d_6) δ =13.1 (CH_3), 28.7 (CH_2), 29.1 (CH_2), 55.3 (CH_3), 56.2 (CH_3), 60.7 (CH), 68.8 (CH_2), 72.6 (CH_2), 101.5 (CH_{Ar}), 110.9 (CH_{Ar}), 111.5 (CH_{Ar}), 113.1 (C_q), 114.4 (CH_{Ar}), 120.1 (CH_{Ar}), 126.9 (C_q), 129.0 ($2CH_{Ar}$), 130.1 (C_q), 130.5 (C_q), 131.1 ($2CH_{Ar}$), 134.1 (C_q), 135.3 (C_q), 135.9 (C_q), 137.6 (C_q), 143.2 (C_q), 153.2 (C_q), 155.5 (C_q), 167.9 (C_q), 168.5 (C_q), 168.8 (C_q). HRMS (EI-MS) *m/z* calcd for $C_{31}H_{28}Cl_2N_4O_9S$: 702.0954, $[M-H]^+$ found: 702.1018. Rf (petroleum ether/ethyl acetate = 2/8) 0.47.

2.1.5.11. *2-(3-(3-(2-(1-(4-Chlorobenzoyl)-5-methoxy-2-methyl-1H-indol-3-yl)acetamido)-4-oxothiazolidin-2-yl)phenoxy)ethyl nitrate* **(6k)** was obtained from 2-(3-((2-(2-(1-(4-chlorobenzoyl)-5-methoxy-2-methyl-1*H*-indol-3-yl)acetyl)hydrazineylidene)methyl)phenoxy)ethyl nitrate **(5k)** as pale yellow solid in 63% yield, m.p. 170-172 °C. ^{1}H NMR (400 MHz, DMSO-d_6) δ = 2.09 (s, 3H), 3.52 (s, 2H), 3.70 (s, 3H), 3.71 (d, *J* = 15.8 Hz, 1H), 3.88 (dd, *J* = 15.9 Hz, 1.8 Hz, 1H), 4.25 (q, *J* = 3.8 Hz, 2H), 4.86 (t, *J* = 4.3 Hz, 2H), 5.75 (d, *J* = 1.5 Hz, 1H), 6.67 (dd, *J* = 9.0 Hz, 2.5 Hz, 1H), 6.92 (d, *J* = 9.0 Hz, 1H), 6.85 - 7.01 (m, 3H), 7.01 (d, *J* = 2.5, 1H), 7.25 (t, *J* = 7.9 Hz, 1H), 7.65 (s, 4H), 10.43 (s, 1H). ^{13}C NMR (101 MHz, DMSO-d_6) δ =13.1 (CH_3), 28.7 (CH_2), 29.1 (CH_2), 55.3 (CH_3), 61.2 (CH), 64.0 (CH_2), 72.0 (CH_2), 101.6 (CH_{Ar}), 111.6 (CH_{Ar}), 113.0 (CH_{Ar}), 113.1 (CH_{Ar}), 114.4 (C_q), 115.1 (CH_{Ar}), 120.2 (CH_{Ar}), 129.0 ($2CH_{Ar}$), 129.8 (C_q), 130.1 (CH_{Ar}), 130.5 (C_q), 131.1 ($2CH_{Ar}$), 134.1 (C_q), 135.2 (C_q), 137.6 (C_q), 140.2 (C_q), 155.5 (C_q), 158.0 (C_q), 167.8 (C_q), 168.5 (C_q), 169.0 (C_q). HRMS (EI-MS) *m/z* calcd for $C_{30}H_{27}ClN_4O_8S$: 638.1238, $[M-H]^+$ found: 638.1304. Rf (petroleum ether/ethyl acetate = 2/8) 0.56.

2.1.5.12. *2-(5-(3-(2-(1-(4-Chlorobenzoyl)-5-methoxy-2-methyl-1H-indol-3-yl)acetamido)-4-oxothiazolidin-2-yl)-2-methoxyphenoxy)ethyl nitrate* **(6l)** was obtained from 2-(5-((2-(2-(1-(4-chlorobenzoyl)-5-methoxy-2-methyl-1*H*-indol-3-yl)acetyl)hydrazineylidene)methyl)-2-methoxy-

phenoxy)ethyl nitrate **(5l)** as pale yellow solid in 25% yield, m.p. 176-178 °C. ^{1}H NMR (400 MHz, DMSO-d_6) δ = 2.07 (s, 3H), 3.50 (s, 2H), 3.70 (s, 3H), 3.71 (d, *J* = 15.8 Hz, 1H), 3.74 (s, 3H), 3.84 (dd, *J* = 15.9 Hz, 1.7 Hz, 1H), 4.04 - 4.33 (m, 2H), 4.84 (t, *J* = 4.4 Hz, 2H), 5.71 (s, 1H), 6.68 (dd, *J* = 9.0 Hz, 2.5 Hz, 1H), 6.86 (s, 1H), 6.81 - 6.93 (m, 1H), 6.93 (d, *J* = 9.0 Hz, 1H), 7.00 (d, *J* = 4.9 Hz, 1H), 7.00 (d, *J* = 4.3 Hz, 1H), 7.65 (s, 4H), 10.31 (s, 1H). ^{13}C NMR (101 MHz, DMSO-d_6) δ = 13.1 (CH_3), 28.7 (CH_2), 29.3 (CH_2), 55.3 (CH_3), 55.5 (CH_3), 61.4 (CH), 64.9 (CH_2), 72.0 (CH_2), 101.6 (CH_{Ar}), 111.5 (CH_{Ar}), 111.6 (CH_{Ar}), 112.5 (C_q), 113.1 (CH_{Ar}), 114.4 (CH_{Ar}), 121.3 (CH_{Ar}), 129.0 ($2CH_{Ar}$), 130.1 (C_q), 130.1 (C_q), 130.5 (C_q), 131.1 ($2CH_{Ar}$), 134.1 (C_q), 135.3 (C_q), 137.6 (C_q), 147.3 (C_q), 149.6 (C_q), 155.5 (C_q), 167.8 (C_q), 168.3 (C_q), 168.8 (C_q). HRMS (EI-MS) *m/z* calcd for $C_{31}H_{29}ClN_4O_9S$: 668.1344, $[M-H]^+$ found: 668.1407. Rf (toluene/acetonitrile = 6/4) 0.58.

2.1.2.13. *2-(5-(3-(2-(1-(4-Chlorobenzoyl)-5-methoxy-2-methyl-1H-indol-3-yl)acetamido)-4-oxo-thiazolidin-2-yl)-2-nitrophenoxy)ethyl nitrate* **(6m)** was obtained from 2-(5-((2-(2-(1-(4-chlorobenzoyl)-5-methoxy-2-methyl-1*H*-indol-3-yl)acetyl)hydrazineylidene)methyl)-2-nitro-phenoxy)ethyl nitrate **(5m)** as pale yellow in 20% yield 17%, m.p. 152-154 °C. ^{1}H NMR (400 MHz, DMSO-d_6) δ = 2.14 (s, 3H), 3.54 (s, 2H), 3.66 (s, 3H), 3.75 (d, *J* = 15.9 Hz, 1H), 3.95 (dd, *J* = 15.9 Hz, 1.8 Hz, 1H), 4.24 - 4.44 (m, 2H), 4.87 (t, *J* = 4.4 Hz, 2H), 5.85 (d, *J* = 1.6 Hz, 1H), 6.65 (dd, *J* = 9.0 Hz, 2.5 Hz, 1H), 6.88 (d, *J* = 9.0 Hz, 1H), 6.93 (d, *J* = 2.5 Hz, 1H), 7.17 (dd, *J* = 8.4 Hz, 1.7 Hz, 1H), 7.35 (d, *J* = 1.7 Hz, 1H), 7.65 (d, *J* = 1.4 Hz, 4H), 7.85 (d, *J* = 8.3 Hz, 1H), 10.49 (s, 1H). ^{13}C NMR (101 MHz, DMSO-d_6) δ = 13.1 (CH_3), 28.8 (CH_2), 29.1 (CH_2), 55.3 (CH_3), 60.4 (CH), 66.0 (CH_2), 71.2 (CH_2), 101.6 (CH_{Ar}), 111.3 (CH_{Ar}), 113.0 (CH_{Ar}), 114.0 (CH_{Ar}), 114.4 (C_q), 119.9 (CH_{Ar}), 125.5 (CH_{Ar}), 129.0 ($2CH_{Ar}$), 130.1 (C_q), 130.4 (C_q), 131.1 ($2CH_{Ar}$), 134.1 (C_q), 135.4 (C_q), 137.6 (C_q), 139.1 (C_q), 145.6 (C_q), 150.7 (C_q), 155.5 (C_q), 167.8 (C_q), 168.6 (C_q), 168.8 (C_q). HRMS (EI-MS) *m/z* calcd for $C_{30}H_{26}ClN_5O_{10}S$: 683.1089, $[M-H]^+$ found: 683.1155. Rf (toluene/acetonitrile = 6/4) 0.6.

2.1.2.14. *2-(3-(3-(2-(1-(4-Chlorobenzoyl)-5-methoxy-2-methyl-1H-indol-3-yl)acetamido)-4-oxo-thiazolidin-2-yl)-4-nitrophenoxy)ethyl nitrate* **(6n)** was obtained from 2-(3-((2-(2-(1-(4-chlorobenzoyl)-5-methoxy-2-methyl-1*H*-indol-3-yl)acetyl)hydrazineylidene)methyl)-4-nitrophe-noxy)ethyl nitrate **(5n)** as pale yellow in yield 35%, m.p. 180-182 °C. ^{1}H NMR (400 MHz, DMSO-d_6) δ = 2.12 (s, 3H), 3.56 (d, *J* = 4.7 Hz, 2H), 3.64 (d, *J* = 15.8 Hz, 1H), 3.69 (s, 3H), 3.93 (dd, *J* = 15.8 Hz, 1.9 Hz, 1H), 4.44 - 4.57 (m, 2H), 4.93 (t, *J* = 4.4 Hz, 2H), 6.18 (d, *J* = 1.8

Hz, 1H), 6.67 (dd, *J* = 9.0 Hz, 2.5 Hz, 1H), 6.90 (d, *J* = 9.0 Hz, 1H), 6.98 (d, *J* = 2.5 Hz, 1H), 7.09 - 7.20 (m, 2H), 7.58 - 7.70 (m, 4H), 8.12 (d, *J* = 9.0 Hz, 1.1 Hz, 1H), 10.63 (s, 1H). ^{13}C NMR (101 MHz, DMSO-d_6) δ = 13.1 (CH_3), 28.1 (CH_2), 28.9 (CH_2), 55.3 (CH_3), 57.4 (CH), 65.0 (CH_2), 71.6 (CH_2), 101.5 (CH_{Ar}), 111.5 (CH_{Ar}), 112.5 (C_q), 113.0 (CH_{Ar}), 114.5 (CH_{Ar}), 114.8 (CH_{Ar}), 128.3 (CH_{Ar}), 129.0 ($2CH_{Ar}$), 130.1 (C_q), 130.4 (C_q), 131.1 ($2CH_{Ar}$), 134.1 (C_q), 135.3 (C_q), 137.6 (C_q), 138.4 (C_q), 140.2 (C_q), 155.5 (C_q), 162.5 (C_q), 167.8 (C_q), 168.7 (C_q), 169.3 (C_q). HRMS (EI-MS) *m/z* calcd for $C_{30}H_{26}ClN_5O_{10}S$: 683.1089, $[M-H]^+$ found: 683.1151. Rf (petroleum ether/ethyl acetate = 2/8) 0.73.

2.1.2.15.*2-(2-Bromo-3-(3-(2-(1-(4-chlorobenzoyl)-5-methoxy-2-methyl-1H-indol-3-yl)acetamido)-4-oxothiazolidin-2-yl)-6-methoxyphenoxy)ethyl nitrate* **(6o)** was obtained from 2-(2-bromo-3-((2-(2-(1-(4-chlorobenzoyl)-5-methoxy-2-methyl-1*H*-indol-3-yl)acetyl)hydrazineylidene)methyl)-6-methoxyphenoxy)ethyl nitrate **(5o)** as pale yellow in yield 52%, m.p. 184-186 °C. ^{1}H NMR (400 MHz, DMSO-d_6) δ = 2.10 (s, 3H), 3.55 (d, *J* = 4.5 Hz, 2H), 3.70 (s, 3H), 3.83 (s, 3H), 3.65 - 3.96 (m, 2H), 4.04 - 4.33 (m, 2H), 4.82 (t, *J* = 4.3 Hz, 2H), 6.02 (s, 1H), 6.66 (dd, *J* = 9.0 Hz, 2.5 Hz, 1H), 6.91 (d, *J* = 9.0 Hz, 1H), 7.02 (d, *J* = 2.5 Hz, 1H), 7.21 (d, *J* = 51.3 Hz, 2H), 7.65 (d, *J* = 1.4 Hz, 4H), 10.54 (s, 1H). ^{13}C NMR (101 MHz, DMSO-d_6) δ = 13.1(CH_3), 28.8 ($2CH_2$), 55.3 (CH_3), 56.2 (CH_3), 60.7 (CH), 68.7 (CH_2), 72.7 (CH_2), 101.5 (CH_{Ar}), 111.6 (CH_{Ar}), 112.5 (CH_{Ar}), 113.1 (CH_{Ar}), 114.4 (CH_{Ar}), 117.7 (C_q), 129.0 ($2CH_{Ar}$), 130.1 (C_q), 130.5 (C_q), 131.1 ($2CH_{Ar}$), 134.1 (C_q), 135.3 (C_q), 137.6 (C_q), 144.1 (C_q), 153.0 (C_q), 155.5 (C_q), 167.8 (C_q), 168.7 (C_q), 169.3 (C_q). HRMS (EI-MS) *m/z* calcd for $C_{31}H_{28}BrClN_4O_9S$: 746.0449, $[M-H]^+$ found: 746.0506. Rf (petroleum ether/ethyl acetate = 2/8) 0.62.

2.1.2.16. *2-(2-(3-(2-(1-(4-Chlorobenzoyl)-5-methoxy-2-methyl-1H-indol-3-yl)acetamido)-4-oxothiazolidin-2-yl)phenoxy)ethyl nitrate* **(6p)** was obtained from 2-(2-((2-(2-(1-(4-chlorobenzoyl)-5-methoxy-2-methyl-1*H*-indol-3-yl)acetyl)hydrazineylidene)methyl)phenoxy)ethyl nitrate **(5p)** as pale yellow in yield 34%, m.p. 175-177 °C. ^{1}H NMR (250 MHz, DMSO-d_6) δ = 2.11 (s, 3H), 3.54 (s, 2H), 3.65 (d, *J* = 15.8 Hz, 1H), 3.68 (s, 3H), 3.78 (dd, *J* = 15.8 Hz, 1.8 Hz, 1H), 3.99 - 4.35 (m, 2H), 4.50 - 4.88 (m, 2H), 5.99 (d, *J* = 1.5 Hz, 1H), 6.68 (dd, *J* = 9.0 Hz, 2.5 Hz, 1H), 6.93 (dd, *J* = 9.0 Hz, 0.4 Hz, 1H), 6.96 - 7.08 (m, 3H), 7.23 - 7.43 (m, 2H), 7.65 (s, 4H), 10.44 (s, 1H). ^{13}C NMR (101 MHz, DMSO-d_6) δ =13.1 (CH_3), 28.7 (CH_2), 28.8 (CH_2), 55.3 (CH, CH_3) 64.4 (CH_2), 71.8 (CH_2), 101.5 (CH_{Ar}), 111.6 (CH_{Ar}), 112.3 (CH_{Ar}), 113.2 (C_q), 114.4 (CH_{Ar}), 121.1 (CH_{Ar}), 126.8 (CH_{Ar}), 127.5 (C_q), 129.0 ($2CH_{Ar}$), 129.9 (CH_{Ar}), 130.1 (C_q), 130.5

(C_q), 131.1 ($2CH_{Ar}$), 134.2 (C_q), 135.3 (C_q), 137.6 (C_q), 155.6 (C_q), 155.6 (C_q), 167.8 (C_q), 168.6 (C_q), 169.2 (C_q). HRMS (EI-MS) *m/z* calcd for $C_{30}H_{27}ClN_4O_8S$: 639.1238, $[M-H]^+$ found: 638.1303. Rf (petroleum ether/ethyl acetate = 2/8) 0.64.

2.1.2.17. *2-(2-(4-(3-(2-(1-(4-Chlorobenzoyl)-5-methoxy-2-methyl-1H-indol-3-yl)aceta-mido)-4-oxothiazolidin-2-yl)phenoxy)ethoxy)ethyl nitrate* **(6q)** was obtained from 2-(2-(4-((2-(2-(1-(4-chlorobenzoyl)-5-methoxy-2-methyl-1*H*-indol-3-yl)acetyl)hydrazineylidene)methyl)phenoxy) ethoxy)ethyl nitrate **(5q)** as pale yellow in yield 27%, m.p. 132-134 °C. ^{1}H NMR (400 MHz, DMSO-d_6) δ = 2.09 (s, 3H), 3.49 (s, 2H), 3.70 (d, *J* = 15.9 Hz, 1H), 3.71 (s, 3H), 3.73 - 3.82 (m, 4H), 3.84 (dd, *J* = 15.9 Hz, 1.7 Hz, 1H), 3.97 - 4.28 (m, 2H), 4.56 - 4.78 (m, 2H), 5.71 (s, 1H), 6.69 (dd, *J* = 8.9 Hz, 2.5 Hz, 1H), 6.86 (d, *J* = 8.5 Hz, 2H), 6.94 (d, *J* = 8.9 Hz, 1H), 7.01 (d, *J* = 2.5 Hz, 1H), 7.27 (d, *J* = 8.5 Hz, 2H), 7.65 (s, 4H), 10.34 (s, 1H). ^{13}C NMR (101 MHz, DMSO-d_6) δ = 13.2 (CH_3), 28.7 (CH_2), 29.3 (CH_2), 55.3 (CH_3), 61.2 (CH), 66.5 (CH_2), 67.1 (CH_2), 68.9 (CH_2), 72.9 (CH_2), 101.7 (CH_{Ar}), 111.5 (CH_{Ar}), 113.2 (C_q), 114.4 ($2CH_{Ar}$), 114.4 (CH_{Ar}), 129.0 ($2CH_{Ar}$), 129.1 ($2CH_{Ar}$), 129.9 (C_q), 130.1 (C_q), 130.5 (C_q), 131.1 ($2CH_{Ar}$), 134.2 (C_q), 135.2 (C_q), 137.6 (C_q), 155.5 (C_q), 158.9 (C_q), 167.8 (C_q), 168.4 (C_q), 168.8 (C_q). HRMS (EI-MS) *m/z* calcd for $C_{32}H_{31}ClN_4O_9S$: 682.1500, $[M-H]^+$ found: 682.1561. Rf (toluene/acetonitrile = 6/4) 0.67.

2.1.2.18. *2-(2-(4-(3-(2-(1-(4-Chlorobenzoyl)-5-methoxy-2-methyl-1H-indol-3-yl)acetamido)-4-oxothiazolidin-2-yl)-2-methoxyphenoxy)ethoxy)ethyl nitrate* **(6r)** was obtained from 2-(2-(4-((2-(2-(1-(4-chlorobenzoyl)-5-methoxy-2-methyl-1*H*-indol-3-yl)acetyl)hydrazineylidene)methyl)-2-methoxyphenoxy)ethoxy)ethyl nitrate **(5r)** as pale yellow in yield 25%, m.p. 135-136 °C. ^{1}H NMR (400 MHz, DMSO-d_6) δ = 2.08 (s, 3H), 3.51 (s, 2H), 3.70 (s, 6H), 3.63 - 3.89 (m, 6H), 3.98 - 4.10 (m, 2H), 4.53 - 4.82 (m, 2H), 5.72 (s, 1H), 6.68 (dd, *J* = 8.9 Hz, 2.4 Hz, 1H), 6.83 (s, 2H), 6.93 (d, *J* = 8.9 Hz, 1H), 6.97 (s, 1H), 7.01 (d, *J* = 2.4 Hz, 1H), 7.65 (s, 4H), 10.33 (s, 1H). ^{13}C NMR (101 MHz, DMSO-d_6) δ = 13.2 (CH_3), 28.7 (CH_2), 29.3 (CH_2), 55.3 (CH_3), 55.4 (CH_3), 61.5 (CH), 66.6 (CH_2), 67.8 (CH_2), 68.9 (CH_2), 72.9 (CH_2), 101.6 (CH_{Ar}), 110.9 (CH_{Ar}), 111.5 (CH_{Ar}), 112.6 (C_q), 113.2 (CH_{Ar}), 114.4 (CH_{Ar}), 120.2 (CH_{Ar}), 129.0 ($2CH_{Ar}$), 130.1 (C_q), 130.4 (C_q), 130.6 (C_q), 131.1 ($2CH_{Ar}$), 134.2 (C_q), 135.2 (C_q), 137.6 (C_q), 148.4 (C_q), 149.0 (C_q), 155.5 (C_q), 167.8 (C_q), 168.4 (C_q), 168.9 (C_q). HRMS (EI-MS) *m/z* calcd for $C_{33}H_{33}ClN_4O_{10}S$: 712.1606, $[M-H]^+$ found: 712.1667. Rf (toluene/acetonitrile = 6/4) 0.49.

2.1.2.19. *2-(2-(4-(3-(2-(1-(4-Chlorobenzoyl)-5-methoxy-2-methyl-1H-indol-3-yl)acetamido)-4-oxothiazolidin-2-yl)-2-ethoxyphenoxy)ethoxy)ethyl nitrate* **(6s)** was obtained from 2-(2-(4-((2-(2-(1-(4-chlorobenzoyl)-5-methoxy-2-methyl-1*H*-indol-3-yl)acetyl)hydrazineylidene)methyl)-2-ethoxyphenoxy)ethoxy)ethyl nitrate **(5s)** as pale yellow in yield 27%, m.p. 136-138 °C. ^{1}H NMR (400 MHz, DMSO-d_6) δ = 1.27 (t, *J* = 6.9 Hz, 3H), 2.08 (s, 3H), 3.50 (s, 2H), 3.70 (d, *J* = 15.9 Hz, 1H), 3.70 (s, 3H), 3.77 (t, *J* = 4.7 Hz, 2H), 3.79 - 3.86 (m, 3H), 3.86 - 4.02 (m, 2H), 4.05 (t, *J* = 4.8 Hz, 2H), 4.65 - 4.72 (m, 2H), 5.70 (s, 1H), 6.67 (dd, *J* = 8.9 Hz, 2.4 Hz, 1H), 6.76 - 6.88 (m, 2H), 6.92 (d, *J* = 8.9 Hz, 1H), 6.95 (s, 1H), 7.01 (d, *J* = 2.4 Hz, 1H), 7.65 (s, 4H), 10.32 (s, 1H). ^{13}C NMR (101 MHz, DMSO-d_6) δ = 13.1 (CH_3), 14.6 (CH_3), 28.7 (CH_2), 29.3 (CH_2), 55.3 (CH_3), 61.5 (CH), 63.9 (CH_2), 66.6 (CH_2), 68.1 (CH_2), 68.9 (CH_2), 72.9 (CH_2), 101.6 (CH_{Ar}), 111.5 (CH_{Ar}), 112.5 (CH_{Ar}), 113.1 (C_q), 113.2 (CH_{Ar}), 114.4 (CH_{Ar}), 120.3 (CH_{Ar}), 129.0 ($2CH_{Ar}$), 130.1 (C_q), 130.5 (C_q), 130.6 (C_q), 131.1 ($2CH_{AR}$), 134.2 (C_q), 135.2 (C_q), 137.6 (C_q), 148.3 (C_q), 148.7 (C_q), 155.5 (C_q), 167.8 (C_q), 168.3 (C_q), 168.8 (C_q). HRMS (EI-MS) *m/z* calcd for $C_{34}H_{35}ClN_4O_{10}S$: 726.1762, $[M-H]^+$ found: 726.1823. Rf (toluene/acetonitrile = 6/4) 0.55.

2.2. In silico docking study

The selectivity of the new NO-IND-TZDs (**6a-s**) for COX isoenzymes (COX-1 and COX-2) was studied using AutoDock 4.2.6 software. The results expressed as docking score were compared to indomethacin (IND), diclofenac (DCF) and celecoxib (CCB), used as reference drugs.

2.2.1 *Generate the receptor coordinate file (RCF)*

X-ray crystallographic structure of the ligand-enzyme complex were downloaded from RCSB Protein Data Bank, for COX-1 (pdb code: 4o1z) and COX-2 (pdb code: 3nt1) and processed prior to docking. The corresponding ligand-enzyme complexes were used to remove the ligands, the water molecules, cofactors and ions that should not be included in the receptor by a text editor. After that, each receptor was converted to PDBQT format file using AutoDock 4.2.6 by reading the coordinates, adding charges, merging non-polar hydrogens and assigning appropriate atom types.

2.2.2. *Generate the ligand coordinate file (LCF)*

Dimensional structures of the compounds (**6a-s**) were sketched in ChemDraw and after that were converted to PDB coordinate files using Chimera 1.14. Each LCF contain special

keywords recognized by AutoDock 4.2.6 like ROOT, ENDROOT, BRANCH, and ENDBRANCH that establish a rigid set of atoms and rotatable groups of atoms that are connected to the rigid root. As well, TORSDOF is used in estimating the change in free energy caused by the loss of torsional degrees of freedom upon binding. Each structure was energy minimized and converted to PDBQT format file using AutoDock4.2.6. A docking method for study the interaction between a single ligand with a single receptor, with explicit calculation of affinity maps, was applied. The receptors were kept rigid and the ligands were allowed to be flexible.

2.2.3. *Preparing the grid parameter file* (GPF)

The GPF specifies the PDBQT files for the receptor and the parameters for generating the atomic affinity maps. For COX-1 was used a grid box of 73x78x82 points with a spacing of 0.375 Å between grid points and the grid box center was put on x = 251.00, y = 104.00 and z = 1.364. COX-2 was enclosed in a 74x72x86 grid box having 0.375 Å spacing and -37.882, -50.853 and -21.24 as x, y and z center. The ligand binding site of COX-1 and COX-2 respectively is identified by using protein visualization software such as DSvisualizer, PyMol and Chimera 1.14.

2.2.4. *Preparing the docking parameter file (DPF*)

The DPF consist of which grid map files to use, which ligand molecule to dock, what is its center and number of torsions, which docking algorithm to use and how many runs to do. For doing the conformation search, was applied the Lamarckian Genetic Algorithm (LGA) with the following parameters: number of individuals in the population (300), the maximum number of 27,000 generations simulated during each LGA run, the maximum number of evaluation at 25,000,000, a mutation rate of 0.02 and a cross over rate of 0.80, while remaining docking parameters were set to default. The ligands were allowed to move within the target proteins to achieve the lowest energy conformations and the number of runs for each docking procedure was set to 200. The selected ligands were docked against COX-1 and COX-2 using AutoDock 4.2.6 to identify their selectivity. After performing molecular docking simulation of the selected ligand molecules against the COX isoenzymes, the best ligand molecules were evaluated on the basis of their binding energy against the COX receptor. All the results obtained by molecular docking simulation were evaluated on the basis of hydrophilic and lipophilic interactions obtained between the binding residues present in the active ligand binding site of the macromolecule and

ligand. The dockings experiments were clustered with a root mean square deviation (RMSD) of 0.5 Å and evaluated by PyMOL software. Most energetically favored orientations were selected for next research.

2.3. In silico ADME-Tox study

ADME-Tox (Absorption, Distribution, Metabolism, Excretion and Toxicity) study offers important data to predict the pharmacokinetic properties and toxicity degree of new candidates, during the drug discovery process [72–74]. The ADME-Tox profile of the new NO-IND-TZDs (**6a-s**) was predicted using *SwissADME* (http://www.swissadme.ch) and *pkCSM-pharmacokinetics* (http://structure.bioc.cam.ac.uk/pkcsm) tools. *SwissADME* provide an overall assessment of the pharmacokinetics profile of small molecules by most relevant computational methods [75,76] and *pkCSM-pharmacokinetics* is a new method based on graph signatures and experimental data [77]. The most important ADME-Tox properties provided from the ADME-Tox tools were selected to predict toxicity profile of the NO-IND-TZDs.

2.4. *In vitro radical scavenging assay*

The free radical scavenging activity of the new NO-IND-TZDs (**6a-s**) was evaluated using 2,2-diphenyl-1-picrylhydrazyl radical (DPPH) assay with slight modification [78–80]. The IND and aspirin (ASP), as reference drugs, and vitamin C, as standard antioxidant, were used.

Preparation of DPPH and test solutions. A weighed amount of DPPH (29.71 mg, 75.34 µmol) was dissolved by sonication in 50 mL methanol of analytical grade and kept in darkness. After 30 min, a sample of 10 mL was taken and made up to 100 mL with methanol. The resulted DPPH solution (150.68 µM) was stored in the darkness at room temperature and used up on the day of preparation. The stock solutions (2600 µM) of tested derivatives (**6a-s**) were prepared in DMSO, then serially diluted with methanol to obtain different concentrations (2600 µM, 1500 µM, 700 µM, 620 µM, 530 µM, 440 µM, 350 µM, 260 µM and 120 µM). The serially diluted solutions of IND and ASP were prepared in the same manner with tested derivatives (**6a-s**). The serially diluted solutions of vitamin C were prepared by dilution of freshly prepared solution (2619 µM) with methanol to make different concentrations (152.26 µM, 132.7 µM, 112.27µM, 95.26 µM, 77.62 µM, 54.63 µM, 40.3 µM, 20.54 µM).

DPPH assay procedure. 500 µL from each sample of the tested compounds (**6a-s**), reference drug (IND, ASP) and vitamin C was added to 1000 µL of DPPH solution. Two blanks (blank 1:500 µL of methanol and 1000 µL of DPPH and blank 2: 1500 µL methanol) were also used. The mixture was kept for 3 h in the darkness at room temperature. Thereafter, a 270 µL aliquot of each sample tube was added in a 96 well plate. The absorbance was then measured at 517 nm using Tecan Sunrise Remote Microplate Reader TW/ML-Abbott F039306. All tests were performed in quadruplicate.

The DPPH radical-inhibiting capacity (inhibition/scavenging activity) (%) was calculated using the following formula [63]:

$$\text{Inhibition (Scavenging activity) \%} = [(A_{CS}-A_s)/A_{CS}] \times 100 \quad (1)$$

where: A_{cs} is the difference between absorbance of blank 1 and blank 2 and A_s is the difference between the absorbance of tested sample and blank 2.

To calculate IC_{50} ($f_{(x)} = 50$) of each tested compounds, the inhibition ratios ($f_{(x)}$) were plotted against the sample concentration (x). The results for each experiment were represented by a dose-response curve and were used two types of regression lines (f(x)): a sigmoid curve and a quadratic line.

The DPPH radical scavenging activity of each tested compounds was expressed also as the vitamin C equivalent antioxidant capacity (CEAC) and was calculated using the following formula [64]:

$$CEAC = IC_{50(\text{vit. C})}/IC_{50(\text{sample})} \quad (2)$$

here: $IC_{50(\text{vit. C})}$ is the concentration of vitamin C required for 50% inhibition and $IC_{50(\text{sample})}$ is concentration of tested compounds (**6a-s)** and reference drugs, respectively, required for 50% inhibition. The higher CEAC value means the higher DPPH radical scavenging activity.

2.5. *In vitro anti-inflammatory assay*

To predict the anti-inflammatory effects of the new NO-IND-TDZs (**6a-s**), a modified Mizushima's test was used [81,82]. The test which assures a significant correlation between the *in vitro* and *in vivo* effects is based on denaturing effect on specific proteins. A solution of bovine serum albumin (BSA) 0.2% in 0.9% NaCl/DMSO = 6/4 was used. Two controls (positive and negative), as well as reference drugs (IND, ASP), were also used. The positive control consisted of the action of 0.1 M hydrochloric acid, as denaturing agent, in 0.9% NaCl, on the

0.2% BSA solution. The negative control consisted of untreated 0.2% BSA solution. Each sample (**6a-s**, IND, ASP) was tested at different concentration (50 µM, 100 µM and 150 µM). The test samples and controls were incubated at 38°C for 5 h. The degree of denaturation of BSA was evaluated by measuring the increase in optical density at 450 nm, measured using Tecan Sunrise Remote Microplate Reader TW/ML-Abbott F039306. All tests were performed in quadruplicate. The maximum value of the absorbance at 450 nm of the positive control was considered as the 100% effect. Results, expressed as averages of the percentage values (% effect), were plotted versus the concentration of tested sample.

2.6. *In vitro nitric oxide release measurement*

To evaluate the nitric oxide release, the new NO-IND-TZDs (**6a-s**) were subjected to Griess colorimetric method [83,84]. The Griess reagents consists of 0.34% (wt/v) *N*-(1-naphthyl)ethylenediamine (NED) solution in DMSO, 3.4% (wt/v*)* sulfanilamide (SULF) in 10% (wt/v*)* phosphoric acid and a mixture between of 3.4% (wt/v) SULF and 1.07% (wt/v) mercuric chloride (SULF-$HgCl_2$) in 10% (wt/v*)* phosphoric acid. The NO released from the sample is spontaneous oxidized to NO_2^-, which subsequently reacts with the Griess reagents to form an azo dye. S-nitroso-N-acetyl-penicillamine (SNAP), sodium nitropruside (SNP) and nitroglycerine (NTG), were used as reference NO donors.

The experiments were carried out in neutral (phosphate buffer solution - PBS) and acidic (hydrochloric acid solution - HCl) experimental conditions, in presence or absence of L-glutathione (GSH): PBS (pH 7.5), PBS-GSH (pH 7.51), HCl (pH 1.55) and HCl-GSH (pH 1.56)

Preparation of sodium nitrite and test solutions

A fresh sodium nitrite stock solution (0.1 M sodium nitrite in distilled water) was prepared and was standardized using the procedure reported in the European Pharmacopoeia (real molarity = 0.0999, molarity factor = 0.999)[85]. Next, a solution of 100 µM sodium nitrite was prepared by diluting of 1 mL of the stock solution to 1000 mL with MeOH/H_2O = 1/1 (v/v) mixture. Then, serially diluted solutions, containing different concentrations (100 µM, 50 µM, 25 µM, 12.50 µM, 6.25 µM, 3.125 µM, 1.56 µM and 0.78 µM), were prepared by dilution with MeOH/H_2O = 1/1 (v/v) mixture. The tested compounds (**6a-s**) and reference NO donors (SNAP, SNP, NTG) were dissolved in DMSO and water, respectively, to afford a stock solution of 2600 µM.

The preparation of nitrite standard curve

An aliquot of 170 µL sodium nitrite solution (in the range of 0.78-100 µM) was added to 50 µL solution of SULF in a 96 well plate. After 10 min, 50 µL of NED solution was added and the absorbance of the formed pink-red azo dye was measured at 540 nm, after 20 min. A blank sample (contain 170 µL PBS, 50 µL SULF and 50 µL NED) was performed under the similar conditions. All tests were performed five times for each concentration and the average absorbance was calculated. The calibration curve was constructed by plotting the average absorbance value in relation with the corresponding sodium nitrite concentration.

NO release assay

A solution of 100 µM NO-IND-TZDs (**6a-s**) and reference NO donors (SNAP, SNP, NTG) was prepared by dilute 80 µL of each stock solution (2600 µM) with 2 mL of PBS, PBS-GSH, HCl and HCl-GSH. These solutions were kept at 37-38°C for 120 min, after that an aliquot of 170 µL of the each solution was measured and added to 50 µL of SULF and SULF-$HgCl_2$ respectively in a 96 well plate. After 10 min, 50 µL of NED solution was added and the absorbance of the formed pink-red azo dye was measured at 540 nm, after 20 min. A blank sample (contain 170 µL PBS/PBS-GSH/HCl/HCl-GSH, 50 µL SULF/SULF-$HgCl_2$ and 50 µL NED) was performed under the similar conditions. All tests were performed in quadruplicate.

The percentage (%) of NO release was calculated using the following formula [83]:

$$\% \text{ NO} = (C_{f\,NO} \times 100)/C_{t\,NO} \quad (3)$$

where: $C_{f\,NO}$ is the found concentration of NO (µM) and $C_{t\,NO}$ is the theoretical concentration of NO (µM).

2.7. Statistical analysis

The results were expressed as mean value ± standard deviation (SD) and the analysis was performed using IBM SPSS Statistics 23 for Windows. The statistical significance of the results was assessed by the one-way and two-way analysis of variance (ANOVA's test) followed by Tukey's HSD test used to compare the differences among samples. A p value < 0.05 was considered statistically significant.

3. Results and discussion

3.1. Chemistry

The synthesis of new NO-IND-TZDs (**6a-s**) was based on chemical modulation of IND at carboxylic group and involved several steps: (i) synthesis of the halide-ethoxy-benzaldehyde derivatives (**2a-s**); (ii) synthesis of the nitrate ester benzaldehyde derivatives **(3a-s)**; (iii) synthesis of the IND hydrazone derivatives (**5a–s**) and (iv) condensation of IND hydrazone derivatives (**5a–s**) with mercaptoacetic acid to obtain the finally derivatives (**6a-s**) (Fig. 3).

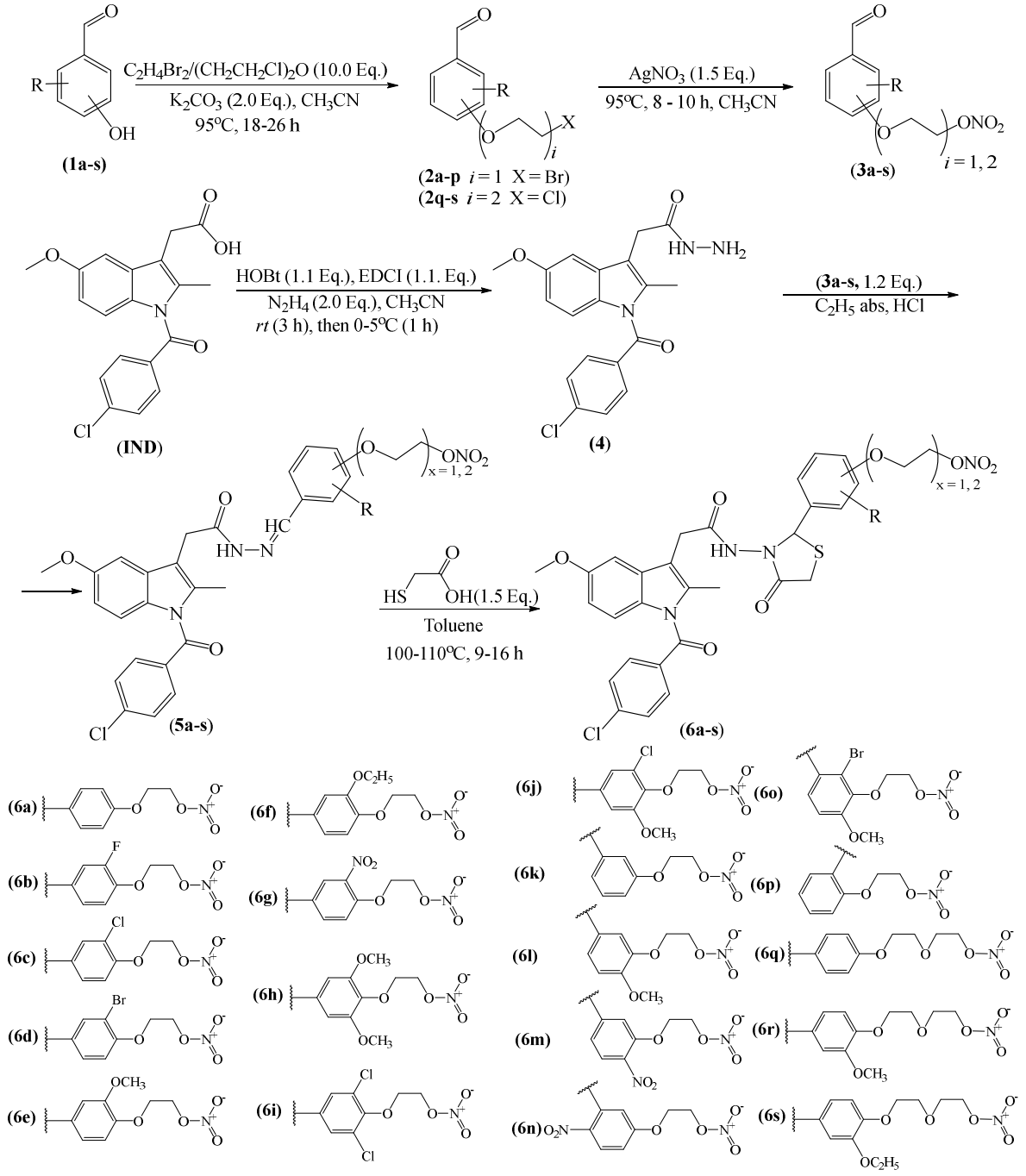

Fig. 3. The synthesis of the new NO-IND-TZDs (**6a-s**).

For the synthesis of the nitrate ester benzaldehydes **(3a-s)** different substituted hydroxy-benzaldehydes (**1a-s**) were reacted with 1,2-dibromoethane or bis(2-chloroethyl)ether respectively, when corresponding halide-ethoxy-benzaldehydes (**2a-s**) were obtained, based on an SN_2 Williamson ether synthesis. Then the intermediaries (**2a-s**) were reacted with silver nitrate ($AgNO_3$) to form the compounds **3a-s**. In the next step, the IND hydrazide (**4**), obtained by a peptide coupling reaction between IND and hydrazine hydrate, was reacted with nitrate ester benzaldehydes **(3a-s),** when new IND hydrazone derivatives (**5a-s**) were obtained. These intermediaries were subjected to an annelation with mercaptoacetic acid to obtain the final derivatives (**6a-s**).

The chemical structure of all synthesized compound (intermediaries and finally derivatives) was proved on the basis of NMR and HR mass spectral methods.

In the ^{1}H NMR spectra of *nitrate ester benzaldehydes* (**3a-s**) it was found the characteristic multiplet signals corresponding to methylene protons close to the electron withdrawing nitrate ester group (-CH_2-ONO_2) that appear more deshielded (δ 4.80-5.00, m, 2H) compared with the protons close to halide (-CH_2-X) (δ 3.75 - 3.90, m, 2H) from halide-ethoxy-benzaldehyde derivatives **(2a-s)**. At the same time, ^{13}C NMR signal for -$\underline{C}H_2$-ONO_2 was observed in range of δ 71.06-72.66 ppm compared to the signal of the same carbon from derivatives (**2a-s)** (in range of δ 30.40-31.60 ppm).

The final NO-IND-TZDs *(***6a-s)** showed the multiplet signals of protons and secondary carbon of methylene (-CH_2-ONO_2) in the range of δ 4.80-4.90 ppm and δ 64.00-69.00 ppm, respectively. The presence of 1,3-thiazolidine-4-one scaffold in the structure of NO-IND-TZDs *(***6a-s)** was proved in the NMR spectra by the characteristic signals of protons and carbons corresponding to methine (=CH-) and methylene (-CH_2-) group. In ^{1}H NMR spectra, the signal of =CH- was observed in the range of δ 5.70-6.00 ppm. For -CH_2- there were diastereotopic protons, that have different chemical shifts δ 3.70 (d, *J* = 15.9Hz, 1H) respectively δ 3.90 (dd, *J* = 15.9Hz, 1.7 Hz, 1H) ppm. In ^{13}C NMR spectra, signal of the =CH- group was observed in the range of δ 60.0-61.4 ppm and of the -CH_2- group at δ 28.9-29.6 ppm. The protons and carbon signals of other aliphatic and aromatic fragments of **6a-s** were observed at expected values of chemical shift. The presence of the signals above mentioned confirmed correct cyclization reaction of IND hydrazone derivatives (**5a–s**) to form 1,3-thiazolidine-4-one ring and preserved

the nitrate ester moiety in the **6a-s**. Moreover the NMR spectral data coupled with mass spectra strong support the proposed structures of the all synthesized compounds.

3.2. In silico docking study

The X-ray crystallographic structures used in this study were selected in term of the quality of the atomic model obtained from the crystallographic data [86]. A murine COX-2 (PDB ID 3nt1) and an ovine COX-1 (PDB ID 4o1z) X-ray crystallographic structures were selected to study the predicted binding mode of the ligands with COX isoenzymes. The PDB 3nt1 and PDB 4o1z were described as COX-2 and COX-1 structures respectively with highest resolution to date, 1.7 Å and 2.4 Å, respectively [87], which means that there is a more confidence in the location of atoms in the electron density map. Also the R-value was less 0.16, indicating a strong agreement between the crystallographic model and the experimental X-ray diffraction data [88,89].

To validate the computational method, it was used the RSMD variation (less than 2Å) for IND, DCF and CCB individually, as reference drugs, into the active site of both COX-1 and COX-2 isoforms and we found the same binding cleft residues reported by other authors [90–92] The IND and DCF are non selective COX inhibitors, that inhibit both types of the COX enzymes, whereas CCB is a preferentially COX-2 selective inhibitor. It was found also that all reference drugs have polar interactions with the catalytic site of both COX-1 and COX-2.

As expected, IND was approximately equipotent against COX-1 and COX-2, but more active against COX-2 than DCF (Table 1), although the both drugs belong to the same chemical class, being acetic acid derivatives. More specific, it was showed that IND and DCF bound deeply into the COX-2 active site in very similar conformation, when their corresponding carboxylate moiety forms two strong hydrogen bonds to the side chain of Arg120 (1.8 Å) and Tyr355 (2.7 Å). In addition, IND formed an extra hydrogen bond with Ser530 (3.2 Å) through benzoyl moiety, which explains why IND showed an enhancing affinity to COX isoenzymes compared to DCF.

It was noted that the free carboxylate moiety, common for IND and DCF, is responsible for non selective inhibition of the COX isoenzymes, being in accordance with the literature data [93,94]. That's why it forms a salt bridge with the basic nitrogen of Arg120, being responsible for the conformational change of COX isoenzymes.

Referring to the CCB, which is a substituted pyrazole derivative, it was showed that the most important for binding to COX are its phenyl sulfonamide substituent and pyrazole ring. Sulfonamide group forms four strong hydrogen bonds with the side chains of Gly519 (3.3 Å), His90 (2.2 Å), Gly354 (3.3 Å) and Leu352 (2.1 Å) of the enlarged polar pocket from COX-2. Moreover, pyrazole ring interacts with Tyr355 (3.3 Å) *via* an extra hydrogen bond, which explain high COX-2 selectivity of CCB.

In order to calculate the Gibbs free energies (ΔG) of NO-IND-TZDs (**6a-s**) each ligand-receptor complex was subjected to careful analysis for ideal docked poses on the basis of least binding energy scores and maximum number of cluster conformations and the results are presented in Table 1.

Table 1

The Gibbs free energies values (ΔG) and inhibition effect rate (Ki) of NO-IND-TZDs (**6a-s)** and of reference drugs (IND, DCF, CCB) for COX-1 and COX-2.

Ligand	COX-1		COX-2		Selectivity index $\log_{10}(Ki_{COX\text{-}1}/Ki_{COX\text{-}2})$
	ΔG (kcal/mol)	Ki (nM)	ΔG (kcal/mol)	Ki (nM)	
6a	-12.23	1.09	-8.27	872.40	-2.903
6b	-10.96	9.18	-10.07	41.59	-0.656
6c	-13.08	0.26	-11.89	1.94	-0.877
6d	-11.90	1.90	-11.07	7.74	-0.609
6e	-10.96	9.20	-8.73	397.62	-1.635
6f	-11.06	7.83	-11.07	7.74	0.005
6g	-10.62	16.32	-8.06	1240	-1.880
6h	-9.56	98.66	-7.68	2350	-1.376
6i	-12.43	0.77	-9.76	70.25	-1.957
6j	-11.60	3.15	-10.45	21.85	-0.841
6k	-13.72	0.09	-9.10	213.93	-3.387
6l	-11.87	1.98	-10.12	38.28	-1.286
6m	-10.91	10.12	-10.34	26.56	-0.419
6n	-11.29	5.34	-9.06	229.29	-1.632
6o	-10.34	26.52	-11.40	4.41	0.779
6p	-12.42	0.79	-8.52	568.34	-2.855
6q	-11.73	2.51	-10.44	22.22	-0.947
6r	-12.01	1.57	-10.07	41.36	-1.420
6s	-11.29	5.29	-8.97	266.20	-1.701
IND	-9.98	48.23	-10.35	25.72	0.273
DCF	-8.12	1120.00	-8.63	468.54	0.378
CCB	-8.37	737.59	-10.31	27.52	1.428

In order to establish the statistical significance of the difference between the receptors while removing ligand variances from the overall error variance, a two-way ANOVA analysis was applied. In the same manner, the difference between the ligands while removing the receptor variances from the overall error variance term was also analyzed. The results established a statistically significant difference between receptors ($F(0.5, 1, 21) = 17.4616$, $p = 0.0004$, Fcrit = 4.3247) and no difference between ligands (F(0.5, 21, 21) =1.3707, p =0.2380, Fcrit =2.0841).

Therefore, the ligand's (**6a-s**) effect over the COX-1 and COX-2 isoenzymes don't differ significantly (the compounds have affinity to the both receptors), but the accessibility of COX-1 and COX-2 for binding the ligands differ significantly. The estimated free binding energy of the reference drugs (IND, DCF and CCB) has a higher negative value for the COX-2 than COX-1, so less energy is needed to stabilize the drug at the ligand binding center (Table 1).

To estimate the selectivity of docked NO-IND-TZDs (**6a-s**) for COX isoenzymes a selectivity index was calculated based on logarithm of ratio between calculated inhibitory constant (Ki) for COX-1 and COX-2 ($\log_{10}Ki_{COX\text{-}1}/Ki_{COX\text{-}2}$) (Table 1, Fig. 4).

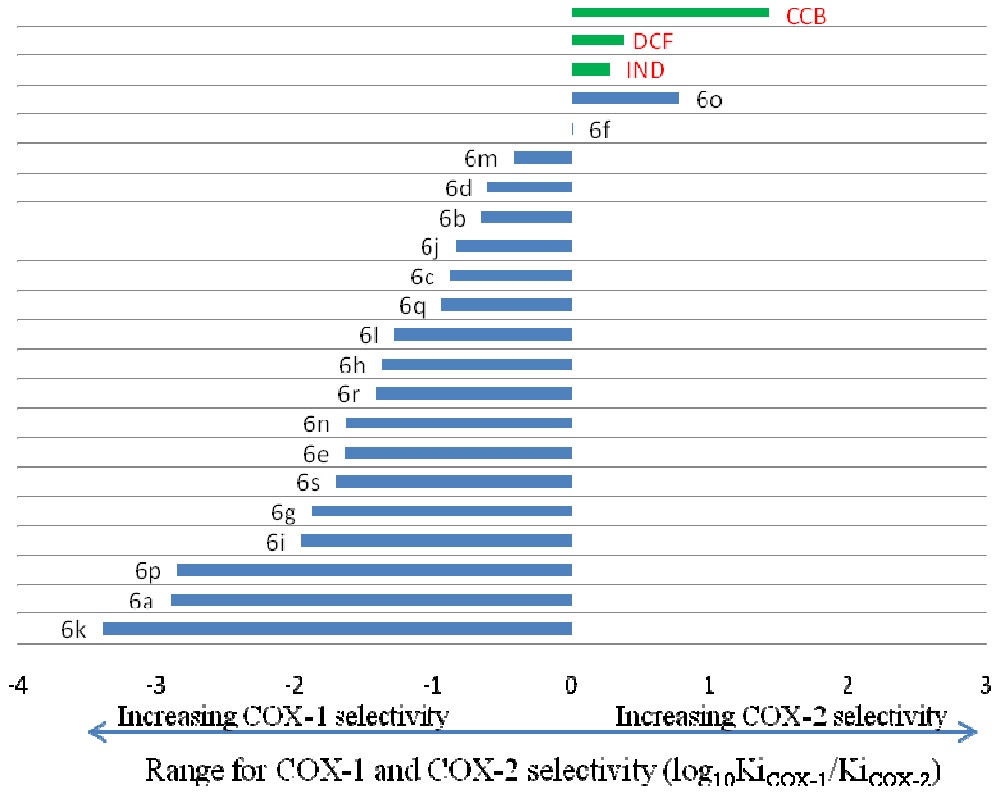

Fig. 4. The COX selectivity of NO-IND-TZDs (**6a-s**) in respect to references drugs.

It was noted that studied compounds are COX-1 selective except **6o,** which is COX-2 selective, with improved selective index in reference with IND and DCF (Fig. 4).

The COX binding pocket is a hydrophobic channel that is extended from the membrane binding domain of the COX isoenzymes that comprises four α-helices that create a hydrophobic surface to the core of the catalytic domain. At the apex of the channel, both isoenzymes have two important amino acids Ser530 and Tyr385. Ser530 is the amino acid targeted by different NSAIDs and influences the COX stereochemistry in prostaglandins synthesis. The catalytic residue Tyr385 is located at the top of the cannel and is involved in the hydroperoxidase activity. Arg120 and Tyr355 are two charged amino acids present in the COX active site of both isoenzymes, which form together a narrow constriction in the channel towards the bottom of the COX active site. The main difference between the active sites of both COX isoenzymes is the replacement of Ile (Ile434 and Ile523) in COX-1 by less bulky amino acid Val (Val434 and Val523) in COX-2. The loss of a single methylene group (Ile *vs* Val) is sufficient to open a secondary internal hydrophobic side pocket in COX-2 that enlarging the volume of the active site by approximately 25% and giving access to Arg513 replaced in COX-1 by a His.

The binding mode of NO-IND-TZDs (**6a-s)** to COX-1 side pocket is quite similar (Fig. 5a) for all compounds, they having affinity for hydrophobic channel. It was noted that NO releasing chain and 1,3-thiazolidine-4-one moiety interact with amino acids from entrance of the active site (Arg120, Tyr355, Glu524, Val116) while the indole structure (IND) interacts with the amino acids from inside of pocket (Ala527, Ser530, Tyr385, Ile523).

Referring to the binding of NO-IND-TZDs (**6a-s)** to COX-2 it was noted differences between compounds. However it was observed that all compounds interact with amino acids both from the narrow constriction and the inside of COX-2 active site, especially with the site pocket (delimited by Val523, Phe518, Arg513, Ala516, Gln192, His90, Tyr355) and extra space (delimited by Leu384, Leu503, Tyr385, Trp387) (Fig. 5b).

Based on docking results we can appreciate that NO-IND-TZDs (**6a-s)** are bulky and can block the access of arachidonic acid (physiological substrate) to the active site of COX isoenzymes.

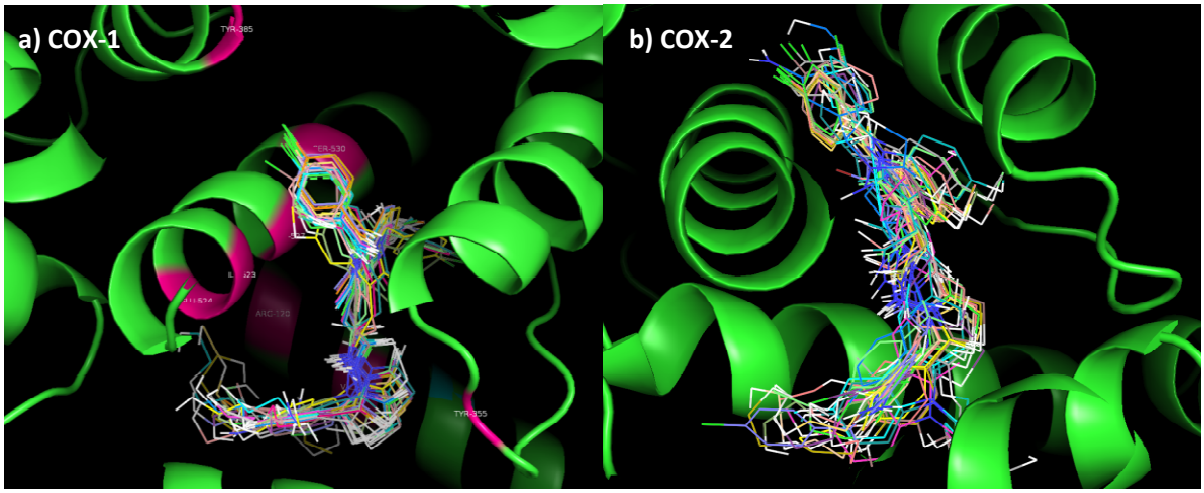

Fig. 5. Binding mode of **6a-s** to the active site of COX-1 (a) and COX-2 (b).

3.3. In silico ADME-Tox study

Using the ADME-Tox evaluation, the pharmacokinetic properties and toxicity degree of the synthesized NO-IND-TZDs (**6a-s**) were predicted and the results are summarized in Table 2.

It is known that oral absorption of the drug is influenced by solubility, permeability (active and passive) across the gastrointestinal tract wall and first pass metabolism [73]. The absorption of our compounds was predicted from lipophilicity, water solubility, percentage of intestinal human absorption (HIA) properties and P-glycopretein (P-gp) inhibitor properties.

The *water solubility* was predicted using the *Silicos IT LogSw* descriptor (SwissADME) depending on which was gave a qualitative estimation of the solubility class [75]. *LogSw* values for NO-IND-TZDs were predicted to range from – 9.36 to – 7.54, being considered poorly soluble.

The *lipophilicity* was predicted using the *Consensus LogPo/w* descriptor (SwissADME), which is the arithmetic mean of five computational methods values [75]. This parameter has a significant influence on various pharmacokinetic properties such as the absorption, distribution, permeability, as well as the routes of drugs clearance [95]. Compounds with a *LogPo/w* higher than 1 or less than 4 are generally considered to have optimal physico-chemical and ADME properties for oral route [96] whereas log*Po/w* > 5 (high lipophilicity) often contributes to high metabolic turnover, low solubility and poor oral absorption [96]. For our compounds, the predicted values of *LogPo/w* ranged from 2.88 to 4.74 (Table 2).

The *pkCSM pharmacokinetics* prediction showed a good human intestinal absorption for NO-IND-TZDs, which ranged from 91.23% to 100%. These results support their good absorption in the small intestine and predict also their capacity to inhibit *P-glycoprotein I/II transport*.

Using pkCSM-pharmacokinetics, the *drug distribution* in terms of the blood brain barrier (BBB) permeability, the volume of distribution (VDss) and the fraction unbound, could be also predicted. For tested NO-IND-TZDs, the predicted values of VDss ranged from – 1.28 to – 0.66 and of fraction unbound ranged from 0.127 to 0.273. The lower VDss (< -0.15) are in agreement with lower value for the fraction of drug molecules in the plasma which are unbound (free) to proteins. It is known that only the unbound fraction of the drug is active whereas the high binding to proteins can affect both the pharmacokinetics and pharmacodynamics of drugs [95,97].

The BBB permeability is assessed using two parameters, one qualitative (BBB) and another one quantitative (LogBB). Depending of the BBB parameter value the drugs are classified as drugs with high and low permeability. More specific, a LogBB value higher 0.3 means that drug readily cross the blood brain barrier while a value less than -1, indicates a reduced permeability for this barrier [77]. BBB permeability values of NO-IND-TZDs were predicted to range from – 2.41 to - 1.49 which means that are poorly distributed to the brain.

The metabolism of NO-IND-TZDs, based on inhibition of the main cytochromes (CYP) of the P450 family (CYP1A2, CYP2C19, CYP2C9, CYP2D6 and CYP3A4), descriptors (SwissADME) was also estimated. CYP2C19 is involved in detoxifying of potential carcinogens or bio-activating environmental procarcinogens [98], CYP2C9 is the major enzyme that metabolizes drugs with a low therapeutic index [99] and CYP2D6 is very polymorphic and it metabolizes ~20% of drugs [100]. Referring to the CYP2D6, it is known that reduced or lacked activity of this enzyme reduce efficacy of the drugs or increase the occurrence of adverse effects [100]. Our compounds were predicted to inhibit all tested CYP enzymes except CYP1A2 and CYP2D6 (Tabel 2).

The *excretion* of the drugs is measured by total clearance (CLtot) and can be achieved by either the kidney and/or the liver where drugs are eliminated in the form of urine or bile, respectively [95]. Using the CLtot descriptor of pkCSM pharmacokinetics it was forecast that excretion of NO-IND-TZDs varies between – 0.174 and 0.401 log(mL/min/kg).

The assessment of *drugs toxicity*, in terms of hepatotoxicity, oral acute toxicity (LD_{50}) values, maximum tolerated dose (MRTD) and mutagenic potential using bacteria (AMES), was predicted by using pkCSM-pharmacokinetics. The hepatotoxicity descriptor predicted that all molecules could present hepatotoxicity. Predicted LD_{50} values ranged from 2.492 to 2.982 mol/kg and for MRTD between 0.47 and 0.58 log(mg/kg/day), which means the tested compounds could be toxic, but many studies, including *in vivo*, must be performed in order to confirm it. Also, most of the tested compounds showed negative results for AMES toxicity (excepting **6g**, **6m** and **6n**) indicating that they do not have mutagenic potential.

Table 2

The ADME-Tox profile of NO-IND-TZDs (**6a-s)** predicted using SwissADME and pkCSM-pharmacokinetics tools.

Comp.	Cons. Log P*o/w*	Silicos-IT LogS*w*	HIA (%)	VDss (human) (Log L/kg)	Fraction unbound (human)	BBB permeability (Log BB)	CLtot (Log mL/min/kg)	MRTD (human) (Log mg/kg/day)	LD_{50} (mol/kg)
6a	3.79	-8.23	100	-0.867	0.129	-1.496	-0.053	0.509	2.674
6b	4.01	-8.48	100	-0.972	0.136	-1.68	-0.096	0.527	2.714
6c	4.21	-8.79	100	-0.83	0.135	-1.648	0.007	0.525	2.639
6d	4.36	-8.96	100	-0.817	0.136	-1.656	-0.174	0.527	2.639
6e	3.77	-8.31	100	-0.869	0.25	-2.111	0.086	0.514	2.971
6f	4.06	-8.7	100	-0.804	0.256	-2.135	0.04	0.524	2.953
6g	2.99	-7.54	96.219	-1.236	0.211	-1.924	0.012	0.472	2.528
6h	3.75	-8.39	100	-0.876	0.262	-2.34	0.224	0.514	2.969
6i	4.76	-9.36	100	-0.767	0.147	-2.267	0.044	0.493	2.656
6j	4.22	-8.88	100	-0.845	0.155	-2.327	0.142	0.488	2.725
6k	3.8	-8.23	95.014	-0.864	0.128	-1.493	-0.047	0.515	2.67
6l	3.7	-8.31	91.227	-0.865	0.152	-1.708	0.084	0.53	2.733
6m	3.06	-7.54	92.26	-1.18	0.208	-1.976	-0.048	0.473	2.523
6n	2.88	-7.54	97.895	-1.276	0.238	-1.915	0.112	0.527	2.492
6o	4.29	-9.04	100	-0.811	0.156	-1.868	0.069	0.545	2.719
6p	3.75	-8.23	95.132	-0.885	0.127	-1.49	0.074	0.52	2.659
6q	3.84	-8.71	95.338	-0.774	0.142	-1.713	0.261	0.58	2.634
6r	3.85	-8.8	100	-0.722	0.266	-2.386	0.401	0.55	2.982
6s	4.04	-9.18	100	-0.66	0.273	-2.41	0.355	0.557	2.962

Briefly, the ADME-Tox profile predicted for NO-IND-TZDs (**6a-s**) consisted of optimal physico-chemical and ADME properties for oral administration, good absorption in the small intestine, low fraction unbound value and poorly distributed to the brain. As for metabolism the

tested compounds do not inhibit the CYP2D6 which is determinant in biotransformation processes and could have some degree of hepatotoxicity.

3.4. In vitro radical scavenging assay

The most used method to evaluate the radical scavenging effect is based on the reduction of DPPH, which is violet in ethanol solution, to yellow, in the presence of a proton or electron donating agent [101]. In order to measure the anti radicalic effect of NO-IND-TZDs, the concentration needed to decrease by 50% the initial DPPH concentration (IC_{50}), was calculated. A lower IC_{50} means a higher antioxidant effect. The values found for tested compounds (**6a-s**), reference drugs (IND and ASP) and vitamin C are showed in Table 3.

Table 3

The IC_{50} and CEAC values of NO-IND-TZDs (**6a-s**) referring to the DPPH radical scavenging effect.

Comp.	IC_{50} (mM)[a]	CEAC[a]	Comp.	IC_{50} (mM)[a]	CEAC[a]
6a	2.63 ± 0.02	0.0280 ± 0.003	**6l**	2.22 ± 0.01	0.0333 ± 0.002
6b	2.18 ± 0.01	0.0339 ± 0.002	**6m**	2.32 ± 0.01	0.0318 ± 0.001
6c	2.28 ± 0.01	0.0324 ± 0.002	**6n**	0.54 ± 0.01	0.1370 ± 0.010
6d	2.21 ±0.02	0.0334 ± 0.002	**6o**	2.17 ± 0.02	0.0341 ± 0.004
6e	2.46 ± 0.06	0.0300 ± 0.008	**6p**	1.82 ± 0.05	0.0405 ± 0.003
6f	2.58 ± 0.04	0.0286 ± 0.004	**6q**	2.78 ± 0.12	0.0266 ± 0.012
6g	2.20 ± 0.01	0.0335 ± 0.002	**6r**	2.14 ± 0.01	0.0345 ± 0.004
6h	15.64 ±1.00	0.0047 ± 0.003	**6s**	2.20 ± 0.01	0.0336 ± 0.003
6i	2.32 ± 0.01	0.0318 ± 0.002	**ASP**	4.58 ± 0.09	0.0162 ± 0.004
6j	2.25 ± 0.01	0.0329 ± 0.003	**IND**	54.36 ± 7.93	0.0014 ± 0.0002
6k	2.78 ± 0.04	0.0266 ± 0.003	**Vit C**	0.07 ± 0.01	1 ± 0

[a] The data are expressed as the mean ±SD, $n = 4$.

Moreover, to compare the antioxidant effect of the tested compounds (**6a-s)** to vitamin C, the CEAC value, that represents how many times tested compounds are more active than vitamin C, was also calculated (Fig. 6). Using one-way ANOVA test there was determined that there is a statistically significant difference ($F(20, 63) = 11891.16$, $p < 0.05$) between tested compounds. Analysis of the results revealed that all tested compounds have improved antioxidant effect compared to reference drugs (IND, ASP), the CEAC values ranging between 0.266-0.137. It can

appreciate the majority of compounds are around 23 times more active than IND (CEAC = 0.0014 ± 0.0002) and 2 times more active than ASP (CEAC = 0.016 ± 0.004). The most active compound was **6n** (CEAC = 0.137 ± 0.01), which has on the second position of 1,3-thiazolidne-4-one scaffold the 2-(4-nitrophenoxy)-ethyl nitrate as substituent, being around 100 times more active than IND. Compared to vitamin C, used as a positive control, all tested compounds were less active, the CEAC values being less than 1.

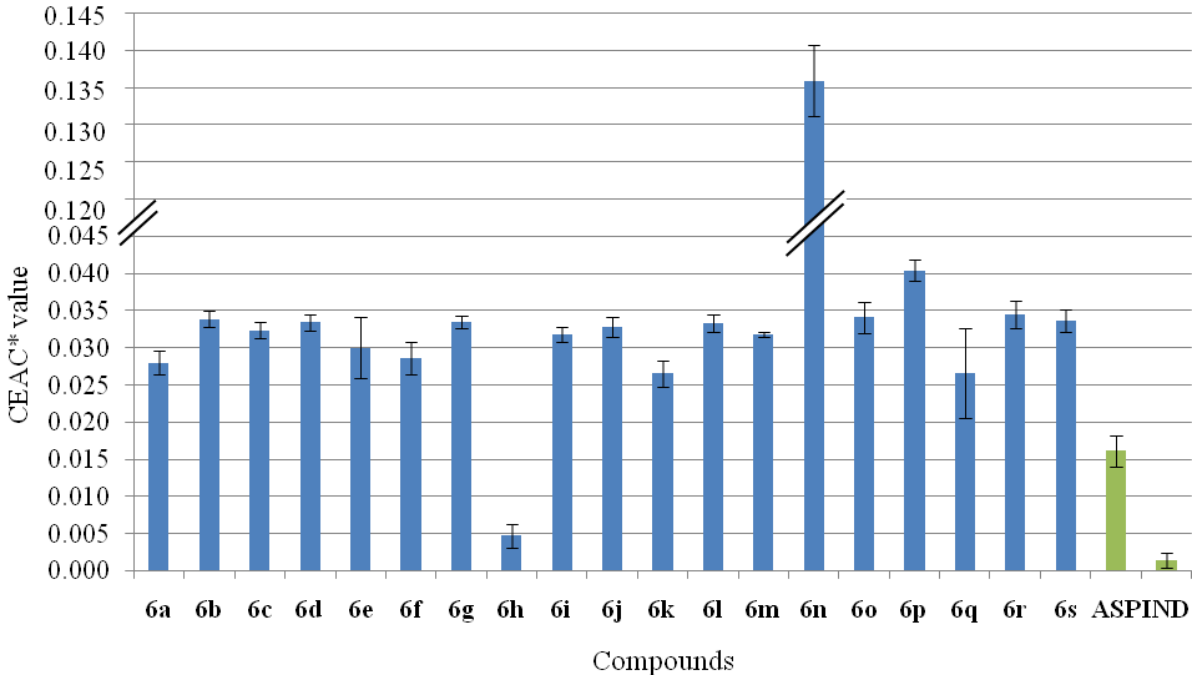

Fig. 6. The DPPH radical scavenging activity of NO-IND-TZDs (**6a-s**) and of reference drugs (IND, ASP) expressed as CEAC values (* mean ± SD, *n* = 4).

3.5. In vitro anti-inflammatory assay

The discovery of new drugs is focused primary to identification of a ligand that binds to the target protein with high affinity [102–104]. It is known that NSAIDs are strong ligands to enzymatic and non-enzymatic proteins, being proved that their anionic radicals interact with the polar amino acids of proteins whereas their lipophilic moieties are fixed into hydrophobic site of proteins [105]. Referring to the COX, different mechanisms of inhibition are known. For example, ASP has a unique therapeutic action and irreversibly inhibits COX-1 and COX-2, due to covalent acetylation of the enzymes [106-109] while IND and other aryl acetic acid

derivatives inhibit COX by a conformational change of protein [106]. In order to study the mechanism of inhibition of newly synthesized NO-IND-TZDs, IND and ASP were used as reference NSAIDs. Literature notes that ASP also induce acetylation of multiple proteins (such as human serum albumin, fibrinogen, p53, cellular protein) by *in vitro* and *in vivo* assays and extensive ASP therapy give rise of anti-acetylated serum albumin antibodies [110-112].

These interactions make changes on the native structure of the proteins as the modification of the secondary, tertiary or quaternary structure without the breaking of covalent bonds. As result, a variety of easily quantifiable physico-chemical effects are produced, which are used to predict the anti-inflammatory effects of different compounds [82].

The Mizushima's test used to evaluate the anti-inflammatory effects of the new NO-IND-TZDs **(6a-s)** is a nephelometric assay based on thermal denaturation of BSA [113]. When a chemical is incubated with a protein (BSA), an increase in optical density will occur as a result of protein precipitation [81]. Literature data report that the native states of the proteins are stable in hydrophobic solvents, whereas the proteins tend to lose their native structure in polar organic solvents like DMSO, DMFA or trifluoroethanol [114]. In addition, it was suggested that the effect of DMSO on the proteins stability depends on the concentration [115].

Because the tested compounds (**6a-s)** have poor solubility in water, DMSO (40%) was used as solvent. The our study showed that BSA, 0.2% in 0.9% NaCl/DMSO = 6/4 remained stable after incubation at 38°C for 5 h and no turbidity was observed. In similar conditions, the tested compounds (**6a-s)** cause an intense precipitation of BSA, resulting a cloudy solution.

The results, expressed as denaturation effects (%) at different concentration (50 µM, 100 µM and 150 µM) in reference with positive control (100%) are presented in Fig. 7. Using two-way ANOVA test there was determined that there is a statistically significant interaction ($F(40, 189) = 49644.649$, $p < 0.05$) between concentration and type of tested compounds on BSA denaturation process.

It was noted that the tested compounds (**6a-s**) were able to increase the albumin denaturation in a concentration dependent manner, the higher concentrations increase the denaturation effect (Fig. 8). For example, the compounds **6a**, **6k** and **6p** showed a statistically significant increasing of denaturation effect ($p < 0.05$) at 150 µM but there were no difference ($p = 0.701$) at 50 µM and 100 µM respectively. At 150 µM, compound **6k** was more active (15.04 ± 0.02%) compared with **6a** (8.44 ± 0.02%) and **6p** (3.33 ± 0.02%). Therefore, in relation with

chemical structure, we can conclude that the presence of 3-phenoxy moiety on second position of thiazolidine-4-one scaffold enhance the anti-inflammatory activity.

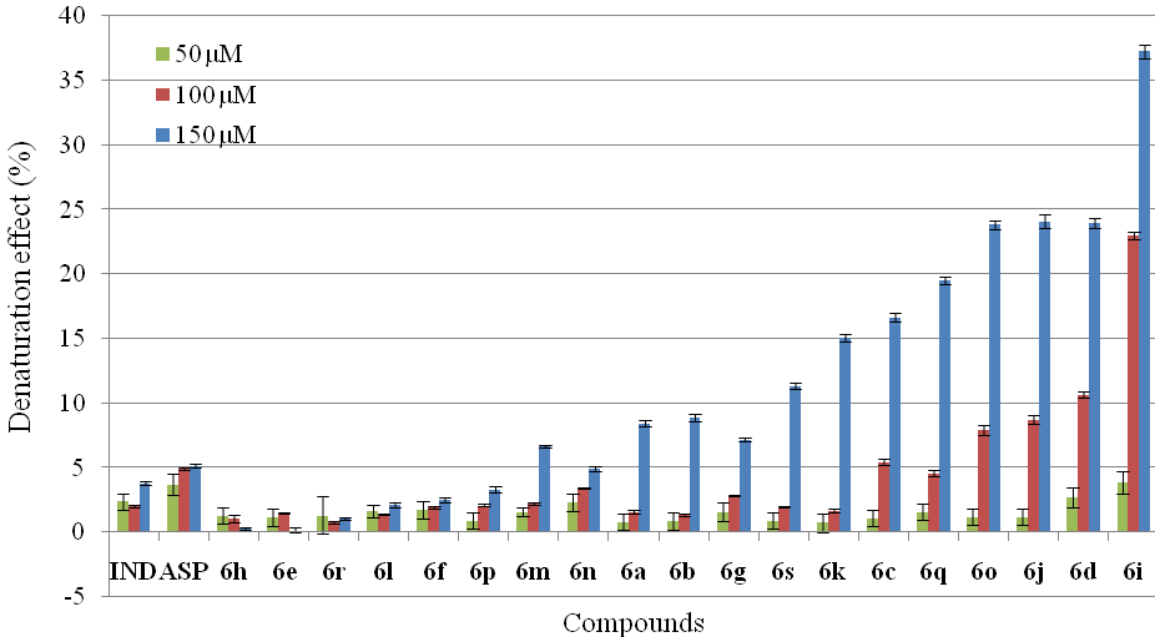

Fig. 7. The effects of NO-IND-TZDs (**6a-s**) and of reference drugs (IND, ASP) on BSA denaturation process.

As expected, ASP (4.78 ± 0.18%) bonded BSA significantly stronger ($p < 0.05$) than IND (2.65 ± 0.23%). We also noted that, comparing with the reference drugs (IND and ASP), that have the denaturation effect less 5%, the derivatives **6k**, **6c**, **6q**, **6o**, **6j**, **6d** and **6i** showed to be more active, with value between 15% and 37%.

The analysis of the results revealed that the substitution of the aromatic ring on 1,3-thiazolidne-4-one scaffold with electron withdrawing groups (like Cl, Br) as well as increase of -O-CH_2-CH_2- spacer length (from 1 unit to 2 units) increase the denaturation effect and thus promote interaction with non enzymatic proteins. The most active compound, in term of anti-inflammatory effects was **6i** which contain a (2,6-dichloro-phenoxy)ethyl nitrate moiety.

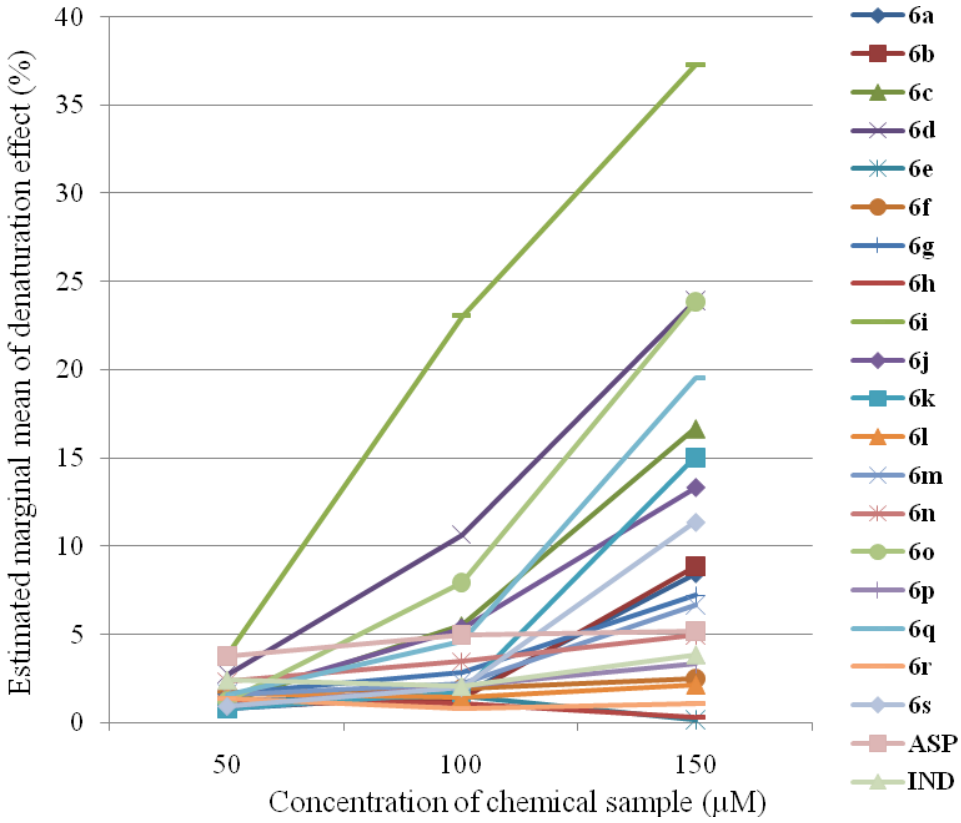

Fig. 8. The marginal mean of denaturation effect of NO-IND-TZDs (**6a-s**) and of reference drugs (IND, ASP).

3.6. In vitro nitric oxide release measurement

For detection and quantification of *in vitro* NO release by NO-IND-TZDs **(6a-s)**, a modified colorimetric Griess assay, based on decomposition of nitrate ester moiety in presence of Hg^{2+} and thiol based compounds, was used. The experiment included also reference NO donors, such as SNAP, SNP, NTG, which belong at different classes. So, NTG is a representative organic nitrate which requires specific thiol and/or enzymatic activation to generate NO, SNP is a metal nitrosyl compound that spontaneously releases NO at physiological pH and SNAP is an S-nitrosothiol which is rapidly decompose in presence of metal ions, such as Cu^{+}, Fe^{2+}, Hg^{2+} and Ag^{+}.

The NO releasing from the NO-IND-TZDs (**6a-s**) was studied in different experimental conditions in order to mimics the intestinal (PBS, PBS-GSH), and gastric (HCl, HCl-GSH) environmental conditions and the results are presented in Fig. 9 and 10.

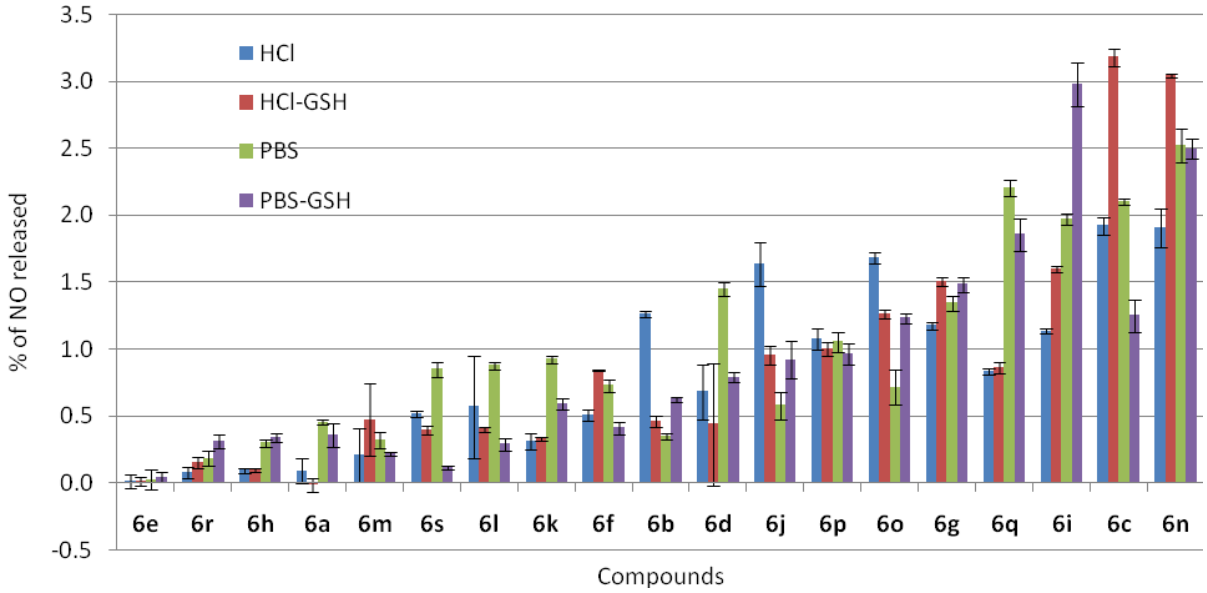

Fig. 9. The percentage (%) of NO released by NO-IND-TZDs (**6a-s**) in different experimental conditions (PBS, PBS-GSH, HCl HCl-GSH), relative to theoretical maximum release of 1.0 mol NO/mol tested compound) (n = 4)

As expected, there was a statistically significant difference between reference NO donors, as determined by one-way ANOVA ($F(2,93) = 60.729$, $p<0.05$). Post hoc comparisons using the Tukey HSD test indicated that the mean score for SNAP (52.70 ± 16.82) was significantly different than the SNP (3.97 ± 1.21) and NTG (0.49 ± 0.18) (Fig. 10). Also, by two way ANOVA it was found there was not a statistically significant interaction between used Griess reagents (NED – SULF/SULF-$HgCl_2$) and experimental conditions (PBS, PBS-GSH, HCl, HCl-GSH) on NO released (($F(3,88) = 1.029$, $p = 0.384$). Moreover, there was no statistically significant difference in mean of NO released by changing the experimental conditions (p = 0.669), but the presence of Hg^{2+} in Griess reagents increased significantly the quantified amount of NO (p = 0.002). These results suggest that the Hg^{2+} decompose the *S*-nitrosothiol from SNAP. In addition, the presence of GSH in the experimental medium can fix the free NO to form a stable S-nitrosothiol (GS-NO). It was noted also that the experimental pH did not influence significantly the amount of NO released from reference NO donors.

In order to study the interaction effects of used Griess reagents and experimental conditions on NO released from nitrate ester moiety of tested compounds (**6a-s**), two-way

ANOVA test was applied. It was found that there is no statistically significant interaction between them ($F(3, 600) = 1.454$, $p = 0.226$). Moreover, it was noted that the adding of $HgCl_2$ to SULF solution do not increase significantly the total amount of NO released from nitrate ester moiety ($F(1, 600) = 0.629$, $p = 0.428$). A statistically significant interaction between structure of compounds (**6a-s**) and experimental conditions ($F(54, 532) = 29.908$, $p < 0.05$) was noted. All these results suggest that the presence of Hg^{2+} in Griess reagents do not influence the amount of NO released by NO-IND-TZDs but it is strongly influenced by the structure of tested compounds and experimental conditions (pH and GSH presence).

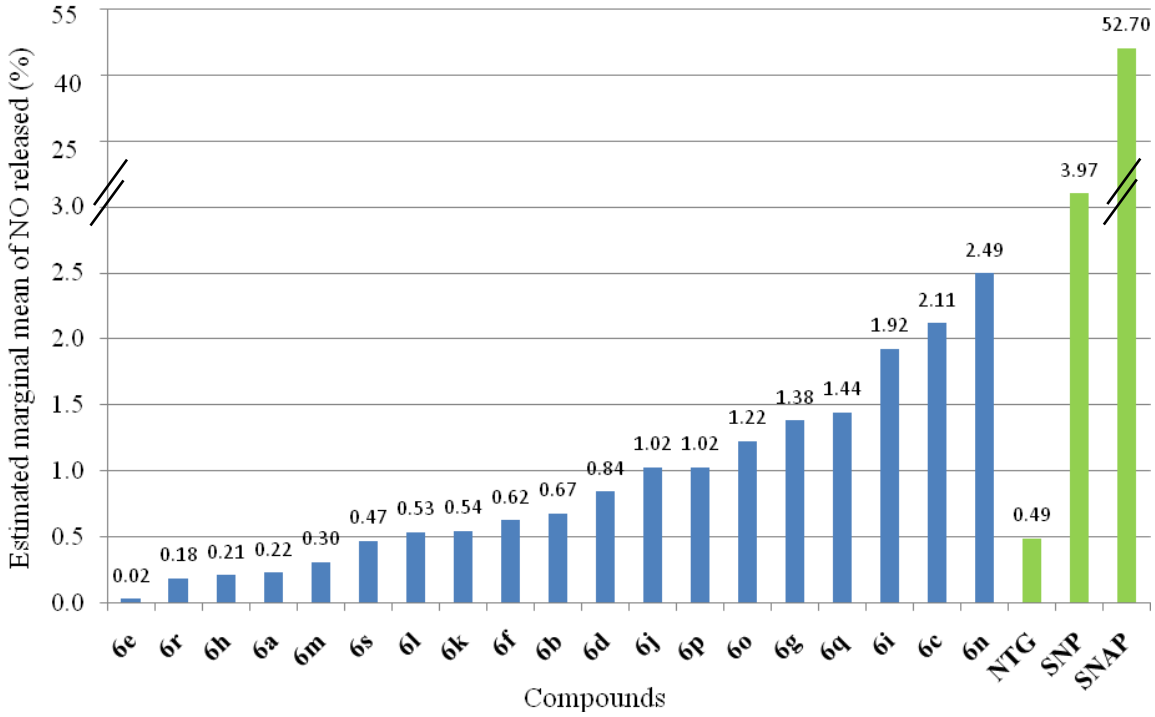

Fig. 10. The estimated marginal means of NO (%) release by NO-IND-TZDs (**6a-s**) compared to reference NO donors (NTG, SNP and SNAP).

By estimated marginal mean of NO released it was showed that the most of the tested compounds (**6a-s**) released more NO compared with NTG (Fig. 10). It was noted that the amount of NO released is influence by the position of nitrate ester moiety on aromatic ring and also by the number and type of the substituents on aromatic ring. The most proper position of nitrate ester moiety is *ortho*, **6p** (2-oxy-ethylnitrate) being more active than **6k** (3-oxy-ethylnitrate) and **6a** (4-oxy-ethylnitrate). Referring to the substitution of phenoxy-ethylnitrate moiety the presence

of electron withdrawing groups (Cl, Br, NO_2) on aromatic ring increase the NO, the most active compounds being **6o**, **6g**, **6q**, **6i**, **6c** and **6n** (Fig. 9, 10). Of these, the best compound was **6n** that consist of an oxy-ethylnitrate (*meta*) and nitro (*ortho*) radicals on aromatic ring.

In this research it was noted a strong correlation between the theoretical studies (*in silico*) with the biological tests (*in vitro*). Based on *in vitro* assay results the compounds **6k**, **6c**, **6q**, **6o**, **6j**, **6d** and **6i** showed to be the most active in term of the anti-inflammatory effects, interacting strongly with non-enzymatic proteins (BSA). These results are supported also by *in silico* docking study when the same compounds showed the higher affinity for COX isoenzyme, having thus an improved anti-inflammatory effect compared to IND. In addition, the ADME-Tox study revealed that the NO-IND-TZDs are generally proper for oral administration, having optimal physico-chemical and ADME properties. These results are in agreement with the *in vitro* assays results when an improved antioxidant effect and increase NO release were observed for tested NO-IND-TZDs, when compared to IND and NTG, respectively.

4. Conclusion

In order to improve the clinical efficiency of IND, especially for long-term use, new nitric oxide-releasing indomethacin derivatives with 1,3-thiazolidine-4-one scaffold (NO-IND-TZDs) have been synthesized, based on the beneficial effects of 1,3-thiazolidine-4-one scaffold and NO, the last one being known as an important endogenous molecule, including its critical role in GI mucosal defense. The synthesized NO-IND-TZDs were biologically evaluated using *in silico* and *in vitro* assays. The molecular docking results revealed that most of the synthesized NO-IND-TZDs are selective COX-1 inhibitors, except **6o** (with (*2-bromo-6-methoxy*phenoxy)ethyl nitrate moiety) which is COX-2 selective. Based on ADME-Tox profile, it can be concluded that NO-IND-TZDs are suitable for oral administration, showing a good absorption in the small intestine, a low fraction unbound value and a reduced distribution to the brain. The tested compounds also showed improved radical scavenging effects, the highest radical scavenging effect being noted for **6n**, which contains a 2-(*4-nitro*-phenoxy)ethyl nitrate moiety. In addition, for this compound it was also noted the highest NO release capacity, which means it could have reduced side effects to GI level such as irritation, bleeding or ulceration. Moreover, the best predicted anti-inflammatory effect, measured as BSA denaturation, was showed by **6i** which contains a (*2,6-*

dichloro-phenoxy)ethylnitrate moiety, which supports the good influence of *chloro* substituent for anti-inflammatory effects.

The results of our study strongly support the potential effect of NO-IND-TZDs as multi-target strategy, targeting the inflammation, oxidative stress and NO release, which encourage us to continue our research with *in vivo* inflammation model assays.

Acknowledgements

The authors would like to thank the Agence Universitaire de la Francophonie and Institute of Atomic Physics (AUF-IFA 2019-2020 grant, contract no. 28/2019), University of Medicine and Pharmacy "Grigore T. Popa" of Iasi grant (contract no.6985/2020), the Region Centre Val de Loire (RTR Motivhealth), the SFR neuroimagerie (SFR FED 4224), the Labex programs SYNORG (ANR-11-LABX-0029) and IRON (ANR-11-LABX-0018-01), the FEDER TECHSAB, the Ligue contre le Cancer du Grand Ouest (comités des Deux Sèvres, du Finistère, de l'Ile et Villaine, du Loir et Cher, de Loire Atlantique, du Loiret, de la Vienne), and the Canceropole Grand Ouest for their financial support.

References

[1] J.N. Fullerton, D.W. Gilroy, Resolution of inflammation: A new therapeutic frontier, Nat. Rev. Drug Discov. 15 (2016) 551–567. https://doi.org/10.1038/nrd.2016.39.

[2] R. Medzhitov, Origin and physiological roles of inflammation, Nature. 454 (2008). https://doi.org/10.1038/nature07201.

[3] M. Mollaei, A. Abbasi, Z.M. Hassan, N. Pakravan, The intrinsic and extrinsic elements regulating inflammation, Life Sci. 260 (2020). https://doi.org/10.1016/j.lfs.2020.118258.

[4] C.N. Serhan, S.K. Gupta, M. Perretti, C. Godson, E. Brennan, Y. Li, O. Soehnlein, T. Shimizu, O. Werz, V. Chiurchiù, A. Azzi, M. Dubourdeau, S.S. Gupta, P. Schopohl, M. Hoch, D. Gjorgevikj, F.M. Khan, D. Brauer, A. Tripathi, K. Cesnulevicius, D. Lescheid, M. Schultz, E. Särndahl, D. Repsilber, R. Kruse, A. Sala, J.Z. Haeggström, B.D. Levy, J.G. Filep, O. Wolkenhauer, The Atlas of Inflammation Resolution (AIR), Mol. Aspects Med. 74 (2020). https://doi.org/10.1016/j.mam.2020.100893.

[5] A.U. Ahmed, An overview of inflammation: Mechanism and consequences, Front. Biol. China. 6 (2011) 274–281. https://doi.org/10.1007/s11515-011-1123-9.

[6] V. Tyagi, V.K. Singh, P.K. Sharma, V. Singh, Essential oil-based nanostructures for inflammation and rheumatoid arthritis, J. Drug Deliv. Sci. Technol. 60 (2020). https://doi.org/10.1016/j.jddst.2020.101983.

[7] M.C. Fantini, I. Guadagni, From inflammation to colitis-associated colorectal cancer in inflammatory bowel disease: Pathogenesis and impact of current therapies, Dig. Liver Dis. (2021). https://doi.org/10.1016/j.dld.2021.01.012.

[8] M. Díaz-Ruiz, M.L. Martínez-Triguero, A. López-Ruiz, F. Fernández-de la Cruz, C. Bañuls, A. Hernández-Mijares, Metabolic disorders and inflammation are associated with familial combined hyperlipemia, Clin. Chim. Acta. 490 (2019) 194–199. https://doi.org/10.1016/j.cca.2018.09.009.

[9] S. Tsalamandris, A.S. Antonopoulos, E. Oikonomou, G. Papamikroulis, G. Vogiatzi, S. Papaioannou, S. Deftereos, D. Tousoulis, The Role of Inflammation in Diabetes: Current Concepts and Future Perspectives, Eur. Cardiol. Rev. 14 (2019) 50–59. https://doi.org/10.15420/ecr.2018.33.1.

[10] D. Karunakaran, A.W. Turner, A.C. Duchez, S. Soubeyrand, A. Rasheed, D. Smyth, D.P. Cook, M. Nikpay, J.W. Kandiah, C. Pan, M. Geoffrion, R. Lee, L. Boytard, H. Wyatt, M.A. Nguyen, P. Lau, M. Laakso, B. Ramkhelawon, M. Alvarez, K.H. Pietiläinen, P. Pajukanta, B.C. Vanderhyden, P. Liu, S.B. Berger, P.J. Gough, J. Bertin, M.E. Harper, A.J. Lusis, R. McPherson, K.J. Rayner, RIPK1 gene variants associate with obesity in humans and can be therapeutically silenced to reduce obesity in mice, Nat. Metab. 2 (2020) 1113–1125. https://doi.org/10.1038/s42255-020-00279-2.

[11] A. Alfaddagh, S.S. Martin, T.M. Leucker, E.D. Michos, M.J. Blaha, C.J. Lowenstein, S.R. Jones, P.P. Toth, Inflammation and cardiovascular disease: From mechanisms to therapeutics, Am. J. Prev. Cardiol. 4 (2020) 100130. https://doi.org/10.1016/j.ajpc.2020.100130.

[12] A.M. Sethwala, I. Goh, J. V Amerena, Combating In fl ammation in Cardiovascular Disease, (2021) 197–206.

[13] T. Wyss-Coray, L. Mucke, Inflammation in neurodegenerative disease - A double-edged sword, Neuron. 35 (2002) 419–432. https://doi.org/10.1016/S0896-6273(02)00794-8.

[14] J.W. Kinney, S.M. Bemiller, A.S. Murtishaw, A.M. Leisgang, A.M. Salazar, B.T. Lamb, Inflammation as a central mechanism in Alzheimer's disease, Alzheimer's Dement. Transl. Res. Clin. Interv. 4 (2018) 575–590. https://doi.org/10.1016/j.trci.2018.06.014.

[15] L.M. Collins, A. Toulouse, T.J. Connor, Y.M. Nolan, Contributions of central and systemic inflammation to the pathophysiology of Parkinson's disease, Neuropharmacology. 62 (2012) 2154–2168. https://doi.org/10.1016/j.neuropharm.2012.01.028.

[16] A. Fishbein, B.D. Hammock, C.N. Serhan, D. Panigrahy, Carcinogenesis: Failure of resolution of inflammation?, Pharmacol. Ther. 218 (2021) 107670. https://doi.org/10.1016/j.pharmthera.2020.107670.

[17] C.G. Honnappa, U.M. Kesavan, A concise review on advances in development of small molecule anti-inflammatory therapeutics emphasising AMPK: An emerging target, Int. J. Immunopathol. Pharmacol. 29 (2016) 562–571. https://doi.org/10.1177/0394632016673369.

[18] K. Wang, J. Xiao, X. Liu, Z. Jiang, Y. Zhan, T. Yin, L. He, F. Zhang, S. Xing, B. Chen, Y. Li, F. Zhang, Z. Kuang, B. Du, J. Gu, AICD: an integrated anti-inflammatory compounds database for drug discovery, Sci. Rep. 9 (2019) 1–10. https://doi.org/10.1038/s41598-019-44227-x.

[19] K. Świacka, A. Michnowska, J. Maculewicz, M. Caban, K. Smolarz, Toxic effects of NSAIDs in non-target species: A review from the perspective of the aquatic environment, Environ. Pollut. 273 (2021) 115891. https://doi.org/10.1016/j.envpol.2020.115891.

[20] A.K. Dwivedi, V. Gurjar, S. Kumar, N. Singh, Molecular basis for nonspecificity of nonsteroidal anti-inflammatory drugs (NSAIDs), Drug Discov. Today. 20 (2015) 863–873. https://doi.org/10.1016/j.drudis.2015.03.004.

[21] G. Kaur, O. Silakari, Multiple target-centric strategy to tame inflammation, Future Med. Chem. 9 (2017) 1361–1376. https://doi.org/10.4155/fmc-2017-0050.

[22] P.G. Conaghan, A turbulent decade for NSAIDs: Update on current concepts of classification, epidemiology, comparative efficacy, and toxicity, Rheumatol. Int. 32 (2012) 1491–1502. https://doi.org/10.1007/s00296-011-2263-6.

[23] N. Moore, M. Duong, S.E. Gulmez, P. Blin, C. Droz, Pharmacoepidemiology of non-steroidal anti-inflammatory drugs, (2019).

[24] P. Pirlamarla, R.M. Bond, FDA labeling of NSAIDs: Review of nonsteroidal anti-inflammatory drugs in cardiovascular disease, Trends Cardiovasc. Med. 26 (2016) 675–680. https://doi.org/10.1016/j.tcm.2016.04.011.

[25] N. Kangwan, J.M. Park, K.B. Hahm, Development of GI-safe NSAID; Progression from the bark of willow tree to modern pharmacology, Curr. Opin. Pharmacol. 19 (2014) 17–23. https://doi.org/10.1016/j.coph.2014.06.003.

[26] S. Lucas, The Pharmacology of Indomethacin, Headache J. Head Face Pain. 56 (2016) 436–446. https://doi.org/10.1111/head.12769.

[27] M.F.A. Mohamed, A.A. Marzouk, A. Nafady, D.A. El-Gamal, R.M. Allam, G.E.D.A. Abuo-

Rahma, H.I. El Subbagh, A.H. Moustafa, Design, synthesis and molecular modeling of novel aryl carboximidamides and 3-aryl-1,2,4-oxadiazoles derived from indomethacin as potent anti-inflammatory iNOS/PGE2 inhibitors, Bioorg. Chem. 105 (2020). https://doi.org/10.1016/j.bioorg.2020.104439.
[28] K. Stachowicz, Indomethacin, a nonselective cyclooxygenase inhibitor, does not interact with MTEP in antidepressant-like activity, as opposed to imipramine in CD-1 mice, Eur. J. Pharmacol. 888 (2020) 173585. https://doi.org/10.1016/j.ejphar.2020.173585.
[29] S. Wongrakpanich, A. Wongrakpanich, K. Melhado, J. Rangaswami, A comprehensive review of non-steroidal anti-inflammatory drug use in the elderly, Aging Dis. 9 (2018) 143–150. https://doi.org/10.14336/AD.2017.0306.
[30] A. Koeberle, O. Werz, Multi-target approach for natural products in inflammation, Drug Discov. Today. 19 (2014) 1871–1882. https://doi.org/10.1016/j.drudis.2014.08.006.
[31] V.L.H. Tatakihara, A.D. Malvezi, C. Panis, R. Cecchini, N.G. Zanluqui, L.M. Yamauchi, M.I.L. Martins, R.V. Da Silva, S.F. Yamada-Ogatta, L.V. Rizzo, M.C. Martins-Pinge, P. Pinge-Filho, Nitric oxide-releasing indomethacin enhances susceptibility to Trypanosoma cruzi infection acting in the cell invasion and oxidative stress associated with anemia, Chem. Biol. Interact. 227 (2015) 104–111. https://doi.org/10.1016/j.cbi.2014.12.024.
[32] J.L. Williams, S. Borgo, I. Hasan, E. Castillo, F. Traganos, B. Rigas, Nitric oxide-releasing nonsteroidal anti-inflammatory drugs (NSAIDs) alter the kinetics of human colon cancer cell lines more effectively than traditional NSAIDs: Implications for colon cancer chemoprevention, Cancer Res. 61 (2001) 3285–3289.
[33] M.N. Hughes, Chemistry of Nitric Oxide and Related Species, in: Methods Enzymol., 2008: pp. 3–19. https://doi.org/10.1016/S0076-6879(08)36001-7.
[34] D. Procházková, N. Wilhelmová, M. Pavlík, Reactive Nitrogen Species and Nitric Oxide, in: Nitric Oxide Action Abiotic Stress Responses Plants, Springer International Publishing, Cham, 2015: pp. 3–19. https://doi.org/10.1007/978-3-319-17804-2_1.
[35] J.O. Lundberg, E. Weitzberg, Nitric Oxide Formation From Inorganic Nitrate, in: Nitric Oxide, Third Edit, Elsevier, 2017: pp. 157–171. https://doi.org/10.1016/B978-0-12-804273-1.00012-0.
[36] D.L.H. WILLIAMS, Nitric oxide in biological systems, in: Nitrosation React. Chem. Nitric Oxide, Elsevier, 2004: pp. 187–198. https://doi.org/10.1016/B978-044451721-0/50012-8.
[37] S. Kumar, R.K. Singh, T.R. Bhardwaj, Therapeutic role of nitric oxide as emerging molecule, Biomed. Pharmacother. 85 (2017) 182–201. https://doi.org/10.1016/j.biopha.2016.11.125.
[38] J.N. Sharma, A. Al-Omran, S.S. Parvathy, Role of nitric oxide in inflammatory diseases, Inflammopharmacology. 15 (2007) 252–259. https://doi.org/10.1007/s10787-007-0013-x.
[39] D.G. Hirst, T. Robson, Nitric Oxide Physiology and Pathology, in: Methods Mol. Biol., 2011: pp. 1–13. https://doi.org/10.1007/978-1-61737-964-2_1.
[40] A. Lanas, Role of nitric oxide in the gastrointestinal tract, Arthritis Res. Ther. 10 (2008) S4. https://doi.org/10.1186/ar2465.
[41] A.P.M. Santana, B.M. Tavares, L.T. Lucetti, F.S. Gouveia, R.A. Ribeiro, P.M.G. Soares, E.H.S. Sousa, L.G.F. Lopes, J.-V.R. Medeiros, M.H.L.P. Souza, The nitric oxide donor cis-[Ru(bpy)2(SO3)NO](PF6) increases gastric mucosa protection in mice – Involvement of the soluble guanylate cyclase/KATP pathway, Nitric Oxide. 45 (2015) 35–42. https://doi.org/10.1016/j.niox.2015.02.002.
[42] F. Spiller, R. Oliveira Formiga, J. Fernandes da Silva Coimbra, J.C. Alves-Filho, T.M. Cunha, F.Q. Cunha, Targeting nitric oxide as a key modulator of sepsis, arthritis and pain, Nitric Oxide. 89 (2019) 32–40. https://doi.org/10.1016/j.niox.2019.04.011.
[43] N. Sahiba, A. Sethiya, J. Soni, D.K. Agarwal, S. Agarwal, Saturated Five-Membered Thiazolidines and Their Derivatives: From Synthesis to Biological Applications, Springer International Publishing, 2020. https://doi.org/10.1007/s41061-020-0298-4.
[44] M.R. Bockman, C.A. Engelhart, J.D. Cramer, M.D. Howe, N.K. Mishra, M. Zimmerman, P. Larson, N. Alvarez-Cabrera, S.W. Park, H.I.M. Boshoff, J.M. Bean, V.G. Young, D.M. Ferguson,

V. Dartois, J.T. Jarrett, D. Schnappinger, C.C. Aldrich, Investigation of (S)-(-)-acidomycin: A selective antimycobacterial natural product that inhibits biotin synthase, ACS Infect. Dis. 5 (2019) 598–617. https://doi.org/10.1021/acsinfecdis.8b00345.
[45] N. Trotsko, Antitubercular properties of thiazolidin-4-ones – A review, Eur. J. Med. Chem. (2021) 113266. https://doi.org/10.1016/j.ejmech.2021.113266.
[46] U. Schmidt, R. Utz, A. Lieberknecht, H. Griesser, B. Potzolli, J. Bahr, K. Wagner, P. Fischer, Amino Acids and Peptides; 59. 1 Synthesis of Biologically Active Cyclopeptides; 9. 2 Synthesis of 16 Isomers of Dolastatin 3; 3 I. Synthesis of the 2-(1-aminoalkyl)-thiazole-4-carboxylic Acids, Synthesis (Stuttg). 1987 (1987) 233–236. https://doi.org/10.1055/s-1987-27899.
[47] M. Mishchenko, S. Shtrygol, D. Kaminskyy, Thiazole-Bearing 4-Thiazolidinones as New Anticonvulsant Agents, (2020).
[48] M. Nazeef, K. Neha, S. Ali, K. Ansari, M. Danish, S.K. Tiwari, V. Yadav, I.R. Siddiqui, Journal of Photochemistry & Photobiology A : Chemistry Visible-light-promoted C e N and C e S bonds formation : A catalyst and solvent-free photochemical approach for the synthesis of 1 , 3-thiazolidin-4- ones, 390 (2020).
[49] Ł. Popiołek, I. Piątkowska-Chmiel, M. Gawrońska-Grzywacz, A. Biernasiuk, M. Izdebska, M. Herbet, M. Sysa, A. Malm, J. Dudka, M. Wujec, New hydrazide-hydrazones and 1,3-thiazolidin-4-ones with 3-hydroxy-2-naphthoic moiety: Synthesis, in vitro and in vivo studies, Biomed. Pharmacother. 103 (2018) 1337–1347. https://doi.org/10.1016/j.biopha.2018.04.163.
[50] S. Huber-Villaume, G. Revelant, E. Sibille, S. Philippot, A. Morabito, S. Dunand, P. Chaimbault, D. Bagrel, G. Kirsch, S. Hesse, H. Schohn, 2-(Thienothiazolylimino)-1,3-thiazolidin-4-ones inhibit cell division cycle 25 A phosphatase, Bioorg. Med. Chem. 24 (2016) 2920–2928. https://doi.org/10.1016/j.bmc.2016.04.063.
[51] A. Pejović, A. Minić, J. Jovanović, M. Pešić, D.I. Komatina, I. Damljanović, D. Stevanović, V. Mihailović, J. Katanić, G.A. Bogdanović, Synthesis, characterization, antioxidant and antimicrobial activity of novel 5-arylidene-2-ferrocenyl-1,3-thiazolidin-4-ones, J. Organomet. Chem. 869 (2018) 1–10. https://doi.org/10.1016/j.jorganchem.2018.05.014.
[52] N. Agrawal, Synthetic and therapeutic potential of 4-thiazolidinone and its analogs, Curr. Chem. Lett. 10 (2021) 119–138. https://doi.org/10.5267/j.ccl.2020.11.002.
[53] L.R.S. Dias, R.R.S. Salvador, Pyrazole carbohydrazide derivatives of pharmaceutical interest, Pharmaceuticals (Basel). 5 (2012) 317–324. https://doi.org/10.3390/ph5030317.
[54] S. Thota, D.A. Rodrigues, P. de S.M. Pinheiro, L.M. Lima, C.A.M. Fraga, E.J. Barreiro, N-Acylhydrazones as drugs, Bioorg. Med. Chem. Lett. 28 (2018) 2797–2806. https://doi.org/https://doi.org/10.1016/j.bmcl.2018.07.015.
[55] E. Ebrahimzadeh, S.A. Tabatabai, R. Vahabpour, Z. Hajimahdi, A. Zarghi, Design, Synthesis, Molecular Modeling Study and Biological Evaluation of New N'-Arylidene-pyrido [2,3-d]pyrimidine-5-carbohydrazide Derivatives as Anti-HIV-1 Agents, Iran. J. Pharm. Res. IJPR. 18 (2019) 237–248. https://doi.org/10.22037/ijpr.2019.112198.13597.
[56] A. Stefanucci, G. Macedonio, S. Dvorácskó, C. Tömböly, A. Mollica, Novel Fubinaca/Rimonabant hybrids as endocannabinoid system modulators, Amino Acids. 50 (2018) 1595–1605. https://doi.org/10.1007/s00726-018-2636-1.
[57] M.P. Dimmito, A. Stefanucci, S. Pieretti, P. Minosi, S. Dvorácskó, C. Tömböly, G. Zengin, A. Mollica, Discovery of orexant and anorexant agents with indazole scaffold endowed with peripheral antiedema activity, Biomolecules. 9 (2019) 1–20. https://doi.org/10.3390/biom9090492.
[58] A. Mollica, S. Pelliccia, V. Famiglini, A. Stefanucci, G. Macedonio, A. Chiavaroli, G. Orlando, L. Brunetti, C. Ferrante, S. Pieretti, E. Novellino, S. Benyhe, F. Zador, A. Erdei, E. Szucs, R. Samavati, S. Dvrorasko, C. Tomboly, R. Ragno, A. Patsilinakos, R. Silvestri, Exploring the first Rimonabant analog-opioid peptide hybrid compound, as bivalent ligand for CB1 and opioid receptors, J. Enzyme Inhib. Med. Chem. 32 (2017) 444–451. https://doi.org/10.1080/14756366.2016.1260565.
[59] A.E. Khodir, Y.A. Samra, E. Said, A novel role of nifuroxazide in attenuation of sepsis-associated

acute lung and myocardial injuries; role of TLR4/NLPR3/IL-1β signaling interruption, Life Sci. 256 (2020) 117907. https://doi.org/https://doi.org/10.1016/j.lfs.2020.117907.
[60] K. Sztanke, A. Maziarka, A. Osinka, M. Sztanke, An insight into synthetic Schiff bases revealing antiproliferative activities in vitro, Bioorg. Med. Chem. 21 (2013) 3648–3666. https://doi.org/https://doi.org/10.1016/j.bmc.2013.04.037.
[61] P.S. Mahajan, M.D. Nikam, V.M. Khedkar, P.C. Jha, D. Sarkar, C.H. Gill, Synthesis, biological evaluation and molecular docking studies of N-acylheteroaryl hydrazone derivatives as antioxidant and anti-inflammatory agents, Res. Chem. Intermed. 42 (2016) 2707–2729. https://doi.org/10.1007/s11164-015-2176-1.
[62] K. Hada, A. Suda, K. Asoh, T. Tsukuda, M. Hasegawa, Y. Sato, K. Ogawa, S. Kuramoto, Y. Aoki, N. Shimma, T. Ishikawa, H. Koyano, Angiogenesis inhibitors identified by cell-based high-throughput screening: Synthesis, structure–activity relationships and biological evaluation of 3-[(E)-styryl]benzamides that specifically inhibit endothelial cell proliferation, Bioorg. Med. Chem. 20 (2012) 1442–1460. https://doi.org/10.1016/j.bmc.2011.12.058.
[63] C.P. Ortmeyer, G. Haufe, K. Schwegmann, S. Hermann, M. Schäfers, F. Börgel, B. Wünsch, S. Wagner, V. Hugenberg, Synthesis and evaluation of a [18 F]BODIPY-labeled caspase-inhibitor, Bioorg. Med. Chem. 25 (2017) 2167–2176. https://doi.org/10.1016/j.bmc.2017.02.033.
[64] M. del Carmen Gimenez-Lopez, M.T. Räisänen, T.W. Chamberlain, U. Weber, M. Lebedeva, G.A. Rance, G.A.D. Briggs, D. Pettifor, V. Burlakov, M. Buck, A.N. Khlobystov, Functionalized Fullerenes in Self-Assembled Monolayers, Langmuir. 27 (2011) 10977–10985. https://doi.org/10.1021/la200654n.
[65] X. Liu, Y. Yang, X. Wang, K. Wang, J. Liu, L. Lei, X. Luo, R. Zhai, F. Fu, H. Wang, Y. Bi, Design, synthesis and biological evaluation of novel α-hederagenin derivatives with anticancer activity, Eur. J. Med. Chem. 141 (2017) 427–439. https://doi.org/10.1016/j.ejmech.2017.09.016.
[66] J. Liu, C. Zhang, H. Wang, L. Zhang, Z. Jiang, J. Zhang, Z. Liu, H. Chen, Incorporation of nitric oxide donor into 1,3-dioxyxanthones leads to synergistic anticancer activity, Eur. J. Med. Chem. 151 (2018) 158–172. https://doi.org/10.1016/j.ejmech.2018.03.072.
[67] A. Nortcliffe, I.N. Fleming, N.P. Botting, D. O'Hagan, Synthesis and anticancer properties of RGD peptides conjugated to nitric oxide releasing functional groups and abiraterone, Tetrahedron. 70 (2014) 8343–8347. https://doi.org/10.1016/j.tet.2014.09.004.
[68] X. Zhang, M. Breslav, J. Grimm, K. Guan, A. Huang, F. Liu, C.A. Maryanoff, D. Palmer, M. Patel, Y. Qian, C. Shaw, K. Sorgi, S. Stefanick, D. Xu, A New Procedure for Preparation of Carboxylic Acid Hydrazides, J. Org. Chem. 67 (2002) 9471–9474. https://doi.org/10.1021/jo026288n.
[69] L.C. Chan, B.G. Cox, Kinetics of Amide Formation through Carbodiimide/ N-Hydroxybenzotriazole (HOBt) Couplings, J. Org. Chem. 72 (2007) 8863–8869. https://doi.org/10.1021/jo701558y.
[70] D. Pires Gouvea, F.A. Vasconcellos, G. dos Anjos Berwaldt, A.C.P.S. Neto, G. Fischer, R.P. Sakata, W.P. Almeida, W. Cunico, 2-Aryl-3-(2-morpholinoethyl)thiazolidin-4-ones: Synthesis, anti-inflammatory in vivo, cytotoxicity in vitro and molecular docking studies, Eur. J. Med. Chem. 118 (2016) 259–265. https://doi.org/10.1016/j.ejmech.2016.04.028.
[71] K.R.A. Abdellatif, M.A. Abdelgawad, H.A.H. Elshemy, S.S.R. Alsayed, Design, synthesis and biological screening of new 4-thiazolidinone derivatives with promising COX-2 selectivity, anti-inflammatory activity and gastric safety profile, Bioorg. Chem. 64 (2016) 1–12. https://doi.org/10.1016/j.bioorg.2015.11.001.
[72] F.X. Domínguez-Villa, N.A. Durán-Iturbide, J.G. Ávila-Zárraga, Synthesis, molecular docking, and in silico ADME/Tox profiling studies of new 1-aryl-5-(3-azidopropyl)indol-4-ones: Potential inhibitors of SARS CoV-2 main protease, Bioorg. Chem. 106 (2021). https://doi.org/10.1016/j.bioorg.2020.104497.
[73] S. Winiwarter, M. Ridderström, A.L. Ungell, T.B. Andersson, I. Zamora, Use of molecular descriptors for absorption, distribution, metabolism, and excretion predictions, in: Compr. Med.

Chem. II, Elsevier, 2006: pp. 531–554. https://doi.org/10.1016/b0-08-045044-x/00140-1.
[74] H. Yu, A. Adedoyin, ADME-Tox in drug discovery: Integration of experimental and computational technologies, Drug Discov. Today. 8 (2003) 852–861. https://doi.org/10.1016/S1359-6446(03)02828-9.
[75] A. Daina, O. Michielin, V. Zoete, SwissADME: A free web tool to evaluate pharmacokinetics, drug-likeness and medicinal chemistry friendliness of small molecules, Sci. Rep. 7 (2017) 1–13. https://doi.org/10.1038/srep42717.
[76] A. Daina, V. Zoete, A BOILED-Egg To Predict Gastrointestinal Absorption and Brain Penetration of Small Molecules, ChemMedChem. (2016) 1117–1121. https://doi.org/10.1002/cmdc.201600182.
[77] D.E.V. Pires, T.L. Blundell, D.B. Ascher, pkCSM: Predicting small-molecule pharmacokinetic and toxicity properties using graph-based signatures, J. Med. Chem. 58 (2015) 4066–4072. https://doi.org/10.1021/acs.jmedchem.5b00104.
[78] T. SHIMAMURA, Y. SUMIKURA, T. YAMAZAKI, A. TADA, T. KASHIWAGI, H. ISHIKAWA, T. MATSUI, N. SUGIMOTO, H. AKIYAMA, H. UKEDA, Applicability of the DPPH Assay for Evaluating the Antioxidant Capacity of Food Additives ^|^ndash; Inter-laboratory Evaluation Study ^|^ndash;, Anal. Sci. 30 (2014) 717–721. https://doi.org/10.2116/analsci.30.717.
[79] H. Abramovič, B. Grobin, N. Poklar Ulrih, B. Cigić, Relevance and Standardization of In Vitro Antioxidant Assays: ABTS, DPPH, and Folin–Ciocalteu, J. Chem. 2018 (2018) 1–9. https://doi.org/10.1155/2018/4608405.
[80] I. Moualek, G. Iratni Aiche, N. Mestar Guechaoui, S. Lahcene, K. Houali, Antioxidant and anti-inflammatory activities of Arbutus unedo aqueous extract, Asian Pac. J. Trop. Biomed. 6 (2016) 937–944. https://doi.org/10.1016/j.apjtb.2016.09.002.
[81] A. Novillo, B. Ekwall, A. Castaño, Protein Precipitation In Vitro as a Measure of Chemical-induced Cytotoxicity: An EDIT Sub-programme, Altern. to Lab. Anim. 29 (2001) 309–324. https://doi.org/10.1177/026119290102900315.
[82] A.S. Loukianov, T.K. Syomina, A.M. Korolev, Conformational Changes in Proteins In Vitro as a Means of Predicting the Acute Toxicities of Chemicals, Altern. to Lab. Anim. 35 (2007) 123–136. https://doi.org/10.1177/026119290703500116.
[83] E.-S.M.N. Abdel-Hafez, G.E.-D.A.A. Abuo-Rahma, M. Abdel-Aziz, M.F. Radwan, H.H. Farag, Design, synthesis and biological investigation of certain pyrazole-3-carboxylic acid derivatives as novel carriers for nitric oxide, Bioorg. Med. Chem. 17 (2009) 3829–3837. https://doi.org/10.1016/j.bmc.2009.04.037.
[84] H.A. Aziz, G.A.I. Moustafa, S.H. Abbas, S.M. Derayea, G.E.-D.A.A. Abuo-Rahma, New norfloxacin/nitric oxide donor hybrids: Synthesis and nitric oxide release measurement using a modified Griess colorimetric method, Eur. J. Chem. 8 (2017) 119–124. https://doi.org/10.5155/eurjchem.8.2.119-124.1549.
[85] Council of Europe, European Pharmacopoeia 10th Edition, 2020.
[86] S. Gore, E. Sanz García, P.M.S. Hendrickx, A. Gutmanas, J.D. Westbrook, H. Yang, Z. Feng, K. Baskaran, J.M. Berrisford, B.P. Hudson, Y. Ikegawa, N. Kobayashi, C.L. Lawson, S. Mading, L. Mak, A. Mukhopadhyay, T.J. Oldfield, A. Patwardhan, E. Peisach, G. Sahni, M.R. Sekharan, S. Sen, C. Shao, O.S. Smart, E.L. Ulrich, R. Yamashita, M. Quesada, J.Y. Young, H. Nakamura, J.L. Markley, H.M. Berman, S.K. Burley, S. Velankar, G.J. Kleywegt, Validation of Structures in the Protein Data Bank, Structure. 25 (2017) 1916–1927. https://doi.org/https://doi.org/10.1016/j.str.2017.10.009.
[87] K.C. Duggan, M.J. Walters, J. Musee, J.M. Harp, J.R. Kiefer, J.A. Oates, L.J. Marnett, Molecular basis for cyclooxygenase inhibition by the non-steroidal anti-inflammatory drug naproxen, J. Biol. Chem. 285 (2010) 34950–34959. https://doi.org/10.1074/jbc.M110.162982.
[88] A.L. Morris, M.W. MacArthur, E.G. Hutchinson, J.M. Thornton, Stereochemical quality of protein structure coordinates, Proteins Struct. Funct. Bioinforma. 12 (1992) 345–364.

https://doi.org/https://doi.org/10.1002/prot.340120407.
[89] G.J. Kleywegt, T.B.T.-M. in E. Alwyn Jones, [11] Model building and refinement practice, in: Macromol. Crystallogr. Part B, Academic Press, 1997: pp. 208–230. https://doi.org/https://doi.org/10.1016/S0076-6879(97)77013-7.
[90] S. Oniga, L. Pacureanu, C. Stoica, M. Palage, A. Crăciun, L. Rusu, E.-L. Crisan, C. Araniciu, COX Inhibition Profile and Molecular Docking Studies of Some 2-(Trimethoxyphenyl)-Thiazoles, Molecules. 22 (2017) 1507. https://doi.org/10.3390/molecules22091507.
[91] S.E. Kassab, M.A. Khedr, H.I. Ali, M.M. Abdalla, Discovery of new indomethacin-based analogs with potentially selective cyclooxygenase-2 inhibition and observed diminishing to PGE2 activities, Eur. J. Med. Chem. 141 (2017) 306–321. https://doi.org/10.1016/j.ejmech.2017.09.056.
[92] S.W. Rowlinson, J.R. Kiefer, J.J. Prusakiewicz, J.L. Pawlitz, K.R. Kozak, A.S. Kalgutkar, W.C. Stallings, R.G. Kurumbail, L.J. Marnett, A Novel Mechanism of Cyclooxygenase-2 Inhibition Involving Interactions with Ser-530 and Tyr-385, J. Biol. Chem. 278 (2003) 45763–45769. https://doi.org/10.1074/jbc.M305481200.
[93] K.M. Knights, A.A. Mangoni, J.O. Miners, Defining the COX inhibitor selectivity of NSAIDs: implications for understanding toxicity, Expert Rev. Clin. Pharmacol. 3 (2010) 769–776. https://doi.org/10.1586/ecp.10.120.
[94] G. Carullo, F. Galligano, F. Aiello, Structure-activity relationships for the synthesis of selective cyclooxygenase 2 inhibitors: an overview (2009-2016), Medchemcomm. 8 (2016) 492–500. https://doi.org/10.1039/c6md00569a.
[95] B. Chandrasekaran, S.N. Abed, O. Al-Attraqchi, K. Kuche, R.K. Tekade, Chapter 21 - Computer-Aided Prediction of Pharmacokinetic (ADMET) Properties, in: R.K.B.T.-D.F.D.P. Tekade (Ed.), Adv. Pharm. Prod. Dev. Res., Academic Press, 2018: pp. 731–755. https://doi.org/https://doi.org/10.1016/B978-0-12-814421-3.00021-X.
[96] Y. Gao, C. Gesenberg, W. Zheng, Oral Formulations for preclinical studies: Principle, design, and development considerations, Elsevier Inc., 2017. https://doi.org/10.1016/B978-0-12-802447-8.00017-0.
[97] A.K. Shakya, B.O. Al-Najjar, P.K. Deb, R.R. Naik, R.K. Tekade, Chapter 8 - First-Pass Metabolism Considerations in Pharmaceutical Product Development, in: R.K.B.T.-D.F.D.C. Tekade (Ed.), Adv. Pharm. Prod. Dev. Res., Academic Press, 2018: pp. 259–286. https://doi.org/https://doi.org/10.1016/B978-0-12-814423-7.00008-3.
[98] Y.A. Ghodke-Puranik, J.K. Lamba, Chapter 7 - Pharmacogenomics, in: B. Patwardhan, R.B.T.-I.A. in D.D. Chaguturu (Eds.), Academic Press, Boston, 2017: pp. 195–234. https://doi.org/https://doi.org/10.1016/B978-0-12-801814-9.00007-6.
[99] A. Dasgupta, Chapter 4 - Genetic Factors Associated With Opioid Therapy and Opioid Addiction, in: A.B.T.-F. the O.E. Dasgupta (Ed.), Elsevier, 2020: pp. 61–88. https://doi.org/https://doi.org/10.1016/B978-0-12-820075-9.00004-1.
[100] R.G. Tirona, R.B. Kim, Chapter 20 - Introduction to Clinical Pharmacology, in: D. Robertson, G.H.B.T.-C. and T.S. (Second E. Williams (Eds.), Academic Press, 2017: pp. 365–388. https://doi.org/https://doi.org/10.1016/B978-0-12-802101-9.00020-X.
[101] D.J. Charles, Antioxidant Assays, in: Antioxid. Prop. Spices, Herbs Other Sources, Springer New York, New York, NY, 2012: pp. 9–38. https://doi.org/10.1007/978-1-4614-4310-0_2.
[102] M.K. Gilson, H.-X. Zhou, Calculation of Protein-Ligand Binding Affinities, Annu. Rev. Biophys. Biomol. Struct. 36 (2007) 21–42. https://doi.org/10.1146/annurev.biophys.36.040306.132550.
[103] H. Gohlke, G. Klebe, Approaches to the Description and Prediction of the Binding Affinity of Small-Molecule Ligands to Macromolecular Receptors, Angew. Chemie Int. Ed. 41 (2002) 2644–2676. https://doi.org/https://doi.org/10.1002/1521-3773(20020802)41:15<2644::AID-ANIE2644>3.0.CO;2-O.
[104] W.L. Jorgensen, The Many Roles of Computation in Drug Discovery, Science (80-.). 303 (2004) 1813 LP – 1818. https://doi.org/10.1126/science.1096361.
[105] S.K. Senthil, P.K. Murugan, S. Selvam, J.P. Chandhana, T.G. Satheesh Babu, E. Kandasamy,

Fluorescence spectroscopic analysis of heavy metal induced protein denaturation, Mater. Today Proc. 33 (2020) 2328–2330. https://doi.org/10.1016/j.matpr.2020.04.693.
[106] A.L. Blobaum, L.J. Marnett, Structural and functional basis of cyclooxygenase inhibition, J. Med. Chem. 50 (2007) 1425–1441. https://doi.org/10.1021/jm0613166.
[107] J. Bienvenu, T. Walzer, U. De Lyon, U. Inserm, Compendium of Inflammatory Diseases, Springer Basel, Basel, 2016. https://doi.org/10.1007/978-3-7643-8550-7.
[108] M.J. Lucido, B.J. Orlando, A.J. Vecchio, M.G. Malkowski, Crystal Structure of Aspirin-Acetylated Human Cyclooxygenase-2: Insight into the Formation of Products with Reversed Stereochemistry, Biochemistry. 55 (2016) 1226–1238. https://doi.org/10.1021/acs.biochem.5b01378.
[109] J. Lei, Y. Zhou, D. Xie, Y. Zhang, Mechanistic insights into a classic wonder drug-aspirin, J. Am. Chem. Soc. 137 (2015) 70–73. https://doi.org/10.1021/ja5112964.
[110] L. Alfonso, G. Ai, R.C. Spitale, G.J. Bhat, Molecular targets of aspirin and cancer prevention, Br. J. Cancer. 111 (2014) 61–67. https://doi.org/10.1038/bjc.2014.271.
[111] Bhat, Does aspirin acetylate multiple cellular proteins? (Review), Mol. Med. Rep. 2 (2009) 667–671. https://doi.org/10.3892/mmr_00000132.
[112] M.H. Tatham, C. Cole, P. Scullion, R. Wilkie, N.J. Westwood, L.A. Stark, R.T. Hay, A Proteomic Approach to Analyze the Aspirin-mediated Lysine Acetylome, Mol. Cell. Proteomics. 16 (2017) 310–326. https://doi.org/10.1074/mcp.O116.065219.
[113] Y. MIZUSHIMA, M. KOBAYASHI, Interaction of anti-inflammatory drugs with serum proteins, especially with some biologically active proteins, J. Pharm. Pharmacol. 20 (1968) 169–173. https://doi.org/10.1111/j.2042-7158.1968.tb09718.x.
[114] A. Pabbathi, S. Patra, A. Samanta, Structural Transformation of Bovine Serum Albumin Induced by Dimethyl Sulfoxide and Probed by Fluorescence Correlation Spectroscopy and Additional Methods, ChemPhysChem. 14 (2013) 2441–2449. https://doi.org/10.1002/cphc.201300313.
[115] A.N.L. Batista, J.M. Batista, L. Ashton, V.S. Bolzani, M. Furlan, E.W. Blanch, Investigation of DMSO-Induced Conformational Transitions in Human Serum Albumin Using Two-Dimensional Raman Optical Activity Spectroscopy, Chirality. 26 (2014) 497–501. https://doi.org/10.1002/chir.22351.